Nucleotide Analogues as Powerful Tools in Exploring G-Quadruplex Folding

I n a u g u r a l d i s s e r t a t i o n

zur

Erlangung des akademischen Grades eines

Doktors der Naturwissenschaften (Dr. rer. nat.)

der

Mathematisch-Naturwissenschaftlichen Fakultät

der

Ernst-Moritz-Arndt-Universität Greifswald

vorgelegt von

Jonathan Dickerhoff

geboren am 22.06.1988

in Cloppenburg

Greifswald, Januar 2017

Dekan:	Prof. Dr. Werner Weitschies
1. Gutachter :	Prof. Dr. Klaus Weisz
2. Gutachter:	Prof. Dr. Heiko Ihmels
3. Gutachter:	Prof. Dr. Clemens Richert
Tag der Promotion:	27. April 2017

Contents

Abbreviations

A	deoxyadenosine
C	deoxycytidine
CD	circular dichroism
dG	deoxyguanosine
DNA	deoxyribonucleic acid
^{F}G	2'-fluoro-2'-deoxyguanosine
G	deoxyguanosine
LNA	locked nucleic acid
N	north
NMR	nuclear magnetic resonance
PM	methylphosphonate
PNA	peptide nucleic acid
PS	phosphorothioate
rG	riboguanosine
RNA	ribonucleic acid
UNA	unlocked nucleic acid
S	south
T	deoxythymidine

1 Scope and Outline

In this dissertation, C2'-modified nucleotides were rationally incorporated into DNA and RNA quadruplexes to gain new insights into their folding process. These nucleic acid secondary structures formed by G-rich sequences attracted increasing interest during the past decades due to their existence *in vivo* and their involvement in many cellular processes. Also, with their unique topology they provide an promising scaffold for various technological applications. Important regions throughout the genome are able to form quadruplexes, emphasizing their high potential as promising drug targets in particular for anti-cancer therapy.

However, the observed structural variability comes hand in hand with a more complex structure prediction. Many driving forces are involved and far from being fully understood. Therefore, a strategy based on the rational incorporation of deoxyguanosine analogues into known structures and subsequent comparison between native and modified forms was developed to isolate specific effects. NMR spectroscopy is particularly suited for analyzing the structural response to the introduced perturbations on an atomic level and for identifying even subtle changes.

In the following, studies are presented that shed light on interactions which could possibly have an effect on the limited diversity of RNA quadruplexes. Additionally, the structural landscape of this class of secondary structures is further explored by editing glycosidic torsion angles using modified nucleotides.

Article I **Sugar-Edge Interactions in a DNA-RNA G-Quadruplex: Evidence of Sequential C-H$\cdots$O Hydrogen Bonds Contributing to RNA Quadruplex Folding**
Dickerhoff, J., Appel, B., Müller, S., Weisz, K. *Angew. Chem. Int. Ed.* 2016, 55, 15162-15165; *Angew. Chem.* 2016, 128, 15386 – 15390.

In this study, remarkable effects of the 2'-hydroxy group were traced by specific substitutions in DNA sequences. Such a deoxyribo- to ribonucleotide substitution offered a rare opportunity to experimentally detect C-H$\cdots$O hydrogen bonds specific for RNA quadruplexes with a possible impact on their restricted folding options.

Article II **Flipping a G-Tetrad in a Unimolecular Quadruplex Without Affecting Its Global Fold**

Dickerhoff, J., Weisz, K. *Angew. Chem. Int. Ed.* 2015, 54, 5588–5591; *Angew. Chem.* 2015, 127, 5680 – 5683.

In this article, a tetrad reversal induced by the incorporation of 2'-fluoro-2'-deoxyguanosines is described. Destabilization of positions with a *syn* glycosidic torsion angle in a (3+1)-hybrid quadruplex resulted in local structural changes instead of a complete refolding. As a consequence the global fold is maintained but features a unique G-core conformation.

Article III **Tracing Effects of Fluorine Substitutions on G-Quadruplex Conformational Transitions**

Dickerhoff, J., Haase, L., Langel, W., Weisz, K., *submitted.*

A detailed analysis of the previously reported tetrad flip is described in this publication. The same substitution strategy was successfully applied to another sequence. In-depth sugar pucker analysis revealed an unusual number of *south* conformers for the 2'-fluoro-2'-deoxyguanosine analogues. Finally, high-resolution structures obtained by restrained molecular dynamics calculations provided insight into conformational effects based on the fluorine orientation.

2 Introduction

The world of biomolecules is mostly dominated by the large and diverse family of proteins. In this context nucleic acids and in particular DNA are often reduced to a simple library of genetic information with its four-letter code. However, they are not only capable of storing this huge amount of data but also of participating in the regulation of replication and transcription. This is even more pronounced for RNA with its increased structural variability. Thus, riboswitches can control the level of translation while ribozymes catalyze chemical reactions, supporting theories based on an RNA world as precursor of today's life.[1]

2.1 G-Quadruplexes and their Significance

In duplex and triplex structures DNA or RNA form base pairs and base triads to serve as their basic units (Figure 1). In contrast, four guanines can associate to a cyclic G-tetrad connected via Hoogsteen hydrogen bonds.[2,3] Stacking of at least two tetrads yields the core of a G-quadruplex with characteristic coordination of monovalent cations such as potassium or sodium to the guanine carbonyl groups.[4] This additional nucleic acid secondary structure exhibits a globular shape with unique properties and has attracted increasing interest over the past two decades.

Starting with the observation of gel formation for guanosine monophosphate more than 100 years ago, a great number of new topologies and sequences have since been discovered.[5] Recently, an experimental analysis of the human genome revealed 716 310 quadruplex forming

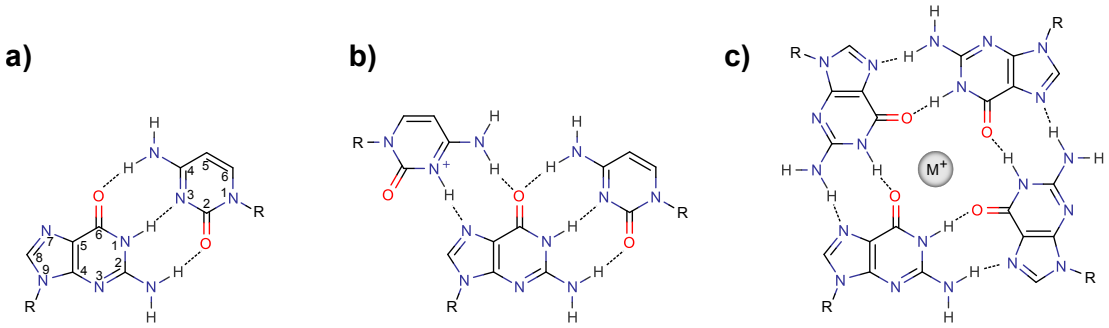

Figure 1: (a) GC base pair, (b) C^+GC triad, and (c) G-tetrad being the basic unit of duplex, triplex and quadruplex structures, respectively. Hydrogen bonds are indicated by dotted lines.

sequences.[6] The clustering of G-rich domains at important genomic regions such as chromosomal ends, promoters, 3'- and 5'-untranslated sequences, splicing sites, and cancer-related genes points to their physiological relevance and mostly excludes a random guanosines distribution. This is further corroborated by several identified proteins such as helicases exhibiting high *in vitro* specificity for quadruplex structures.[7] Furthermore, DNA and RNA quadruplexes can be detected in human and other cells via *in vivo* fluorescence spectroscopy using specific antibodies or chemically synthesized ligands.[8–10]

A prominent example of a quadruplex forming sequence is found at the end of the chromosomes. This so-called telomeric region is composed of numerous tandem repeats such as TTAGGG in human cells and terminated with an unpaired 3'-overhang.[11] In general, these telomers are shortened with every replication cycle until a critical length is reached and cell senescence occurs. However, the enzyme telomerase, found in many cancerous cells, can extent this sequence and enable unregulated proliferation without cell aging.[12] Ligands designed for anti-cancer therapy specifically bind and stabilize telomeric quadruplexes to impede telomerase action, counteracting the immortality of the targeted cancer cells.[13]

Additional cellular processes are also associated with the formation of quadruplexes. For example, G-rich sequences are found in many origins of replication and are involved in the initiation of genome copying.[14,15] Transcription and translation can also be controlled by the formation of DNA or RNA quadruplexes within promoters and ribosome binding sites.[16,17]

Obviously, G-quadruplexes are potential drug targets particularly for anti-cancer treatment. Therefore, a large variety of different quadruplex ligands has been developed over the last years.[18] In contrast to other secondary structures, these ligands mostly stack upon the quadruplex outer tetrads rather then intercalate between tetrads. Also, a groove binding mode was observed in rare cases. Until now, only one quadruplex specific ligand, quarfloxin, reached phase II clinical trials. However, it was withdrawn as a consequence of poor bioavailability despite otherwise promising results.[19,20]

Besides its physiological meaning, many diagnostic and technological applications make use of the quadruplex scaffold. Some structures can act as so-called aptamers and show both strong and specific binding towards proteins or other molecules. One of the best known examples is the high-affinity thrombine binding aptamer inhibiting fibrin-clot formation.[21] In addition, quadruplexes can be used as biosensors for the detection and quantification of metal ions such as potassium. As a consequence of a specific fold induced by the corresponding metal ion, detection is based on either intrinsic quadruplex fluorescence,[22] binding of a fluorescent ligand,[23] or a chemical reaction catalyzed by a formed quadruplex with enzymatic activity (DNAzyme).[24] DNAzymes represent another interesting field of application. Coordination of hemin or copper ions to outer tetrads can, for example, impart peroxidase activity or facilitate an enantioselective Diels-Alder reaction.[25,26]

2.2 Structural Variability of G-Quadruplexes

A remarkable feature of DNA quadruplexes is their considerable structural variability emphasized by continued reports of new folds. In contrast to duplex and triplex structures with their strict complementarity of involved strands, the assembly of the G-core is significantly less restricted. Also, up to four individual strands are involved and several patterns of G-tract directionality can be observed. In addition to all tracts being parallel, either one or two can also show opposite orientation such as in (3+1)-hybrid and antiparallel structures, respectively (Figure 2a-c).[27]

In general, each topology is characterized by a specific pattern of the glycosidic torsion angles *anti* and *syn* describing the relative base-sugar orientation (Figure 2d).[28] An increased number of *syn* conformers is necessary in case of antiparallel G-tracts to form an intact Hoogsten hydrogen bond network within tetrads. The sequence of glycosidic angles also determines the type of stacking interactions within the G-core. Adjacent *syn* and *anti* conformers within a G-tract result in opposite polarity of the tetrads' hydrogen bonds and in a heteropolar stacking. Its homopolar counterpart is found for *anti-anti* or *syn-syn* arrangements.[29]

Finally, the G-tract direction also determines the width of the four quadruplex grooves. Whereas a medium groove is formed between adjacent parallel strands, wide and narrow grooves

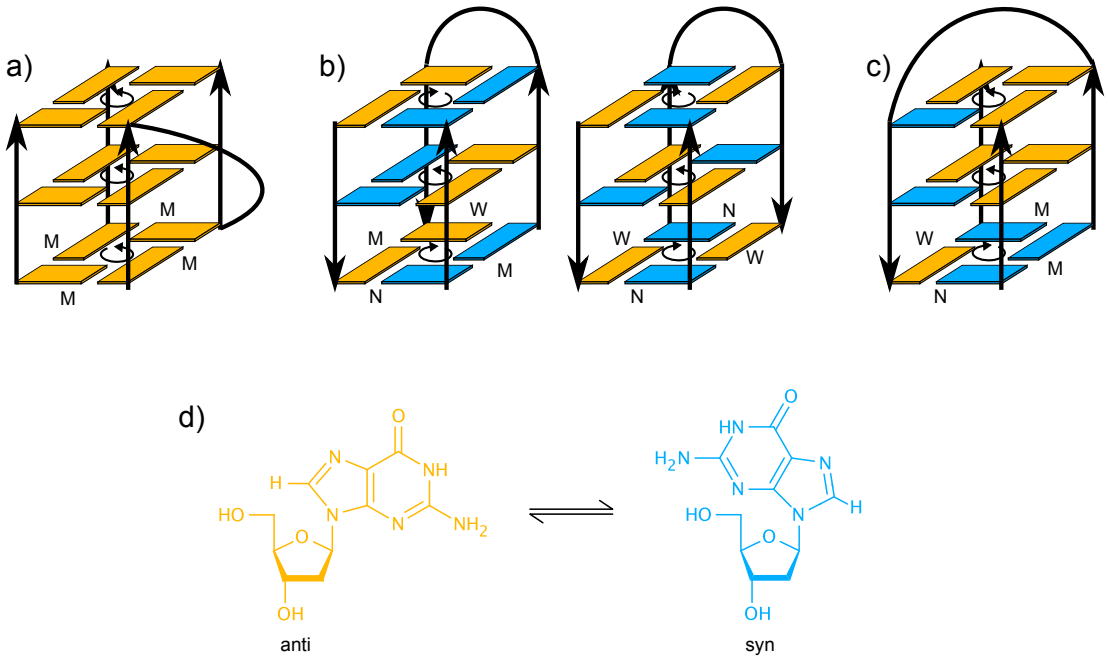

Figure 2: Schematic view of (a) parallel, (b) antiparallel, and (c) (3+1)-hybrid type topologies with propeller, lateral, and diagonal loop, respectively. Medium (M), narrow (N), and wide (W) grooves are indicated as well as the direction of the tetrads' hydrogen bond network. (d) *Syn-anti* equilibrium for dG. The *anti* and *syn* conformers are shown in orange and blue, respectively.

are observed between antiparallel tracts.[30]

Unimolecular quadruplexes may be further diversified through loops of different length. There are three main types of loops, one of which is the propeller loop connecting adjacent parallel tracts while spanning all tetrads within a groove. Antiparallel tracts are joined by loops located above the tetrad. Lateral loops connect neighboring and diagonal loops link oppositely positioned G-tracts (Figure 2). Other motifs include bulges,[31] omitted Gs within the core,[32] long loops forming duplexes,[33] or even left-handed quadruplexes.[34]

Simple sequences with G-tracts linked by only one or two nucleotides can be assumed to adopt a parallel topology. Otherwise, the individual composition and length of loops,[35–37] overhangs, or other features prevent a reliable prediction of the corresponding structure. Many forces can contribute with mostly unknown magnitude or origin. Additionally, extrinsic parameters like type of ion, pH, crowding agents, or temperature can have a significant impact on folding. The quadruplex structural variability is exemplified by the human telomeric sequence and its variants which can adopt all three types of G-tract arrangements.[38–40]

Remarkably, so far most of the discussed variations have not been observed for RNA. Although RNA can generally adopt a much larger variety of foldings facilitated by additional putative 2'-OH hydrogen bonds, RNA quadruplexes are mostly limited to parallel topologies. Even sophisticated approaches using various templates to enforce an antiparallel strand orientation failed.[41,42]

2.3 Modification of G-Quadruplexes

The scientific literature is rich in examples of modified nucleic acids. These modifications are often associated with significant effects that are particularly apparent for the diverse quadruplex. Frequently, a detailed analysis of quadruplexes is impeded by the coexistence of several species. To isolate a particular structure, the incorporation of nucleotide analogues favoring one specific conformer at variable positions can be employed.[43,44] Furthermore, analogues can be used to expand the structural landscape by inducing unusual topologies that are only little populated or in need of very specific conditions. Thereby, insights into the driving forces of quadruplex folding can be gained and new drug targets can be identified. Fine-tuning of certain quadruplex properties, such as thermal stability, nuclease resistance, or catalytic activity can also be achieved.[45,46]

In the following, some frequently used modifications affecting the backbone, guanine base, or sugar moiety are presented (Figure 3). Backbone alterations include methylphosphonate (PM) or phosphorothioate (PS) derivatives and also more significant conversions.[45] These can be 5'-5' and 3'-3' backbone linkages[47] or a complete exchange for an alternative scaffold as seen in peptide nucleic acids (PNA).[48]

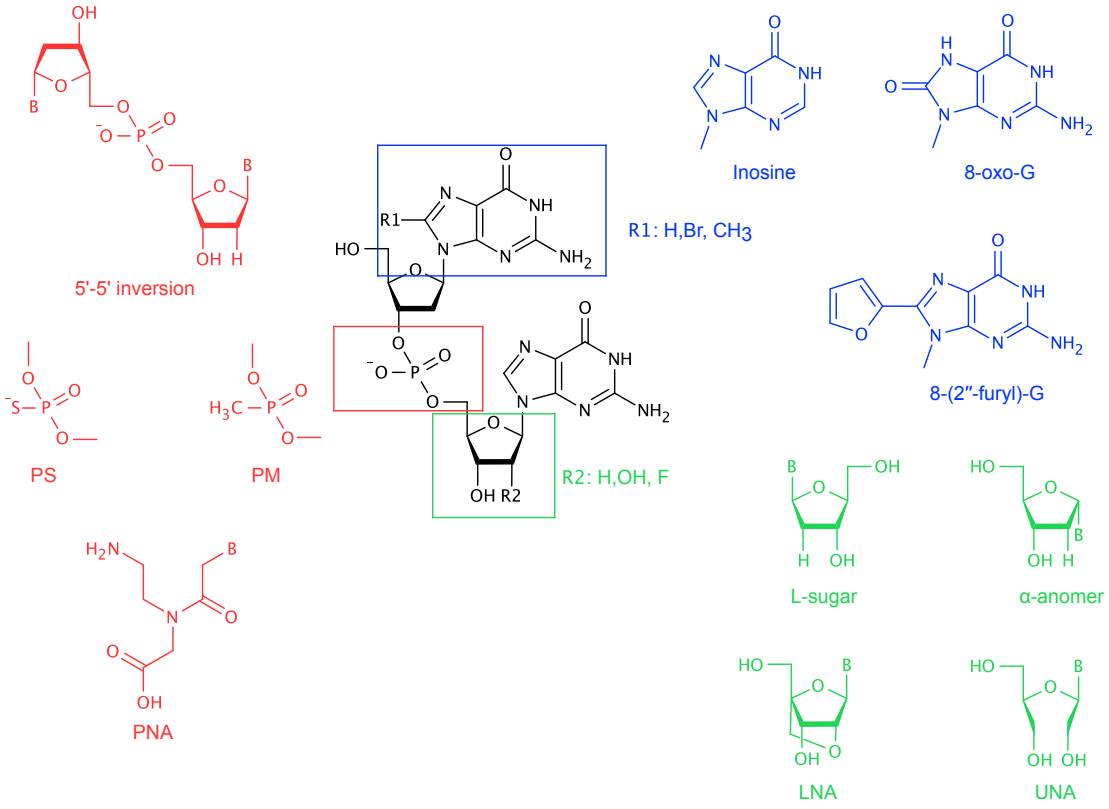

Figure 3: Modifications at the level of base (blue), backbone (red), and sugar (green).

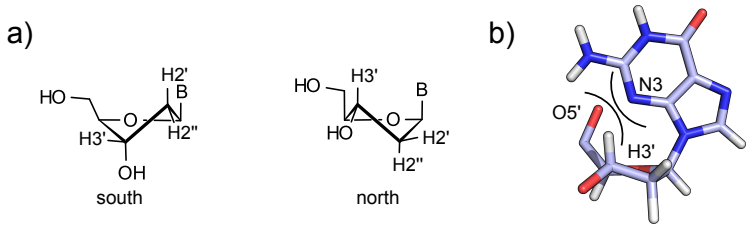

Figure 4: (a) Sugar conformations and (b) the proposed steric clash between a *syn* oriented base and a sugar in *north* conformation.

Most guanine analogues are modified at C8, conserving regular hydrogen bond donor and acceptor sites. Substitution at this position with bulky bromine, methyl, carbonyl, or fluorescent furyl groups is often employed to control the glycosidic torsion angle.[49–52] Space requirements and an associated steric hindrance destabilize an *anti* conformation. Consequently, such modifications can either show a stabilizing effect after their incorporation at a *syn* position or may induce a flip around the glycosidic bond followed by further rearrangements when placed at an *anti* position.[53] The latter was reported for an entire tetrad fully substituted with 8-Br-dG or 8-Methyl-dG in a tetramolecular structure.[49,50] Furthermore, the G-analogue inosine is often used as an NMR marker based on the characteristic chemical shift of its imino proton.[54]

On the other hand, sugar modifications can increase the structural flexibility as observed for unlocked nucleic acids (UNA)[55] or change one or more stereocenters as with α- or L-deoxyribose.[56,57] However, in many cases the glycosidic torsion angle is also affected. The *syn* conformer may be destabilized either by interactions with the particular C2' substituent as observed for the C2'-epimers arabinose and 2'-fluoro-2'-deoxyarabinose or through steric restrictions as induced by a change in sugar pucker.[58–60]

The sugar pucker is defined by the furanose ring atoms being above or below the sugar plane. A planar arrangement is prevented by steric restrictions of the eclipsed substituents. Energetically favored puckers are generally represented by *south*- (S) or *north*- (N) type conformers with C2' or C3' atoms oriented above the plane towards C5' (Figure 4a). Locked nucleic acids (LNA),[61] ribose,[62] or 2'-fluoro-2'-deoxyribose[63] are examples for sugar moieties which prefer the N-type pucker due to structural constraints or gauche effects of electronegative groups at C2'. Therefore, the minimization of steric hindrance between N3 and both H3' and O5' is assumed to shift the equilibrium towards *anti* conformers (Figure 4b).[64]

3 Sugar-Edge Interactions in a DNA-RNA G-Quadruplex: Evidence of Sequential C-H···O Hydrogen Bonds Contributing to RNA Quadruplex Folding

In the first project, riboguanosines (rG) were introduced into DNA sequences to analyze possible effects of the 2'-hydroxy group on quadruplex folding. As mentioned above, RNA quadruplexes normally adopt parallel folds. However, the frequently cited reason that N-type pucker excludes *syn* glycosidic torsion angles is challenged by a significant number of riboguanosine S-type conformers in these structures. Obviously, the 2'-OH is correlated with additional forces contributing to the folding process. The homogeneity of pure RNA quadruplexes hampers the more detailed evaluation of such effects. Alternatively, the incorporation of single rG residues into a DNA structures may be a promising approach to identify corresponding anomalies by comparing native and modified structure.

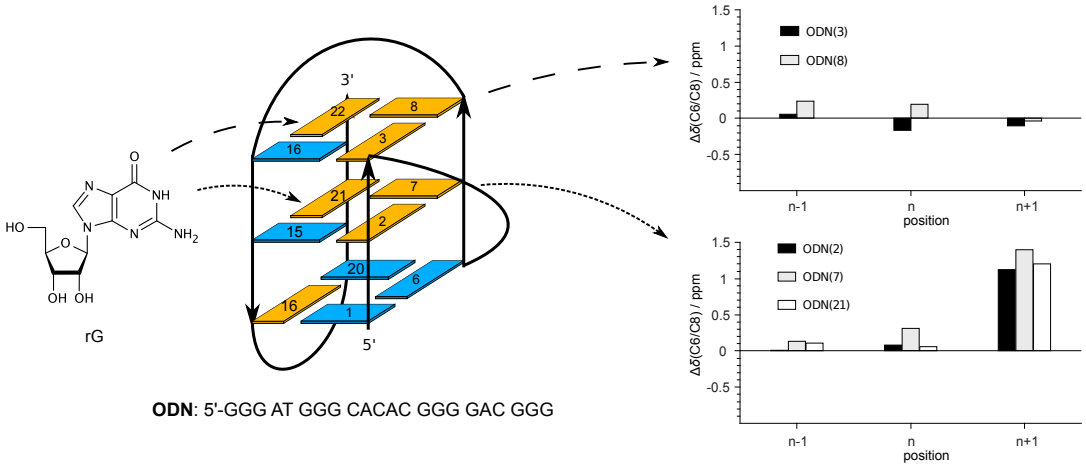

Figure 5: Incorporation of rG at *anti* positions within the central tetrad is associated with a deshielding of C8 in the 3'-neighboring nucleotide. Substitution of position 16 and 22 leads to polymorphism preventing a detailed analysis. The *anti* and *syn* conformers are shown in orange and blue, respectively.

Initially, all *anti* nucleotides of the artificial (3+1)-hybrid structure ODN, comprising all main types of loops, were consecutively exchanged with rG (Figure 5).[65] Positions with the unfavored *syn* conformation were omitted in these substitutions to avoid additional perturbations. A high resemblance to the native form required for a meaningful comparison was found for most rG-modified sequences based on CD and NMR spectra. Also, conservation of the normally unfavored S-type pucker was observed for most riboses. However, guanosines following the rG residues located within the central tetrad showed a significant C8 deshielding effect (Figure 5), suggesting an interaction between C8 and the 2'-hydroxy group of the incorporated rG nucleotide. Similar chemical shift differences were correlated to C-H$\cdots$O hydrogen bonds in literature.[66,67]

Further evidence of such a C-H$\cdots$O hydrogen bond was provided by using a similarly modified parallel topology from the c-MYC promoter sequence.[68] Again, the combination of both an S-type ribose and a C8 deshielded 3'-neighboring base was found and hydrogen bond formation was additionally corroborated by an increase of the one-bond ^{1}J(H8,C8) scalar coupling constant.

The significance of such sequential interactions as established for these DNA-RNA chimeras was assessed via data analysis of RNA structures from NMR and X-ray crystallography. A search for S-type sugars in combination with suitable C8-H$\cdots$O2' hydrogen bond angular and distance parameters could identify a noticeable number of putative C-H$\cdots$O interactions.

One such example was detected in a bimolecular human telomeric sequence (rHT) that was subsequently employed for a further evaluation of sequential C-H$\cdots$O hydrogen bonds in RNA quadruplexes.[69,70] Replacing the corresponding rG3 with a dG residue resulted in a shielding

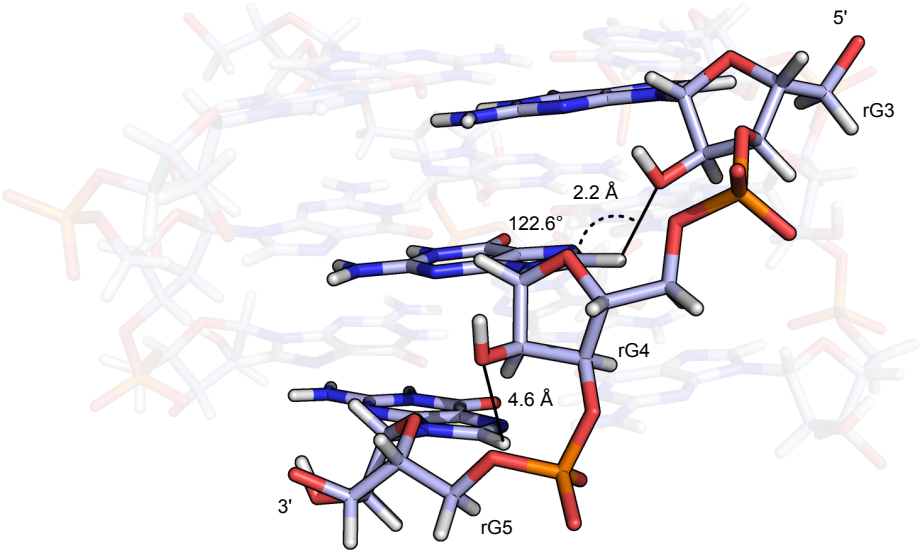

Figure 6: An S-type sugar pucker of rG3 in rHT (PDB: 2KBP) allows for a C-H$\cdots$O hydrogen bond formation with rG4. The latter is an N conformer and is unable to form corresponding interactions with rG5.

of the following C8 as expected for a loss of the predicted interaction (Figure 6).

In summary, a single substitution strategy in combination with NMR spectroscopy provided a unique way to detect otherwise hard to find C-H$\cdots$O hydrogen bonds in RNA quadruplexes. As a consequence of hydrogen bond donors required to adopt an *anti* conformation, *syn* residues in antiparallel and (3+1)-hybrid assemblies are possibly penalized. Therefore, sequential C8-H$\cdots$O2' interactions in RNA quadruplexes could contribute to the driving force towards a parallel topology.

4 Flipping a G-Tetrad in a Unimolecular Quadruplex Without Affecting Its Global Fold

In a second project, 2'-fluoro-2'-deoxyguanosines (^{F}G) preferring *anti* glycosidic torsion angles were substituted for *syn* dG conformers in a quadruplex. Structural rearrangements as a response to the introduced perturbations were identified via NMR spectroscopy.

Studies published in literature report on the refolding into parallel topologies after incorporation of nucleotides with an *anti* conformational preference.[60,62,63] However, a single or full exchange was employed and rather flexible structures were used. Also, the analysis was largely based on CD spectroscopy. This approach is well suited to determine the type of stacking which is often misinterpreted as an effect of strand directionality.[28,71] The interpretation as being a shift towards a parallel fold is in fact associated with a homopolar stacked G-core. Although both structural changes are frequently correlated, other effects such as a reversal of tetrad polarity as observed for tetramolecular quadruplexes can not be excluded without a more detailed structural analysis.

All three *syn* positions within the tetrad following the 5'-terminus (5'-tetrad) of ODN were substituted with ^{F}G analogues to yield the sequence ^{F}ODN. Initial CD spectroscopic studies on the modified quadruplex revealed a negative band at about 240 nm and a large positive band at 260 nm characteristic for exclusive homopolar stacking interactions (Figure 7a). Instead

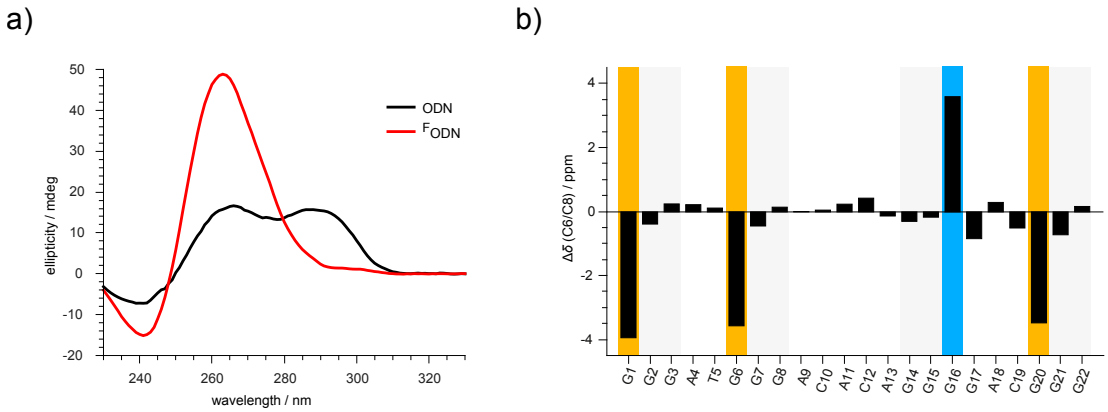

Figure 7: a) CD spectra of ODN and ^{F}ODN, and b) chemical shift differences for C6/C8 of the modified sequence referenced against the native form.

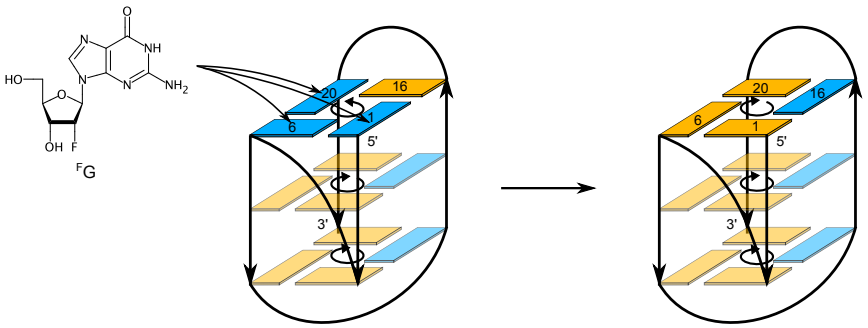

Figure 8: Incorporation of ^{F}G into the 5'-tetrad of ODN induces a tetrad reversal. *Anti* and *syn* residues are shown in orange and blue, respectively.

of assuming a newly adopted parallel fold, NMR experiments were performed to elucidate conformational changes in more detail. A spectral resemblance to the native structure except for the 5'-tetrad was observed, contradicting expectations of fundamental structural differences.

NMR spectral assignments confirmed a (3+1)-topology with identical loops and glycosidic angles of the 5'-tetrad switched from *syn* to *anti* and *vice versa* (Figure 8). This can be visualized by plotting the chemical shift differences between modified and native ODN (Figure 7b), making use of a strong dependency of chemical shifts on the glycosidic torsion angle for the C6 and C8 carbons of pyrimidine and purine bases, respectively.[72,73] Obviously, most residues in ^{F}ODN are hardly affected in line with a conserved global fold. In contrast, C8 resonances of ^{F}G1, ^{F}G6, and ^{F}G20 are shielded by about 4 ppm corresponding to the newly adopted *anti* conformation, whereas C8 of G16 located in the antiparallel G-tract is deshielded due to its opposing *anti-syn* transition.

Taken together, these results revealed for the first time a tetrad flip without any major quadruplex refolding. Apparently, the resulting new topology with antiparallel strands and a homopolar stacked G-core is preferred over more significant changes. Due to its conserved fold, the impact of the tetrad polarity, e.g., on ligand binding, may be determined without interfering effects from loops, overhangs, or strand direction. Consequently, this information could also enable a rational design of quadruplex-forming sequences for various biological and technological applications.

5 Tracing Effects of Fluorine Substitutions on G-Quadruplex Conformational Transitions

In the third project, the previously described reversal of tetrad polarity was expanded to another sequence. The structural changes were analyzed in detail yielding high-resolution structures of modified quadruplexes.

Distinct features of ODN such as a long diagonal loop or a missing overhang may decide whether a tetrad flip or a refolding in a parallel quadruplex is preferred. To resolve this ambiguity, the human telomeric sequence HT was chosen as an alternative (3+1)-hybrid structure comprising three TTA lateral loops and single-stranded termini (Figure 9a).[40] Again, a modified construct ^{F}HT was designed by incorporating ^{F}G at three *syn* positions within the 5'-tetrad and subsequently analyzed via CD and NMR spectroscopy. In analogy to ^{F}ODN, the experimental data showed a change of tetrad polarity but no refolding into a parallel topology, thus generalizing such transitions for this type of quadruplex.

In literature, an N-type pucker exclusively reported for ^{F}G in nucleic acids is suggested to be the driving force behind a destabilization of *syn* conformers. However, an analysis of sugar pucker for ^{F}ODN and ^{F}HT revealed that two of the three modified nucleotides adopt an S-type conformation. These unexpected observations indicated differences in positional impact; thus, the 5'-tetrad of ODN was mono- and disubstituted with ^{F}G to identify their specific contribution to structural changes. A comparison of CD spectra demonstrated the crucial role of the N-type nucleotide in the conformational transition. Although critical for a tetrad flip, an exchange of at least one additional residue was necessary for complete reversal. Apparently, based on these results S conformers also show a weak prefererence for the *anti* conformation, indicating additional forces at work that influence the glycosidic torsion angle.

NMR restrained high-resolution structures were calculated for ^{F}HT and ^{F}ODN (Figures 9b-c). As expected, differences to the native form were mostly restricted to the 5'-tetrad as well as to nucleotides of the adjacent loops and the 5'-overhang. The structures revealed an important correlation between sugar conformation and fluorine orientation. Depending on the sugar pucker, F2' points towards one of the two adjacent grooves. Conspicuously, only medium grooves are occupied as a consequence of the N-type sugar that effectively removes the corresponding fluorine from the narrow groove and reorients it towards the medium groove (Figure 10). The narrow groove is characterized by a small separation of the two antiparallel backbones.

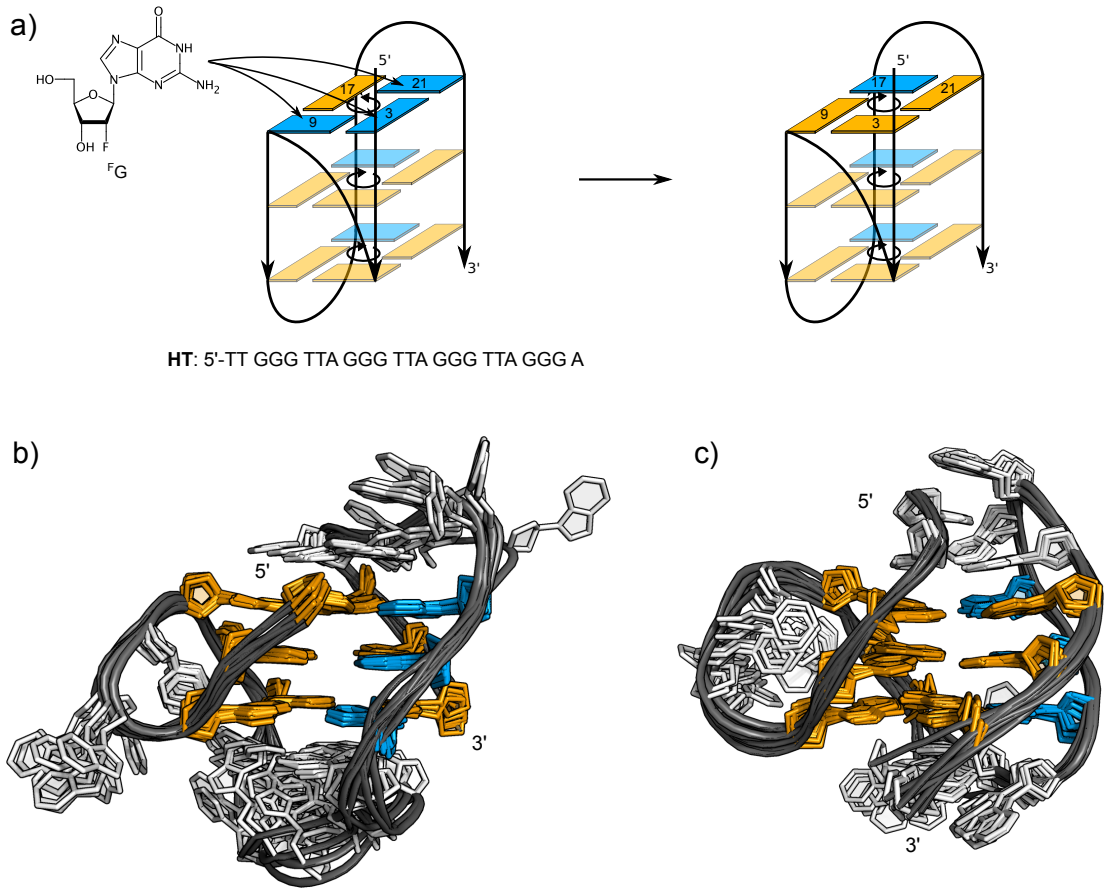

Figure 9: (a) Schematic view of HT and ^{F}HT showing the polarity reversal after ^{F}G incorporation. High-resolution structures of (b) ^{F}ODN and (c) ^{F}HT. Ten lowest-energy states are superimposed and *anti* and *syn* residues are presented in orange and blue, respectively.

Thus, the negative phosphates are close to each other increasing the negative electrostatic potential and mutual repulsion.[74] This is attenuated by a well-ordered spine of water as observed in crystal structures.[75,76]

Because fluorine is both negatively polarized and hydrophobic, its presence within the narrow groove may disturb the stabilizing water arrangement while simultaneously increasing the strongly negative potential.[77,78] From this perspective, the observed adjustments in sugar pucker can be considered important in alleviating destabilizing effects.

Structural adjustments of the capping loops and overhang were noticeable, in particular for ^{F}HT. An AT base pair was formed in both native and modified structures and stacked upon the outer tetrad. However, the *anti* T is replaced by an adjacent *syn*-type T for the AT base pair formation in ^{F}HT, thus conserving the original stacking geometry between base pair and reversed outer tetrad.

In summary, the first high-resolution structures of unimolecular quadruplexes with an in-

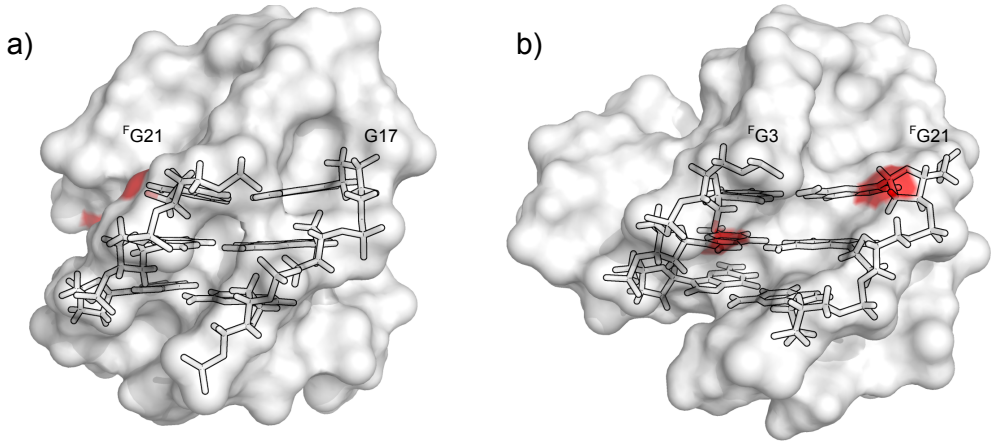

Figure 10: View into (a) narrow and (b) medium groove of ^{F}HT showing the fluorine orientation. F2' of residue ^{F}G21 is removed from the narrow groove due to its N-type sugar pucker. Fluorines are shown in red.

duced tetrad reversal were determined. Incorporated ^{F}G analogues were shown to adopt an S-type pucker not observed before. Both N- and S-type conformations affected the glycosidic torsion angle contrary to expectations and indicated additional effects of F2' on the base-sugar orientation.

A putative unfavorable fluorine interaction within the narrow groove provided a possible explanation for the single N conformer exhibiting a critical role for the tetrad flip. Theoretically, a hydroxy group of ribose may show similar destabilizing effects when located within the narrow groove. As a consequence, parallel topologies comprising only medium grooves are preferred as indeed observed for RNA quadruplexes. Finally, a comparison of modified and unmodified structures emphasized the importance of mostly unnoticed interactions between the G-core and capping nucleotides.

6 Conclusion

In this dissertation the influence of C2'-substituents on quadruplexes has been investigated largely through NMR spectroscopic methods. Riboguanosines with a 2'-hydroxy group and 2'-fluoro-2'-deoxyribose analogues were incorporated into G-rich DNA sequences and modified constructs were compared with their native counterparts.

In the first project, ribonucleotides were used to evaluate the influence of an additional hydroxy group and to assess their contribution for the propensity of most RNA quadruplexes to adopt a parallel topology. Indeed, chemical shift changes suggested formation of C-H$\cdots$O hydrogen bonds between O2' of *south*-type ribose sugars and H8-C8 of the 3'-following guanosine. This was further confirmed for a different quadruplex and additionally corroborated by characteristic changes of C8–H8 scalar coupling constants. Finally, based on published high-resolution RNA structures, a possible structural role of these interactions through the stabilization of hydrogen bond donors in *anti* conformation was indicated.

In a second part, fluorinated ribose analogues with their preference for an *anti* glycosidic torsion angle were incorporated in a (3+1)-hybrid quadruplex exclusively at *syn* positions to induce structural rearrangements. In contrast to previous studies, the global fold in a unimolecular structure was conserved while the hydrogen bond polarity of the modified tetrad was reversed. Thus, a novel quadruplex conformation with antiparallel G-tracts but without any alternation of glycosidic angles along the tracts could be obtained.

In a third project, a corresponding tetrad reversal was also found for a second (3+1)-hybrid quadruplex generalizing this transition for such kind of topology. Remarkably, a *south*-type sugar pucker was observed for most 2'-fluoro-2'-deoxyguanosine analogues that also noticeably affected the *syn-anti* equilibrium. Up to this point, a strong preference for *north* conformers had been assumed due to the electronegative C2'-substituent This conformation is correlated with strong steric interactions in case of a base in *syn* orientation.

To explain the single occurrence of *north* pucker mostly driving the tetrad flip, a hypothesis based on high-resolution structures of both modified sequences was developed. Accordingly, unfavorable interactions of the fluorine within the narrow groove induce a switch of sugar pucker to reorient F2' towards the adjacent medium groove. It is conceivable that other sugar analogues such as ribose can show similar behavior. This provides another explanation for the propensity of RNA quadruplexes to fold into parallel structures comprising only medium

grooves.

In summary, the rational incorporation of modified nucleotides proved itself as powerful strategy to gain more insight into the forces that determine quadruplex folding. Therefore, the results may open new venues to design quadruplex constructs with specific characteristics for advanced applications.

Bibliography

[1] Higgs, P.G. and Lehman, N., The RNA world: molecular cooperation at the origins of life. *Nat. Rev. Genet.* 2015, *16*, 7–17.

[2] Gellert, M., Lipsett, M.N., and Davies, D.R., Helix formation by guanylic acid. *Proc. Natl. Acad. Sci. USA* 1962, *48*, 2013–2018.

[3] Hoogsteen, K., The crystal and molecular structure of a hydrogen-bonded complex between 1-methylthymine and 9-methyladenine. *Acta Crystallogr.* 1963, *16*, 907–916.

[4] Williamson, J.R., Raghuraman, M.K., and Cech, T.R., Monovalent cation-induced structure of telomeric DNA: the G-quartet model. *Cell* 1989, *59*, 871–880.

[5] Bang, I., Untersuchungen über die Guanylsäure. *Biochem. Z.* 1910, *26*, 293–311.

[6] Chambers, V.S., Marsico, G., Boutell, J.M., Di Antonio, M., Smith, G.P., and Balasubramanian, S., High-throughput sequencing of DNA G-quadruplex structures in the human genome. *Nat. Biotechnol.* 2015, *33*, 877–881.

[7] London, T.B.C., Barber, L.J., Mosedale, G., Kelly, G.P., Balasubramanian, S., Hickson, I.D., Boulton, S.J., and Hiom, K., FANCJ is a structure-specific DNA helicase associated with the maintenance of genomic G/C tracts. *J. Biol. Chem.* 2008, *283*, 36132–36139.

[8] Schaffitzel, C., Berger, I., Postberg, J., Hanes, J., Lipps, H.J., and Plückthun, A., In vitro generated antibodies specific for telomeric guanine-quadruplex DNA react with Stylonychia lemnae macronuclei. *Proc. Natl. Acad. Sci. USA* 2001, *98*, 8572–8577.

[9] Biffi, G., Tannahill, D., McCafferty, J., and Balasubramanian, S., Quantitative visualization of DNA G-quadruplex structures in human cells. *Nat. Chem.* 2013, *5*, 182–186.

[10] Laguerre, A., Wong, J.M.Y., and Monchaud, D., Direct visualization of both DNA and RNA quadruplexes in human cells via an uncommon spectroscopic method. *Sci. Rep.* 2016, *6*, 32141.

[11] Makarov, V.L., Hirose, Y., and Langmore, J.P., Long G tails at both ends of human chromosomes suggest a C strand degradation mechanism for telomere shortening. *Cell* 1997, *88*, 657–666.

[12] Kim, N.W., Piatyszek, M.A., Prowse, K.R., Harley, C.B., West, M.D., Ho, P.L., Coviello, G.M., Wright, W.E., Weinrich, S.L., and Shay, J.W., Specific association of human telomerase activity with immortal cells and cancer. *Science* 1994, *266*, 2011–2015.

[13] Sun, D., Thompson, B., Cathers, B.E., Salazar, M., Kerwin, S.M., Trent, J.O., Jenkins, T.C., Neidle, S., and Hurley, L.H., Inhibition of human telomerase by a G-quadruplex-interactive compound. *J. Med. Chem.* 1997, *40*, 2113–2116.

[14] Besnard, E., Babled, A., Lapasset, L., Milhavet, O., Parrinello, H., Dantec, C., Marin, J.M., and Lemaitre, J.M., Unraveling cell type–specific and reprogrammable human replication origin signatures associated with G-quadruplex consensus motifs. *Nat. Struct. Mol. Biol.* 2012, *19*, 837–844.

[15] Valton, A.L., Hassan-Zadeh, V., Lema, I., Boggetto, N., Alberti, P., Saintomé, C., Riou, J.F., and Prioleau, M.N., G4 motifs affect origin positioning and efficiency in two vertebrate replicators. *EMBO J.* 2014, *33*, 732–746.

[16] Siddiqui-Jain, A., Grand, C.L., Bearss, D.J., and Hurley, L.H., Direct evidence for a G-quadruplex in a promoter region and its targeting with a small molecule to repress c-MYC transcription. *Proc. Natl. Acad. Sci. USA* 2002, *99*, 11593–11598.

[17] Wieland, M. and Hartig, J.S., RNA quadruplex-based modulation of gene expression. *Chem. Biol.* 2007, *14*, 757–763.

[18] Neidle, S., Quadruplex nucleic acids as novel therapeutic targets. *J. Med. Chem.* 2016, *59*, 5987–6011.

[19] Drygin, D., Siddiqui-Jain, A., O'Brien, S., Schwaebe, M., Lin, A., Bliesath, J., Ho, C.B., Proffitt, C., Trent, K., Whitten, J.P., Lim, J.K.C., Von Hoff, D., Anderes, K., and Rice, W.G., Anticancer activity of CX-3543: a direct inhibitor of rRNA biogenesis. *Cancer Res.* 2009, *69*, 7653–7661.

[20] Balasubramanian, S., Hurley, L.H., and Neidle, S., Targeting G-quadruplexes in gene promoters: a novel anticancer strategy? *Nat. Rev. Drug Discov.* 2011, *10*, 261–275.

[21] Bock, L.C., Griffin, L.C., Latham, J.A., Vermaas, E.H., and Toole, J.J., Selection of single-stranded DNA molecules that bind and inhibit human thrombin. *Nature* 1992, *355*, 564–566.

[22] Kwok, C.K., Sherlock, M.E., and Bevilacqua, P.C., Decrease in RNA folding cooperativity by deliberate population of intermediates in RNA G-quadruplexes. *Angew. Chem. Int. Ed.* 2013, *52*, 683–686.

[23] Li, T., Wang, E., and Dong, S., Parallel G-quadruplex-specific fluorescent probe for monitoring DNA structural changes and label-free detection of potassium ion. *Anal. Chem.* 2010, *82*, 7576–7580.

[24] Yang, X., Li, T., Li, B., and Wang, E., Potassium-sensitive G-quadruplex DNA for sensitive visible potassium detection. *Analyst* 2010, *135*, 71–75.

[25] Travascio, P., Witting, P.K., Mauk, A.G., and Sen, D., The peroxidase activity of a hemin−DNA oligonucleotide complex: free radical damage to specific guanine bases of the DNA. *J. Am. Chem. Soc.* 2001, *123*, 1337–1348.

[26] Wang, C., Jia, G., Zhou, J., Li, Y., Liu, Y., Lu, S., and Li, C., Enantioselective Diels-Alder reactions with G-quadruplex DNA-based catalysts. *Angew. Chem. Int. Ed.* 2012, *51*, 9352–9355.

[27] Zhang, S., Wu, Y., and Zhang, W., G-quadruplex structures and their interaction diversity with ligands. *ChemMedChem* 2014, *9*, 899–911.

[28] Karsisiotis, A.I., Hessari, N.M., Novellino, E., Spada, G.P., Randazzo, A., and Webba da Silva, M., Topological characterization of nucleic acid G-quadruplexes by UV absorption and circular dichroism. *Angew. Chem. Int. Ed.* 2011, *50*, 10645–10648.

[29] Lech, C.J., Heddi, B., and Phan, A.T., Guanine base stacking in G-quadruplex nucleic acids. *Nucleic Acids Res.* 2013, *41*, 2034–2046.

[30] Webba da Silva, M., Geometric Formalism for DNA quadruplex folding. *Chem. Eur. J.* 2007, *13*, 9738–9745.

[31] Mukundan, V.T. and Phan, A.T., Bulges in G-quadruplexes: broadening the definition of G-quadruplex-forming sequences. *J. Am. Chem. Soc.* 2013, *135*, 5017–5028.

[32] Heddi, B., Martín-Pintado, N., Serimbetov, Z., Kari, T., and Phan, A.T., G-quadruplexes with (4n -1) guanines in the G-tetrad core: formation of a G-triad·water complex and implication for small-molecule binding. *Nucleic Acids Res.* 2016, *44*, 910–916.

[33] Lim, K.W. and Phan, A.T., Structural basis of DNA quadruplex-duplex junction formation. *Angew. Chem. Int. Ed.* 2013, *52*, 8566–8569.

[34] Chung, W.J., Heddi, B., Schmitt, E., Lim, K.W., Mechulam, Y., and Phan, A.T., Structure of a left-handed DNA G-quadruplex. *Proc. Natl. Acad. Sci. USA* 2015, *112*, 2729–2733.

[35] Hazel, P., Huppert, J., Balasubramanian, S., and Neidle, S., Loop-length-dependent folding of G-quadruplexes. *J. Am. Chem. Soc.* 2004, *126*, 16405–16415.

[36] Guédin, A., Alberti, P., and Mergny, J.L., Stability of intramolecular quadruplexes: sequence effects in the central loop. *Nucleic Acids Res.* 2009, *37*, 5559–5567.

[37] Guédin, A., Gros, J., Alberti, P., and Mergny, J.L., How long is too long? Effects of loop size on G-quadruplex stability. *Nucleic Acids Res.* 2010, *38*, 7858–7868.

[38] Wang, Y. and Patel, D.J., Solution structure of the human telomeric repeat d [$AG_3(T_2$ $AG_3)_3$] G-tetraplex. *Structure* 1993, *1*, 263–282.

[39] Parkinson, G.N., Lee, M.P.H., and Neidle, S., Crystal structure of parallel quadruplexes from human telomeric DNA. *Nature* 2002, *417*, 876–880.

[40] Luu, K.N., Phan, A.T., Kuryavyi, V., Lacroix, L., and Patel, D.J., Structure of the human telomere in K^+ solution: an intramolecular (3 + 1) G-quadruplex scaffold. *J. Am. Chem. Soc.* 2006, *128*, 9963–9970.

[41] Mendoza, O., Porrini, M., Salgado, G.F., Gabelica, V., and Mergny, J.L., Orienting tetramolecular G-quadruplex formation: the quest for the elusive RNA antiparallel quadruplex. *Chem. Eur. J.* 2015, *21*, 6732–6739.

[42] Bonnat, L., Dejeu, J., Bonnet, H., Génnaro, B., Jarjayes, O., Thomas, F., Lavergne, T., and Defrancq, E., Templated formation of discrete RNA and DNA:RNA hybrid G-quadruplexes and their interactions with targeting ligands. *Chem. Eur. J.* 2016, *22*, 3139–3147.

[43] Matsugami, A., Xu, Y., Noguchi, Y., Sugiyama, H., and Katahira, M., Structure of a human telomeric DNA sequence stabilized by 8-bromoguanosine substitutions, as determined by NMR in a K^+ solution. *FEBS J.* 2007, *274*, 3545–3556.

[44] Marušič, M., Veedu, R.N., Wengel, J., and Plavec, J., G-rich VEGF aptamer with locked and unlocked nucleic acid modifications exhibits a unique G-quadruplex fold. *Nucleic Acids Res.* 2013, *41*, 9524–9536.

[45] Saccà, B., Lacroix, L., and Mergny, J.L., The effect of chemical modifications on the thermal stability of different G-quadruplex-forming oligonucleotides. *Nucleic Acids Res.* 2005, *33*, 1182–1192.

[46] Li, C., Zhu, L., Zhu, Z., Fu, H., Jenkins, G., Wang, C., Zou, Y., Lu, X., and Yang, C.J., Backbone modification promotes peroxidase activity of G-quadruplex-based DNAzyme. *Chem. Commun.* 2012, *48*, 8347–8349.

[47] Esposito, V., Virgilio, A., Randazzo, A., Galeone, A., and Mayol, L., A new class of DNA quadruplexes formed by oligodeoxyribonucleotides containing a 3′-3′ or 5′-5′ inversion of polarity site. *Chem. Commun.* 2005, 3953–3955.

[48] Datta, B., Schmitt, C., and Armitage, B.A., Formation of a $PNA_2{-}DNA_2$ hybrid quadruplex. *J. Am. Chem. Soc.* 2003, *125*, 4111–4118.

[49] Esposito, V., Randazzo, A., Piccialli, G., Petraccone, L., Giancola, C., and Mayol, L., Effects of an 8-bromodeoxyguanosine incorporation on the parallel quadruplex structure $[d(TGGGT)]_4$. *Org. Biomol. Chem.* 2004, *2*, 313–318.

[50] Virgilio, A., Esposito, V., Randazzo, A., Mayol, L., and Galeone, A., 8-Methyl-2'-deoxyguanosine incorporation into parallel DNA quadruplex structures. *Nucleic Acids Res.* 2005, *33*, 6188–6195.

[51] Szalai, V.A., Singer, M.J., and Thorp, H.H., Site-specific probing of oxidative reactivity and telomerase function using 7,8-dihydro-8-oxoguanine in telomeric DNA. *J. Am. Chem. Soc.* 2002, *124*, 1625–1631.

[52] Sproviero, M., Fadock, K.L., Witham, A.A., and Manderville, R.A., Positional impact of fluorescently modified G-tetrads within polymorphic human telomeric G-quadruplex structures. *ACS Chem. Biol.* 2015, *10*, 1311–1318.

[53] Dias, E., Battiste, J.L., and Williamson, J.R., Chemical probe for glycosidic conformation in telomeric DNAs. *J. Am. Chem. Soc.* 1994, *116*, 4479–4480.

[54] Smith, F.W. and Feigon, J., Strand orientation in the DNA quadruplex formed from the Oxytricha telomere repeat oligonucleotide d($G_4T_4G_4$) in solution. *Biochemistry* 1993, *32*, 8682–8692.

[55] Pasternak, A., Hernandez, F.J., Rasmussen, L.M., Vester, B., and Wengel, J., Improved thrombin binding aptamer by incorporation of a single unlocked nucleic acid monomer. *Nucleic Acids Res.* 2011, *39*, 1155–1164.

[56] Kolganova, N.A., Varizhuk, A.M., Novikov, R.A., Florentiev, V.L., Pozmogova, G.E., Borisova, O.F., Shchyolkina, A.K., Smirnov, I.P., Kaluzhny, D.N., and Timofeev, E.N., Anomeric DNA quadruplexes: modified thrombin aptamers. *Artif. DNA PNA XNA* 2014, *5*, e28422.

[57] Tran, P.L.T., Moriyama, R., Maruyama, A., Rayner, B., and Mergny, J.L., A mirror-image tetramolecular DNA quadruplex. *Chem. Commun.* 2011, *47*, 5437–5439.

[58] Peng, C.G. and Damha, M.J., G-quadruplex induced stabilization by 2'-deoxy-2'-fluoro-D-arabinonucleic acids (2'F-ANA). *Nucleic Acids Res.* 2007, *35*, 4977–4988.

[59] Lech, C.J., Li, Z., Heddi, B., and Phan, A.T., 2′-F-ANA-guanosine and 2′-F-guanosine as powerful tools for structural manipulation of G-quadruplexes. *Chem. Commun.* 2012, *48*, 11425–11427.

[60] Martín-Pintado, N., Yahyaee-Anzahaee, M., Deleavey, G.F., Portella, G., Orozco, M., Damha, M.J., and González, C., Dramatic effect of furanose C2′ substitution on structure and stability: directing the folding of the human telomeric quadruplex with a single fluorine atom. *J. Am. Chem. Soc.* 2013, *135*, 5344–5347.

[61] Dominick, P.K. and Jarstfer, M.B., A conformationally constrained nucleotide analogue controls the folding topology of a DNA G-quadruplex. *J. Am. Chem. Soc.* 2004, *126*, 5050–5051.

[62] Tang, C.F. and Shafer, R.H., Engineering the quadruplex fold: nucleoside conformation determines both folding topology and molecularity in guanine quadruplexes. *J. Am. Chem. Soc.* 2006, *128*, 5966–5973.

[63] Li, Z., Lech, C.J., and Phan, A.T., Sugar-modified G-quadruplexes: effects of LNA-, 2'F-RNA- and 2'F-ANA-guanosine chemistries on G-quadruplex structure and stability. *Nucleic Acids Res.* 2014, *42*, 4068–4079.

[64] Saenger, W., *Principles of Nucleic Acid Structure*. Springer-Verlag, New York, NY, 1984.

[65] Marušič, M., Ŝket, P., Bauer, L., Viglasky, V., and Plavec, J., Solution-state structure of an intramolecular G-quadruplex with propeller, diagonal and edgewise loops. *Nucleic Acids Res.* 2012, *40*, 6946–6956.

[66] Lichter, R.L. and Roberts, J.D., Carbon-13 nuclear magnetic resonance spectroscopy. Solvent effects on chemical shifts. *J. Phys. Chem.* 1970, *74*, 912–916.

[67] Marques, M.P.M., Amorim da Costa, A.M., and Ribeiro-Claro, P.J.A., Evidence of C−H···O hydrogen bonds in liquid 4-ethoxybenzaldehyde by NMR and vibrational spectroscopies. *J. Phys. Chem. A* 2001, *105*, 5292–5297.

[68] Ambrus, A., Chen, D., Dai, J., Jones, R.A., and Yang, D., Solution structure of the biologically relevant G-quadruplex element in the human c-MYC promoter. implications for G-quadruplex stabilization. *Biochemistry* 2005, *44*, 2048–2058.

[69] Martadinata, H. and Phan, A.T., Structure of propeller-type parallel-stranded RNA G-quadruplexes, formed by human telomeric RNA sequences in K^+ solution. *J. Am. Chem. Soc.* 2009, *131*, 2570–2578.

[70] Collie, G.W., Haider, S.M., Neidle, S., and Parkinson, G.N., A crystallographic and modelling study of a human telomeric RNA (TERRA) quadruplex. *Nucleic Acids Res.* 2010, *38*, 5569–5580.

[71] Masiero, S., Trotta, R., Pieraccini, S., De Tito, S., Perone, R., Randazzo, A., and Spada, G.P., A non-empirical chromophoric interpretation of CD spectra of DNA G-quadruplex structures. *Org. Biomol. Chem.* 2010, *8*, 2683–2692.

[72] Greene, K.L., Wang, Y., and Live, D., Influence of the glycosidic torsion angle on ^{13}C and ^{15}N shifts in guanosine nucleotides: investigations of G-tetrad models with alternating syn and anti bases. *J. Biomol. NMR* 1995, *5*, 333–338.

[73] Fonville, J.M., Swart, M., Vokáčová, Z., Sychrovský, V., Šponer, J.E., Šponer, J., Hilbers, C.W., Bickelhaupt, F.M., and Wijmenga, S.S., Chemical shifts in nucleic acids studied by density functional theory calculations and comparison with experiment. *Chem. Eur. J.* 2012, *18*, 12372–12387.

[74] Marathias, V.M., Wang, K.Y., Kumar, S., Pham, T.Q., Swaminathan, S., and Bolton, P.H., Determination of the number and location of the manganese binding sites of DNA quadruplexes in solution by EPR and NMR in the presence and absence of thrombin. *J. Mol. Biol.* 1996, *260*, 378–394.

[75] Haider, S., Parkinson, G.N., and Neidle, S., Crystal structure of the potassium form of an Oxytricha nova G-quadruplex. *J. Mol. Biol.* 2002, *320*, 189–200.

[76] Hazel, P., Parkinson, G.N., and Neidle, S., Topology variation and loop structural homology in crystal and simulated structures of a bimolecular DNA quadruplex. *J. Am. Chem. Soc.* 2006, *128*, 5480–5487.

[77] Biffinger, J.C., Kim, H.W., and DiMagno, S.G., The polar hydrophobicity of fluorinated compounds. *ChemBioChem* 2004, *5*, 622–627.

[78] O'Hagan, D., Understanding organofluorine chemistry. An introduction to the C–F bond. *Chem. Soc. Rev.* 2008, *37*, 308–319.

Author Contributions

Article I **Sugar-Edge Interactions in a DNA-RNA G-Quadruplex: Evidence of Sequential C-H$\cdots$ Hydrogen Bonds Contributing to RNA Quadruplex Folding**
Dickerhoff, J., Appel, B., Müller, S., Weisz, K. *Angew. Chem. Int. Ed.* 2016, 55, 15162-15165; *Angew. Chem.* 2016, 128, 15386 – 15390.

KW initiated the project. JD designed and performed the experiments. SM and BA provided the DNA-RNA chimeras. KW performed the quantum-mechanical calculations. JD with the help of KW wrote the manuscript that was read and edited by all authors.

Article II **Flipping a G-Tetrad in a Unimolecular Quadruplex Without Affecting Its Global Fold**
Dickerhoff, J., Weisz, K. *Angew. Chem. Int. Ed.* 2015, 54, 5588–5591; *Angew. Chem.* 2015, 127, 5680 – 5683.

KW initiated the project. KW and JD designed and JD performed the experiments. KW with the help of JD wrote the manuscript.

Article III **Tracing Effects of Fluorine Substitutions on G-Quadruplex Conformational Transitions**
Dickerhoff, J., Haase, L., Langel, W., Weisz, K., *submitted.*

KW initiated the project. JD designed and with the help of LH performed the experiments. WL supported the structure calculations. JD with the help of KW wrote the manuscript that was read and edited by all authors.

Prof. Dr. Klaus Weisz

Jonathan Dickerhoff

Article I

G-Quadruplexes

International Edition: DOI: 10.1002/anie.201608275
German Edition: DOI: 10.1002/ange.201608275

Sugar–Edge Interactions in a DNA–RNA G-Quadruplex: Evidence of Sequential C–H···O Hydrogen Bonds Contributing to RNA Quadruplex Folding

*Jonathan Dickerhoff, Bettina Appel, Sabine Müller, and Klaus Weisz**

Abstract: *DNA G-quadruplexes were systematically modified by single riboguanosine (rG) substitutions at anti-dG positions. Circular dichroism and NMR experiments confirmed the conservation of the native quadruplex topology for most of the DNA–RNA hybrid structures. Changes in the C8 NMR chemical shift of guanosines following rG substitution at their 3′-side within the quadruplex core strongly suggest the presence of C8–H···O hydrogen-bonding interactions with the O2′ position of the C2′-endo ribonucleotide. A geometric analysis of reported high-resolution structures indicates that such interactions are a more general feature in RNA quadruplexes and may contribute to the observed preference for parallel topologies.*

G-rich DNA and RNA sequences are both able to form four-stranded structures (G4) with a central core of two to four stacked guanine tetrads that are held together by a cyclic array of Hoogsteen hydrogen bonds. G-quadruplexes exhibit considerable structural diversity depending on the number and relative orientation of individual strands as well as on the type and arrangement of connecting loops. However, whereas significant structural polymorphism has been reported and partially exploited for DNA,[1] variations in folding are strongly limited for RNA. Apparently, the additional 2′-hydroxy group in G4 RNA seems to restrict the topological landscape to almost exclusively yield structures with all four G-tracts in parallel orientation and with G nucleotides in *anti* conformation. Notable exceptions include the spinach aptamer, which features a rather unusual quadruplex fold embedded in a unique secondary structure.[2] Recent attempts to enforce antiparallel topologies through template-guided approaches failed, emphasizing the strong propensity for the formation of parallel RNA quadruplexes.[3] Generally, a C3′-*endo* (N) sugar puckering of purine nucleosides shifts the orientation about the glycosyl bond to *anti*.[4] Whereas free guanine ribonucleotide (rG) favors a C2′-*endo* (S) sugar pucker,[5] C3′-*endo* conformations are found in RNA and DNA–RNA chimeric duplexes with their specific water coordination.[6,7] This preference for N-type puckering has often been invoked as a factor contributing to the resistance of RNA to fold into alternative G4 structures with *syn* guanosines. However, rG nucleotides in RNA quadruplexes adopt both C3′-*endo* and C2′-*endo* conformations (see below). The 2′-OH substituent in RNA has additionally been advocated as a stabilizing factor in RNA quadruplexes through its participation in specific hydrogen-bonding networks and altered hydration effects within the grooves.[8] Taken together, the factors determining the exceptional preference for RNA quadruplexes with a parallel fold remain vague and are far from being fully understood.

The incorporation of ribonucleotide analogues at various positions of a DNA quadruplex has been exploited in the past to either assess their impact on global folding or to stabilize particular topologies.[9–12] Herein, single rG nucleotides favoring *anti* conformations were exclusively introduced at suitable dG positions of an all-DNA quadruplex to allow for a detailed characterization of the effects exerted by the additional 2′-hydroxy group. In the following, all seven *anti*-dG core residues of the ODN(0) sequence, previously shown to form an intramolecular (3+1) hybrid structure comprising all three main types of loops,[13] were successively replaced by their rG analogues (Figure 1 a).

To test for structural conservation, the resulting chimeric DNA–RNA species were initially characterized by recording their circular dichroism (CD) spectra and determining their thermal stability (see the Supporting Information, Figure S1). All modified sequences exhibited the same typical CD signature of a (3+1) hybrid structure with thermal stabilities close to that of native ODN(0) except for ODN(16) with rG incorporated at position 16. The latter was found to be significantly destabilized while its CD spectrum suggested that structural changes towards an antiparallel topology had occurred.

More detailed structural information was obtained in NMR experiments. The imino proton spectral region for all ODN quadruplexes is shown in Figure 2 a. Although only nucleotides in a matching *anti* conformation were used for the substitutions, the large numbers of imino resonances in ODN(16) and ODN(22) suggest significant polymorphism and precluded these two hybrids from further analysis. All other spectra closely resemble that of native ODN(0), indicating the presence of a major species with twelve imino resonances as expected for a quadruplex with three G-tetrads. Supported by the strong similarities to ODN(0) as a result of the conserved fold, most proton as well as C6/C8 carbon resonances could be assigned for the singly substituted hybrids through standard NMR methods, including homonuclear 2D NOE and ^{1}H–^{13}C HSQC analysis (see the Supporting Information).

[*] J. Dickerhoff, Dr. B. Appel, Prof. Dr. S. Müller, Prof. Dr. K. Weisz
Institut für Biochemie
Ernst-Moritz-Arndt-Universität Greifswald
Felix-Hausdorff-Strasse 4, 17487 Greifswald (Germany)
E-mail: weisz@uni-greifswald.de
Supporting information and the ORCID identification number(s) for the author(s) of this article can be found under: http://dx.doi.org/10.1002/anie.201608275.

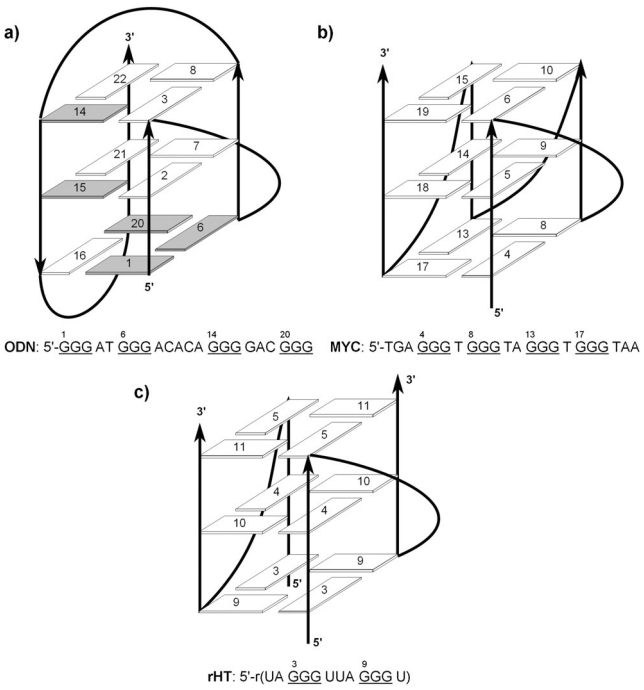

Figure 1. Sequence and topology of the a) ODN, b) MYC, and c) rHT quadruplexes. G nucleotides in *syn* and *anti* conformation are represented by dark and white rectangles, respectively.

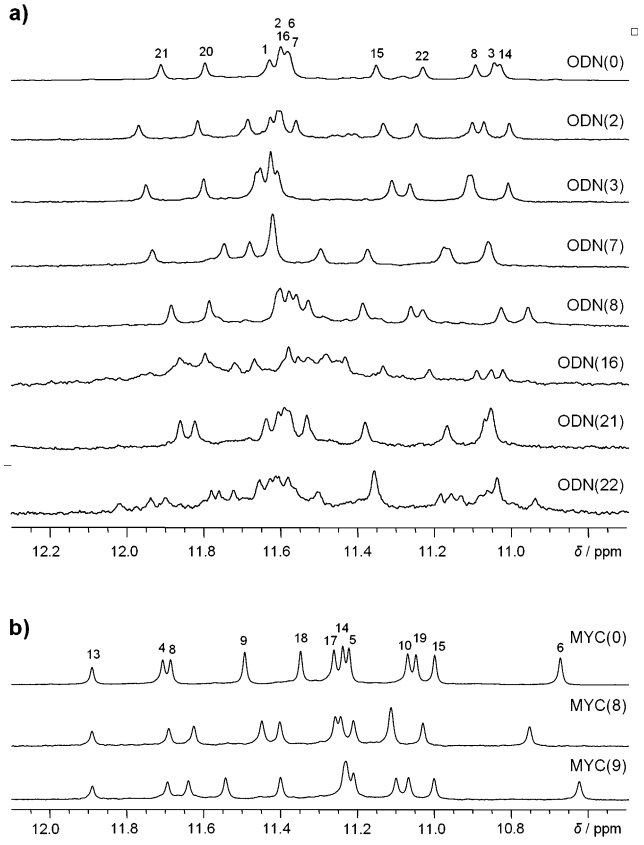

Figure 2. Imino proton spectral regions of the native and substituted quadruplexes for a) ODN at 25 °C and b) MYC at 40 °C in 10 mM potassium phosphate buffer, pH 7. Resonance assignments for the G-tract guanines are indicated for the native quadruplexes.

All 2′-deoxyguanosines in the native ODN(0) quadruplex were found to adopt an S-type conformation. For the modified quadruplexes, sugar puckering of the guanine ribonucleotides was assessed through endocyclic ^{1}H–^{1}H vicinal scalar couplings (Figure S4). The absence of any resolved H1′–H2′ scalar coupling interactions indicates an N-type C3′-*endo* conformation for the ribose sugar in ODN(8). In contrast, the scalar couplings $J(H1',H2') \geq 8$ Hz for the hybrids ODN(2), ODN(3), ODN(7), and ODN(21) are only compatible with pseudorotamers in the south domain.[14] Apparently, most of the incorporated ribonucleotides adopt the generally less favored S-type sugar conformation, matching the sugar puckering of the replaced 2′-deoxyribonucleotide.

Given the conserved structures for the five well-defined quadruplexes with single modifications, chemical-shift changes with respect to unmodified ODN(0) can directly be traced back to the incorporated ribonucleotide with its additional 2′-hydroxy group. A compilation of all imino, H1′, H6/H8, and C6/C8 ^{1}H and ^{13}C chemical shift changes upon rG substitution is shown in Figure S5. Aside from the anticipated differences for the rG modified residues and the more flexible diagonal loops, the largest effects involve the C8 resonances of guanines following a substitution site.

Distinct chemical-shift differences of the guanosine C8 resonance for the *syn* and *anti* conformations about the glycosidic bond have recently been used to confirm a G-tetrad flip in a 2′-fluoro-dG-modified quadruplex.[15] On the other hand, the C8 chemical shifts are hardly affected by smaller variations in the sugar conformation and the glycosidic torsion angle χ, especially in the *anti* region ($-180° < \chi < -120°$).[16] It is therefore striking that in the absence of larger structural rearrangements, significant C8 deshielding effects exceeding 1 ppm were observed exclusively for those guanines that follow the centrally located and S-puckered rG substitutions in ODN(2), ODN(7), and ODN(21) (Figure 3 a). Likewise, the corresponding H8 resonances experience downfield shifts, albeit to a smaller extent; these were particularly apparent for ODN(7) and ODN(21) with $\Delta\delta > 0.2$ ppm (Figure S5). It should be noted, however, that the H8 chemical shifts are more sensitive towards the particular sugar type, sugar pucker, and glycosidic torsion angle, making the interpretation of H8 chemical-shift data less straightforward.[16]

To test whether these chemical-shift effects are reproduced within a parallel G4 fold, the MYC(0) quadruplex derived from the promotor region of the c-MYC oncogene was also subjected to corresponding dG→rG substitutions (Figure 1 b).[17] Considering the pseudosymmetry of the parallel MYC(0) quadruplex, only positions 8 and 9 along one G-tract were subjected to single rG modifications. Again, the ^{1}H imino resonances as well as CD spectra confirmed the conservation of the native fold (Figures 2 b and S6). A sugar pucker analysis based on H1′–H2′ scalar couplings revealed N- and S-type pseudorotamers for rG in MYC(8) and MYC(9), respectively (Figure S7). Owing to the good spectral resolution, these different sugar conformational preferences were further substantiated by C3′ chemical-shift changes, which have been shown to strongly depend on the sugar

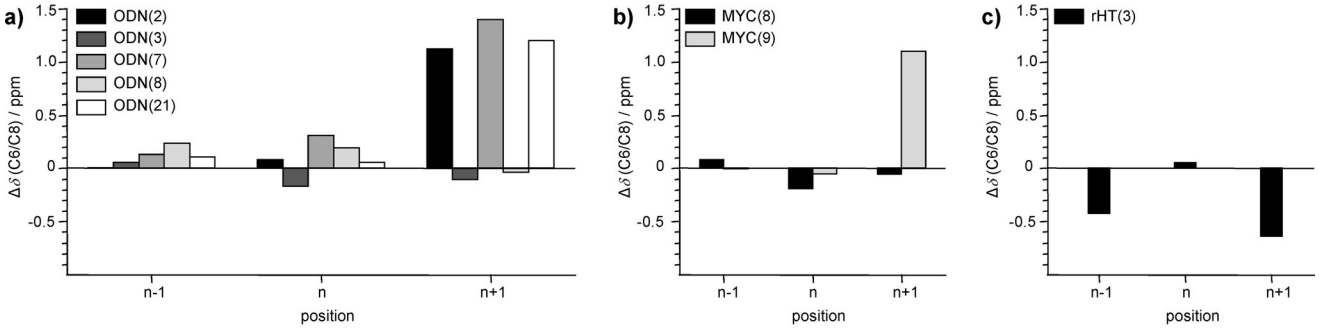

Figure 3. ^{13}C chemical-shift changes of C6/C8 in a) ODN, b) MYC, and c) rHT. The quadruplexes were modified with rG (ODN, MYC) or dG (rHT) at position *n* and referenced against the unmodified DNA or RNA G4.

pucker but not on the χ torsion angle.[16] The significant difference in the chemical shifts (> 4 ppm) of the C3′ resonances of rG8 and rG9 is in good agreement with previous DFT calculations on N- and S-type ribonucleotides (Figure S12). In addition, negligible C3′ chemical-shift changes for other residues as well as only subtle changes of the ^{31}P chemical shift next to the substitution site indicate that the rG substitution in MYC(9) does not exert significant impact on the conformation of neighboring sugars and the phosphodiester backbone (Figure S13).

In analogy to ODN, corresponding ^{13}C-deshielding effects were clearly apparent for C8 on the guanine following the S-puckered rG in MYC(9) but not for C8 on the guanine following the N-puckered rG in MYC(8) (Figure 3b). Whereas an S-type ribose sugar allows for close proximity between its 2′-OH group and the C8–H of the following base, the 2′-hydroxy group points away from the neighboring base for N-type sugars. Corresponding nuclei are even further apart in ODN(3) with rG preceding a propeller loop residue (Figure S14). Thus the recurring pattern of chemical-shift changes strongly suggests the presence of $O2'_{(n)}\cdots H{-}C8_{(n+1)}$ interactions at appropriate steps along the G-tracts in line with the ^{13}C deshielding effects reported for aliphatic as well as aromatic carbon donors in C–H···O hydrogen bonds.[18] Additional support for such interresidual hydrogen bonds comes from comprehensive quantum-chemical calculations on a dinucleotide fragment from the ODN quadruplex, which confirmed the corresponding chemical-shift changes (see the Supporting Information). As these hydrogen bonds are expected to be associated with an, albeit small, increase in the one-bond ^{13}C–^{1}H scalar coupling,[18] we also measured the ^{1}J(C8,H8) values in MYC(9). Indeed, when compared to parent MYC(0), it is only the C8–H8 coupling of nucleotide G10 that experiences an increase by nearly 3 Hz upon rG9 incorporation (Figure 4). Likewise, a comparable increase in ^{1}J(C8,H8) could also be detected in ODN(2) (Figure S15).

We then wondered whether such interactions could be a more general feature of RNA G4. To search for putative CHO hydrogen bonds in RNA quadruplexes, several NMR and X-ray structures from the Protein Data Bank were subjected to a more detailed analysis. Only sequences with uninterrupted G-tracts and NMR structures with restrained sugar puckers were considered.[8,19–24] CHO interactions were identified based on a generally accepted H···O distance cutoff

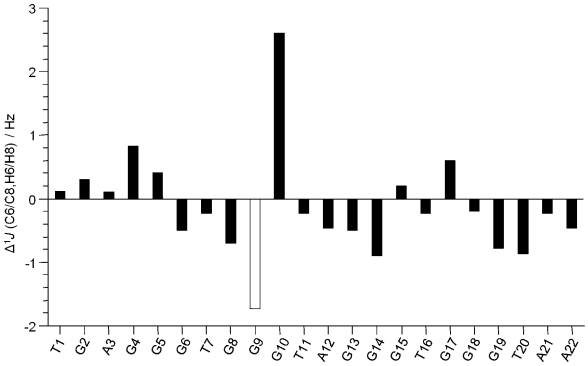

Figure 4. Changes in the C6/C8–H6/H8 ^{1}J scalar coupling in MYC(9) referenced against MYC(0). The white bar denotes the rG substitution site; experimental uncertainty ± 0.7 Hz.

< 3 Å and a CH···O angle between 110–180°.[25] In fact, based on the above-mentioned geometric criteria, sequential Hoogsteen side-to-sugar-edge C8–H···O2′ interactions seem to be a recurrent motif in RNA quadruplexes but are always associated with a hydrogen-bond sugar acceptor in S-configuration, that is, from C2′-*endo* to C3′-*exo* (Table S1). Except for a tetramolecular structure where crystallization often leads to a particular octaplex formation,[23] these geometries allow for a corresponding hydrogen bond in each or every second G-tract.

The formation of CHO hydrogen bonds within an all-RNA quadruplex was additionally probed through an inverse rG→dG substitution of an appropriate S-puckered residue. For this experiment, a bimolecular human telomeric RNA sequence (rHT) was employed whose G4 structure had previously been solved through both NMR and X-ray crystallographic analyses, which yielded similar results (Figure 1c).[8,22] Both structures exhibit an S-puckered G3 residue with a geometric arrangement that allows for a C8–H···O2′ hydrogen bond (Figure 5). Indeed, as expected for the loss of the proposed CHO contact, a significant shielding of G4 C8 was experimentally observed in the dG-modified rHT(3) (Figure 3c). The smaller reverse effect in the RNA quadruplex can be attributed to differences in the hydration pattern and conformational flexibility. A noticeable shielding effect was also observed at the (*n*−1) adenine residue, likely

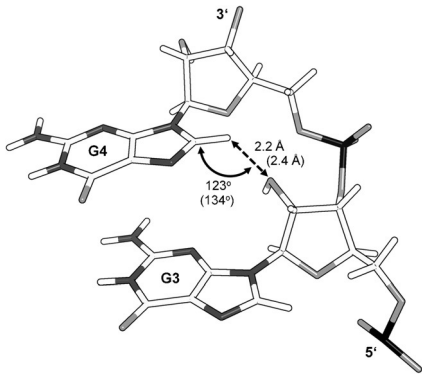

Figure 5. Proposed C–H···O base–sugar hydrogen-bonding interaction between G3 and G4 in the rHT solution structure.[22] Values in parentheses were obtained from the corresponding crystal structure.[8]

reflecting some orientational adjustments of the adjacent overhang upon dG incorporation.

Although CHO hydrogen bonds have been widely accepted as relevant contributors to biomolecular structures, proving their existence in solution has been difficult owing to their small effects and the lack of appropriate reference compounds. The singly substituted quadruplexes offer a unique possibility to detect otherwise unnoticed changes induced by a ribonucleotide and strongly suggest the formation of sequential CHO base–sugar hydrogen bonds in the DNA–RNA chimeric quadruplexes. The dissociation energies of hydrogen bonds with C–H donor groups amount to 0.4–4 kcal mol^{-1} [26] but may synergistically add to exert noticeable stabilizing effects as also seen for i-motifs. In these alternative four-stranded nucleic acids, weak sugar–sugar hydrogen bonds add to impart significant structural stability.[27] Given the requirement of an *anti* glycosidic torsion angle for the 3′-neighboring hydrogen-donating nucleotide, C8–H···O2′ interactions may thus contribute in driving RNA folding towards parallel all-*anti* G4 topologies.

Keywords: DNA–RNA hybrids · G-quadruplexes · hydrogen bonds · NMR spectroscopy

How to cite: *Angew. Chem. Int. Ed.* **2016**, *55*, 15162–15165
Angew. Chem. **2016**, *128*, 15386–15390

[1] a) S. Burge, G. N. Parkinson, P. Hazel, A. K. Todd, S. Neidle, *Nucleic Acids Res.* **2006**, *34*, 5402–5415; b) M. Webba da Silva, *Chem. Eur. J.* **2007**, *13*, 9738–9745.
[2] H. Huang, N. B. Suslov, N.-S. Li, S. A. Shelke, M. E. Evans, Y. Koldobskaya, P. A. Rice, J. A. Piccirilli, *Nat. Chem. Biol.* **2014**, *10*, 686–691.
[3] a) O. Mendoza, M. Porrini, G. F. Salgado, V. Gabelica, J.-L. Mergny, *Chem. Eur. J.* **2015**, *21*, 6732–6739; b) L. Bonnat, J. Dejeu, H. Bonnet, B. Génnaro, O. Jarjayes, F. Thomas, T. Lavergne, E. Defrancq, *Chem. Eur. J.* **2016**, *22*, 3139–3147.
[4] W. Saenger, *Principles of Nucleic Acid Structure*, Springer, New York, **1984**, Chapter 4.
[5] J. Plavec, C. Thibaudeau, J. Chattopadhyaya, *Pure Appl. Chem.* **1996**, *68*, 2137–2144.
[6] a) C. Ban, B. Ramakrishnan, M. Sundaralingam, *J. Mol. Biol.* **1994**, *236*, 275–285; b) E. F. DeRose, L. Perera, M. S. Murray, T. A. Kunkel, R. E. London, *Biochemistry* **2012**, *51*, 2407–2416.
[7] S. Barbe, M. Le Bret, *J. Phys. Chem. A* **2008**, *112*, 989–999.
[8] G. W. Collie, S. M. Haider, S. Neidle, G. N. Parkinson, *Nucleic Acids Res.* **2010**, *38*, 5569–5580.
[9] C.-F. Tang, R. H. Shafer, *J. Am. Chem. Soc.* **2006**, *128*, 5966–5973.
[10] J. Qi, R. H. Shafer, *Biochemistry* **2007**, *46*, 7599–7606.
[11] B. Saccà, L. Lacroix, J.-L. Mergny, *Nucleic Acids Res.* **2005**, *33*, 1182–1192.
[12] N. Martín-Pintado, M. Yahyaee-Anzahaee, G. F. Deleavey, G. Portella, M. Orozco, M. J. Damha, C. González, *J. Am. Chem. Soc.* **2013**, *135*, 5344–5347.
[13] M. Marušič, P. Šket, L. Bauer, V. Viglasky, J. Plavec, *Nucleic Acids Res.* **2012**, *40*, 6946–6956.
[14] F. A. A. M. De Leeuw, C. Altona, *J. Chem. Soc. Perkin Trans. 2* **1982**, 375–384.
[15] J. Dickerhoff, K. Weisz, *Angew. Chem. Int. Ed.* **2015**, *54*, 5588–5591; *Angew. Chem.* **2015**, *127*, 5680–5683.
[16] J. M. Fonville, M. Swart, Z. Vokáčová, V. Sychrovský, J. E. Šponer, J. Šponer, C. W. Hilbers, F. M. Bickelhaupt, S. S. Wijmenga, *Chem. Eur. J.* **2012**, *18*, 12372–12387.
[17] A. Ambrus, D. Chen, J. Dai, R. A. Jones, D. Yang, *Biochemistry* **2005**, *44*, 2048–2058.
[18] a) R. L. Lichter, J. D. Roberts, *J. Phys. Chem.* **1970**, *74*, 912–916; b) M. P. M. Marques, A. M. Amorim da Costa, P. J. A. Ribeiro-Claro, *J. Phys. Chem. A* **2001**, *105*, 5292–5297; c) M. Sigalov, A. Vashchenko, V. Khodorkovsky, *J. Org. Chem.* **2005**, *70*, 92–100.
[19] C. Cheong, P. B. Moore, *Biochemistry* **1992**, *31*, 8406–8414.
[20] H. Liu, A. Matsugami, M. Katahira, S. Uesugi, *J. Mol. Biol.* **2002**, *322*, 955–970.
[21] T. Mashima, A. Matsugami, F. Nishikawa, S. Nishikawa, M. Katahira, *Nucleic Acids Res.* **2009**, *37*, 6249–6258.
[22] H. Martadinata, A. T. Phan, *J. Am. Chem. Soc.* **2009**, *131*, 2570–2578.
[23] M. C. Chen, P. Murat, K. Abecassis, A. R. Ferré-D'Amaré, S. Balasubramanian, *Nucleic Acids Res.* **2015**, *43*, 2223–2231.
[24] J. Deng, Y. Xiong, M. Sundaralingam, *Proc. Natl. Acad. Sci. USA* **2001**, *98*, 13665–13670.
[25] a) G. R. Desiraju, *Acc. Chem. Res.* **1996**, *29*, 441–449; b) M. Brandl, K. Lindauer, M. Meyer, J. Sühnel, *Theor. Chem. Acc.* **1999**, *101*, 103–113.
[26] T. Steiner, *Angew. Chem. Int. Ed.* **2002**, *41*, 48–76; *Angew. Chem.* **2002**, *114*, 50–80.
[27] I. Berger, M. Egli, A. Rich, *Proc. Natl. Acad. Sci. USA* **1996**, *93*, 12116–12121.

Received: August 24, 2016
Revised: September 29, 2016
Published online: November 7, 2016

Angewandte Chemie
Eine Zeitschrift der Gesellschaft Deutscher Chemiker

Supporting Information

Sugar–Edge Interactions in a DNA–RNA G-Quadruplex: Evidence of Sequential C–H···O Hydrogen Bonds Contributing to RNA Quadruplex Folding

*Jonathan Dickerhoff, Bettina Appel, Sabine Müller, and Klaus Weisz**

anie_201608275_sm_miscellaneous_information.pdf

Table of Contents

Materials and methods

Materials. Unmodified DNA oligonucleotides were purchased from *TIB MOLBIOL* (Berlin, Germany). Ribonucleotide-modified oligomers were chemically synthesized on a ABI 392 Nucleic Acid Synthesizer using standard DNA phosphoramidite building blocks, a 2'-*O*-*tert*-butyldimethylsilyl (TBDMS) protected guanosine phosphoramidite and CPG 1000 Å (ChemGenes) as support. A mixed cycle under standard conditions was used according to the general protocol: detritylation with dichloroacetic acid/1,2-dichloroethane (3/97) for 58 s, coupling with phosphoramidites (0.1 M in acetonitrile) and benzylmercaptotetrazole (0.3 M in acetonitrile) with a coupling time of 2 min for deoxy- and 8 min for ribonucleoside phosphoramidites, capping with Cap A THF/acetic anhydride/2,6-lutidine (80/10/10) and Cap B THF/1-methylimidazole (84/16) for 29 s and oxidation with iodine (0.02 M) in THF/pyridine/H_2O (98.6/0.4/10) for 60 s. Phosphoramidite and activation solutions were dried over molecular sieves (4 Å). All syntheses were carried out in the 'trityl-off' mode. Deprotection and purification of the oligomers was carried out as described in detail previously.[1] After purification on a 15% denaturing polyacrylamide gel, bands of product were cut from the gel, and rG-modified oligomers were eluted (0.3 M NaOAc, pH 7.1) followed by ethanol precipitation. The concentrations were determined spectrophotometrically by measuring the absorbance at 260 nm. Samples were obtained by dissolving the corresponding oligonucleotides in a low salt buffer with 10 mM potassium phosphate, pH 7.0, for NMR experiments or in a high salt buffer with 20 mM potassium phosphate, 100 mM KCl, pH 7.0, for UV and CD experiments. Prior to measurements, the samples were annealed by heating to 90 ^{o}C followed by slow cooling to room temperature. Final concentrations of oligonucleotides were 5 μM for the UV and CD experiments and between 0.12 and 0.46 mM for the NMR measurements.

UV melting experiments. UV experiments were performed on a *Cary 100* spectrophotometer equipped with a Peltier temperature control unit (*Varian* Deutschland, Darmstadt). The melting curves were recorded by measuring the absorption of the solution at 295 nm with 2 data points/^{o}C in 10 mm quartz cuvettes. Heating and cooling rates of 0.2 °C/min were employed. Melting temperatures were determined by the intersection of the melting curve and the median of the fitted baselines.

Circular dichroism. CD spectra were acquired with a Jasco J-810 spectropolarimeter at 20 ^{o}C (*Jasco*, Tokyo, Japan). The spectra were recorded with a bandwidth of 1 nm, a scanning speed of 50 nm/min and 10 accumulations. All spectra were blank corrected.

NMR experiments. All NMR spectra were acquired on a Bruker Avance 600 MHz spectrometer equipped with an inverse $^{1}H/^{13}C/^{15}N/^{31}P$ quadruple resonance cryoprobehead and z-field gradients. Data were processed using Topspin 3.1 and analyzed with CcpNmr Analysis.[2] Proton chemical shifts were referenced relative to TSP by setting the H_2O signal in 90% H_2O/10% D_2O to δ_H = 4.78 ppm at 25 °C. For the one- and two-dimensional homonuclear measurements in 90% H_2O/10% D_2O a WATERGATE with w5 element was employed for solvent suppression. Typically, 4K × 900 data points with 32 transients per t_1 increment and a recycle delay of 2 s were collected in t_2 and t_1. Prior to Fourier transformation data were zero-filled to give a 4K × 2K matrix and both dimensions were apodized by squared sine bell window functions. In general, phase-sensitive ^{1}H-^{13}C HSQC experiments optimized for a ^{1}J(C,H) of 170 Hz were acquired with a 3-9-19 solvent suppression scheme in 90% H_2O/10% D_2O employing a spectral width of 7.5 kHz in the indirect ^{13}C dimension, 64 scans at each of 540 t_1 increments and a relaxation delay of 1.5 s between scans. The resolution in t_2 was increased to 8K for the determination of ^{1}J(C6,H6) and ^{1}J(C8,H8). For the analysis of the H3'-C3' spectral region, the DNA was dissolved in D_2O and experiments optimized for a ^{1}J(C,H) of 150 Hz. ^{13}C chemical shifts were referenced relative to TMS by using the indirect referencing method. Phase-sensitive ^{1}H-^{31}P HETCOR experiments adjusted for a ^{1}J(P,H) of 10 Hz were acquired in D_2O employing a spectral width of 730 Hz in the indirect ^{31}P dimension and 512 t_1 increments.

Quantum chemical calculations. Molecular geometries of G-G and rG-G dinucleotides were subjected to a constrained optimization at the HF/6-31G* level of calculation using the Spartan08 program package. DFT calculations of NMR chemical shifts for the optimized structures were subsequently performed with the B3LYP/6-31G** level of density functional theory.

[1] B. Appel, T. Marschall, A. Strahl, S. Müller in *Ribozymes* (Ed.: J. Hartig), Wiley-VCH, Weinheim, Germany, **2012**, pp. 41-49.

[2] W. F. Vranken, W. Boucher, T. J. Stevens, R. H. Fogh, A. Pajon, M. Llinas, E. L. Ulrich, J. L. Markley, J. Ionides, E. D. Laue, *Proteins: Structure, Function, and Bioinformatics* **2005**, *59*, 687–696.

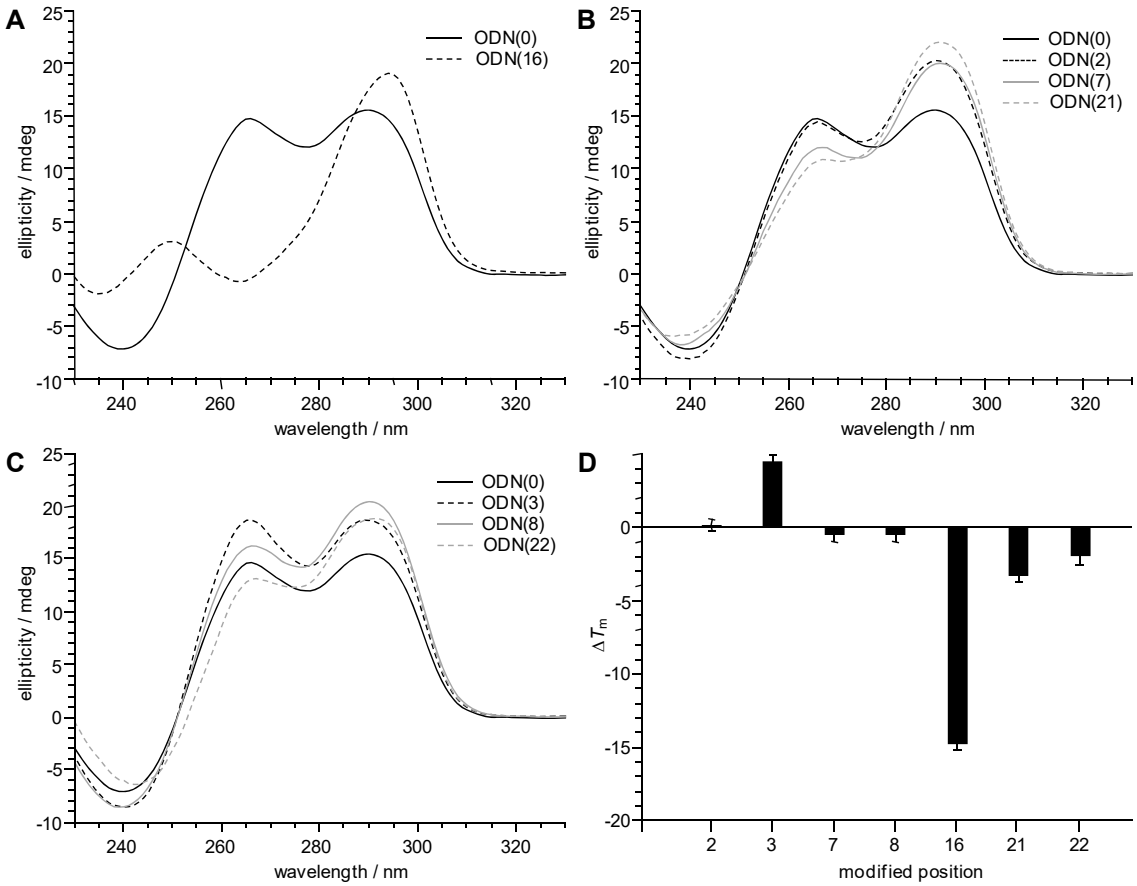

Figure S1. CD spectra of ODN rG-modified in the 5'-tetrad (A), the central tetrad (B), and the 3'-tetrad (C). (D) Changes in melting temperature upon rG substitutions.

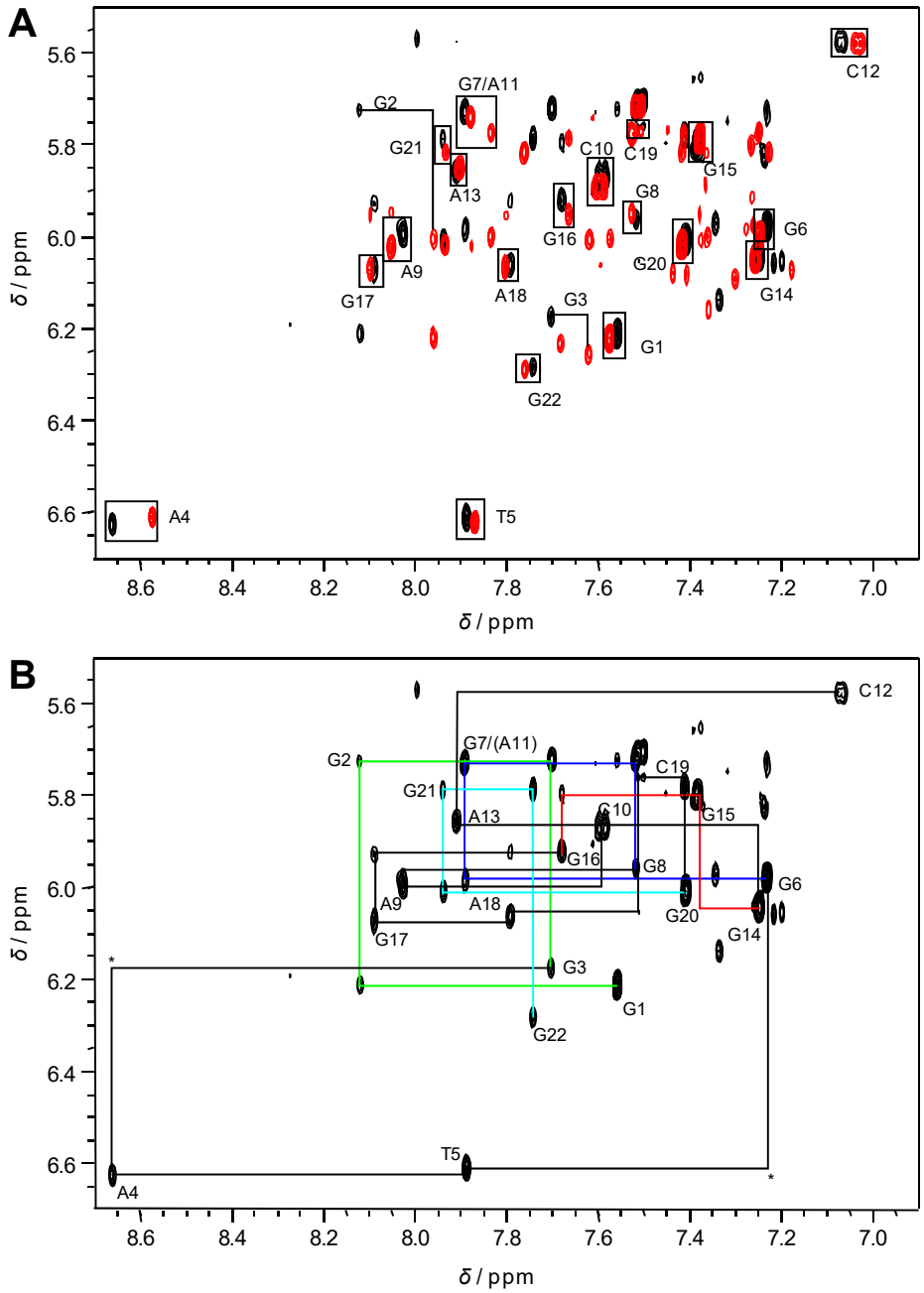

Figure S2. (A) Superposition of the H6/H8–H1' 2D NOE spectral region of ODN(0) (red) and ODN(2) (black). (B) Sequential H6/H8–H1' NOE walks for ODN(2) traced by solid lines. Due to signal overlap for residues G7 and A11 connectivities involving the latter were omitted. NOEs along the four G-tracts are shown in green, blue, red, and cyan; non-observable NOE contacts are marked by asterisks; T = 25 °C, τ_m = 300 ms.

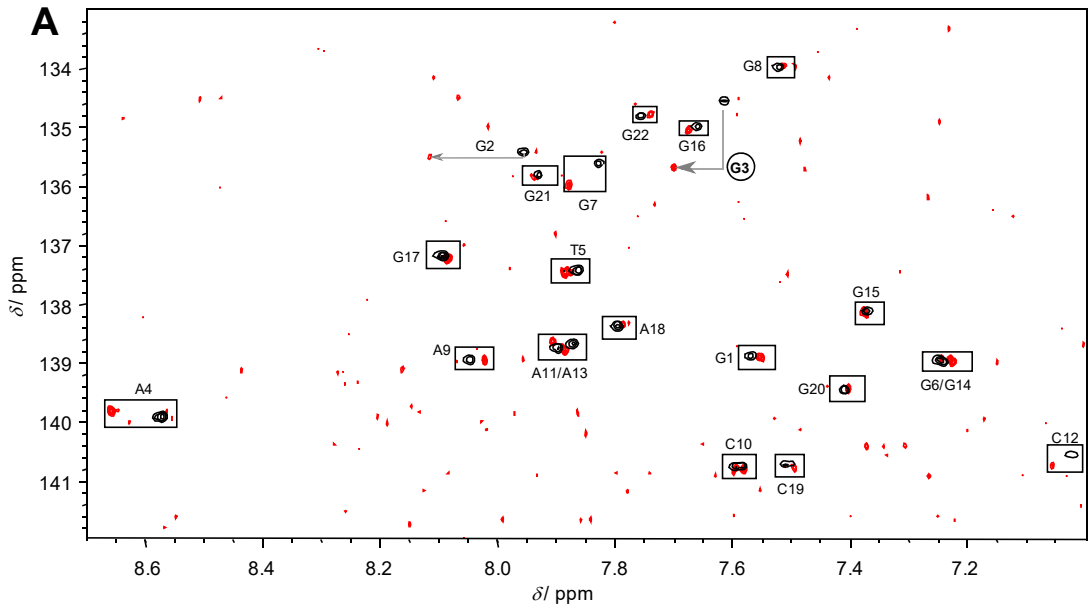
A
δ/ ppm
δ/ ppm
G8
G22
G16
G3
G2
G21
G7
G17
T5
G15
A18
A9
A11/A13
G1
G6/G14
G20
A4
C10
C19
C12

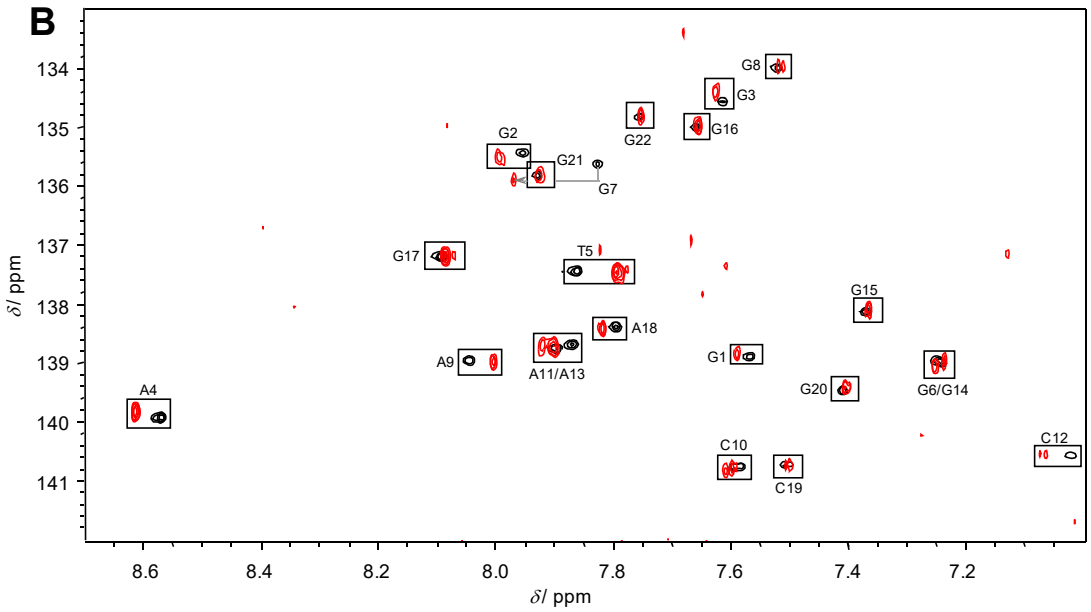
B
δ/ ppm
δ/ ppm
G8
G3
G22
G16
G2
G21
G7
G17
T5
G15
A18
A9
A11/A13
G1
G6/G14
G20
A4
C10
C19
C12

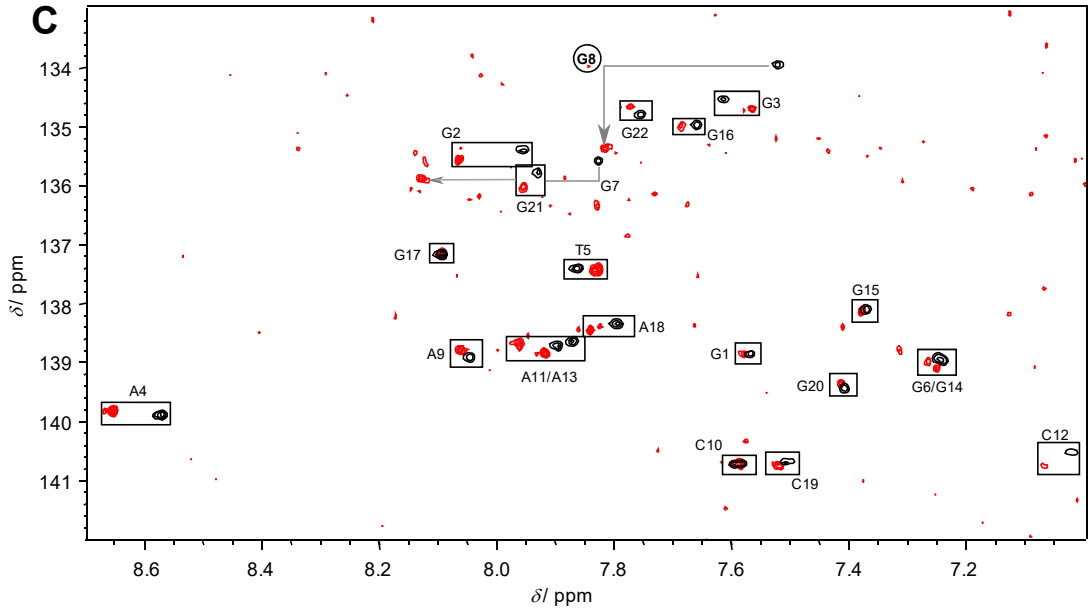
C
δ/ ppm
δ/ ppm
G8
G3
G22
G16
G2
G7
G21
G17
T5
G15
A18
A9
A11/A13
G1
G6/G14
G20
A4
C10
C19
C12

Figure continued

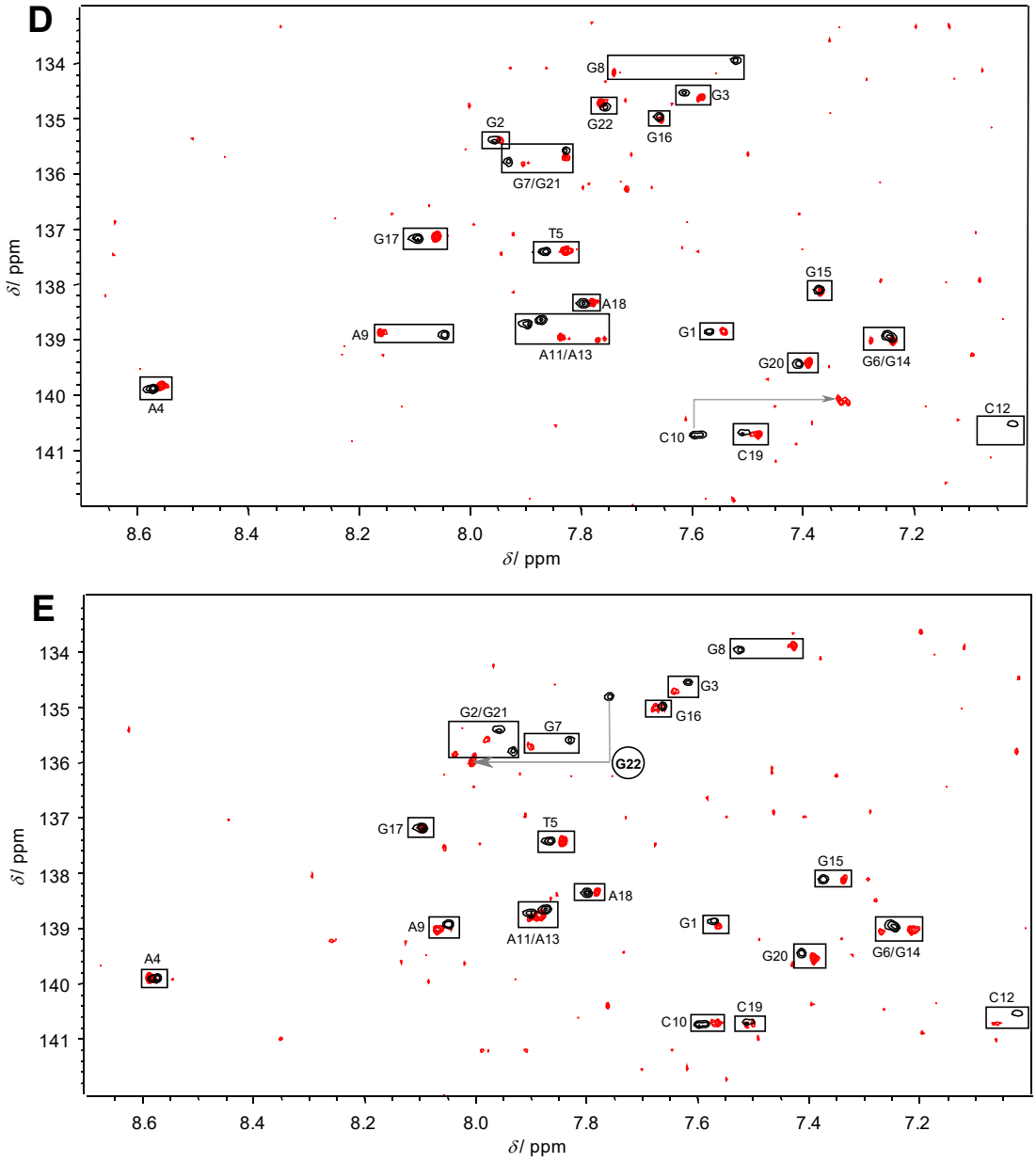

Figure S3. H6/H8–C6/C8 spectral region of ^{1}H-^{13}C HSQC spectra acquired at 25 °C. Spectrum of unmodified ODN(0) (black) is superimposed with ribose-modified (red) ODN(2) (A), ODN(3) (B), ODN7 (C), ODN(8) (D), and ODN(21) (E). Corresponding crosspeaks for the native and substituted quadruplex are combined within rectangular boxes or connected by horizontal and vertical lines; large chemical shift changes in both the ^{13}C and ^{1}H dimension as observed for guanine bases at the 3'-neighboring position of incorporated rG are highlighted.

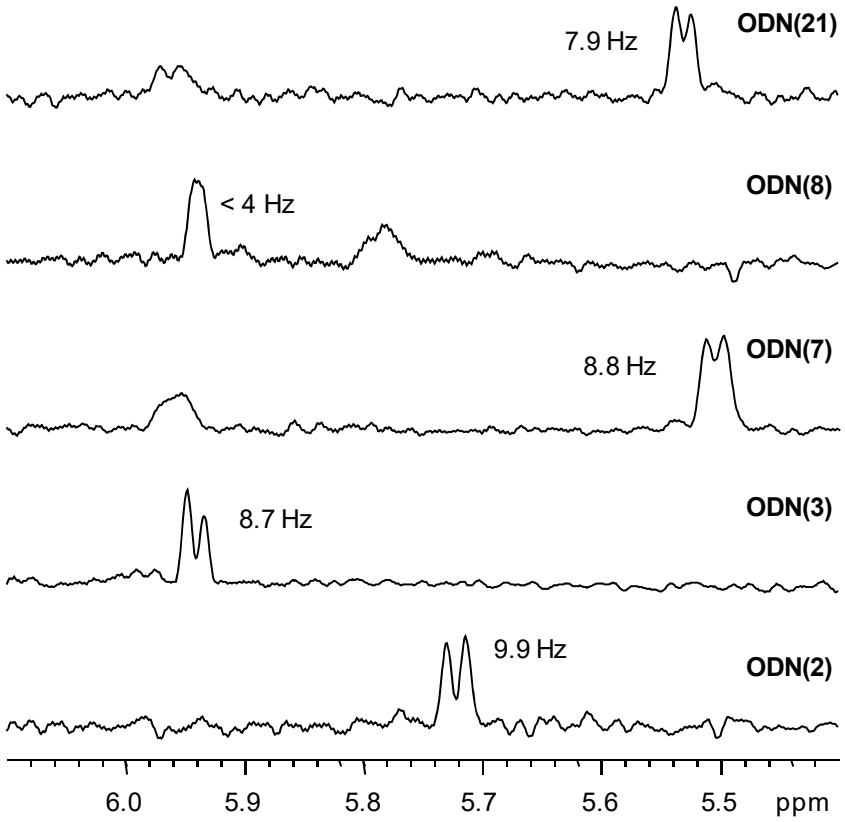

Figure S4. Rows of 2D NOE spectra at $\omega_1=\delta$(H2') showing the anomeric ribose H1' resonance for ODN(2), ODN(3), ODN(7), ODN(8), and ODN(21). Vicinal scalar couplings in the ribose sugar J(H1',H2') were determined by peak fitting routines; the digital resolution is 0.6 Hz/point.

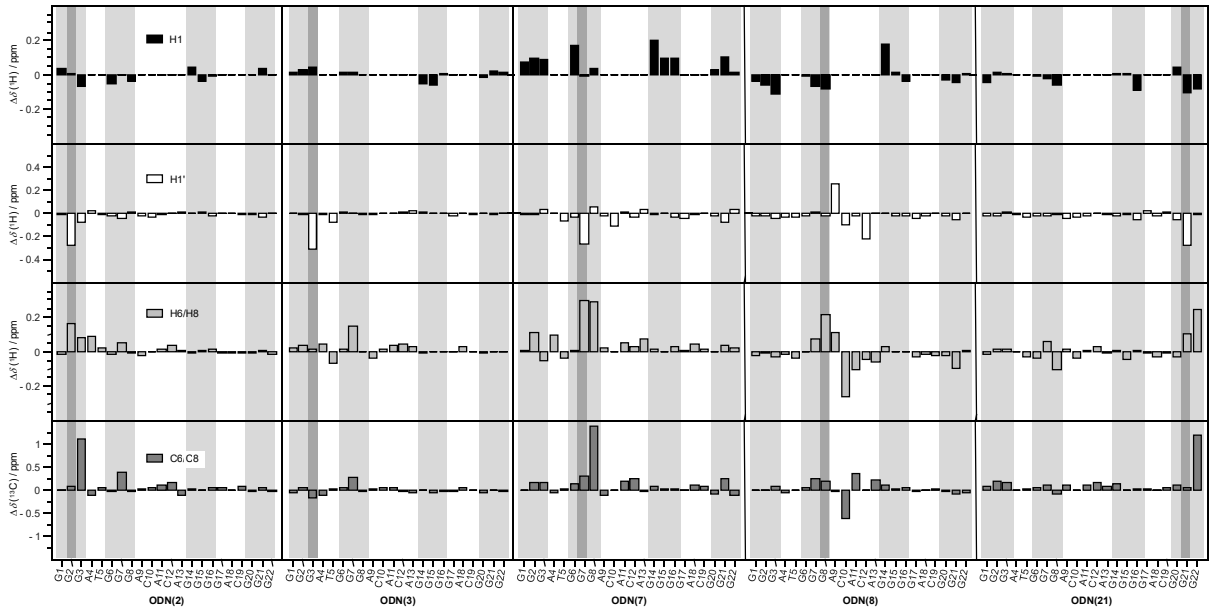

Figure S5. Chemical shift changes of H1, H1', H6/H8, and C6/C8 in rG-substituted ODN referenced against ODN(0); vertical traces in dark and light gray denote rG substitution sites and G-tracts of the quadruplex core, respectively.

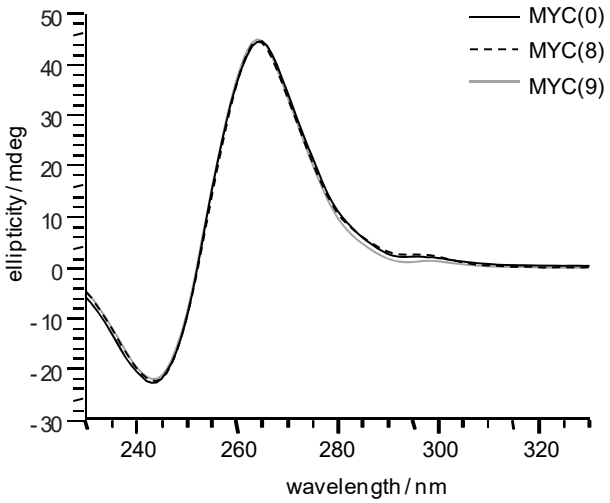

Figure S6. CD spectra of MYC(0) and rG-modified MYC(8) and MYC(9).

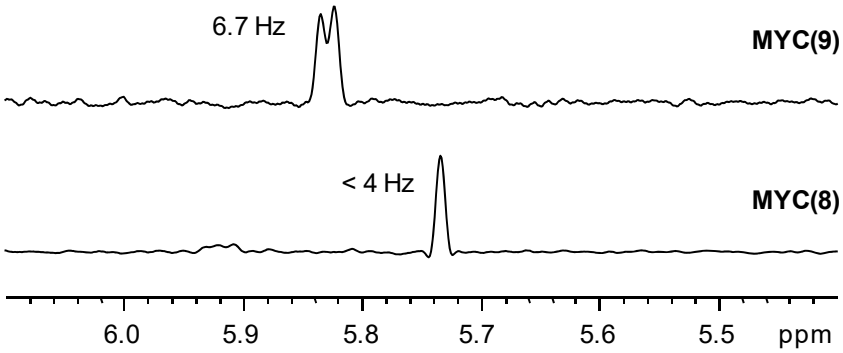

Figure S7. Rows of 2D NOE spectra at $\omega_1=\delta$(H2') showing the anomeric ribose H1' resonance for MYC(8) and MYC(9). Vicinal scalar couplings in the ribose sugar J(H1',H2') were determined by peak fitting routines; the digital resolution is 0.6 Hz/point.

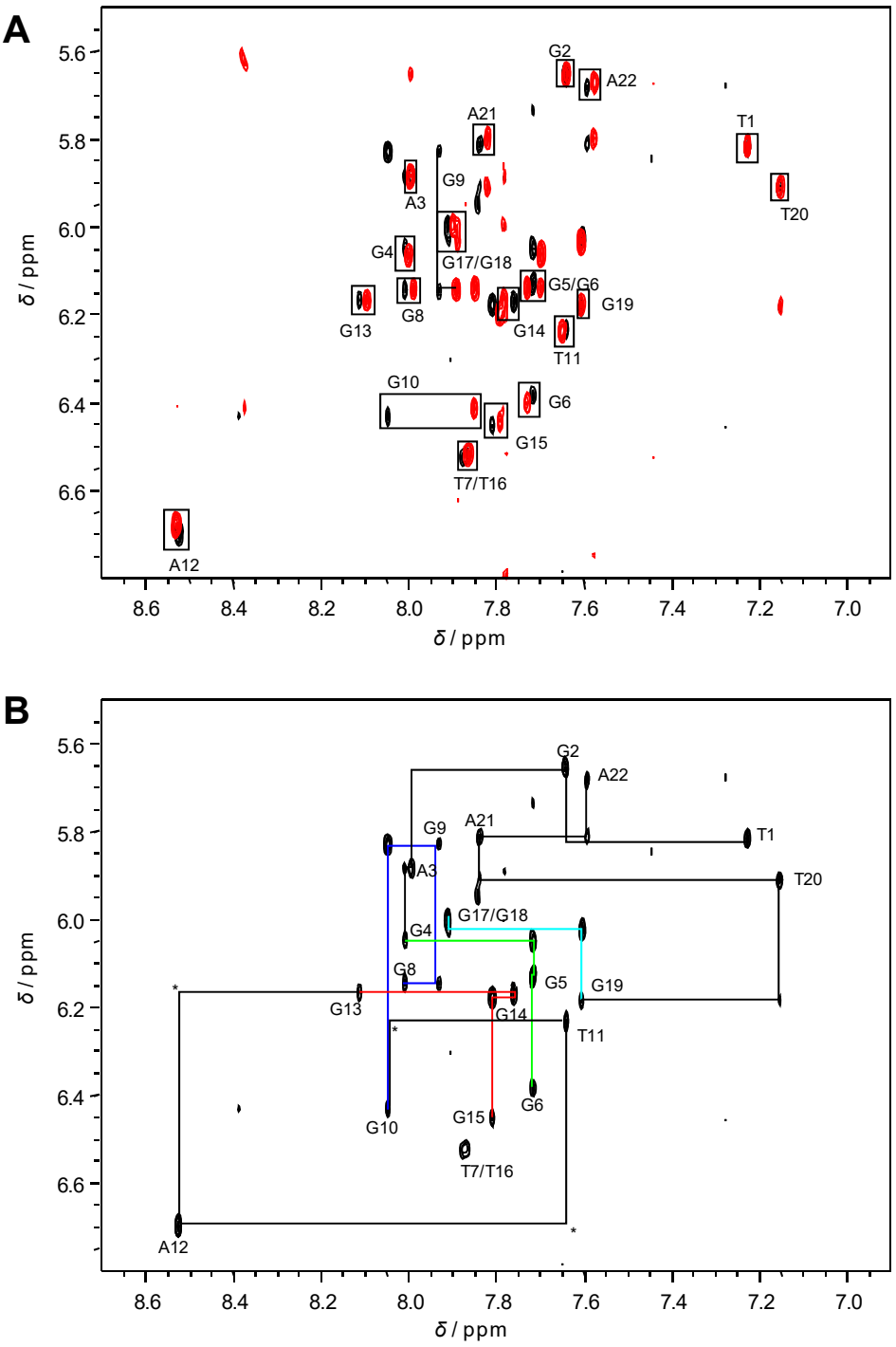

Figure S8. (A) Superposition of the H6/H8–H1' 2D NOE spectral region of MYC(0) (red) and MYC(9) (black). (B) Sequential H6/H8–H1' NOE walks for MYC(9) traced by solid lines. Due to the overlap for residues T7 and T16 connectivities involving the latter were omitted. The NOEs along the four G-tracts are shown in green, blue, red, and cyan; non-observable NOE contacts are marked by asterisks; T = 40 °C, τ_m = 300 ms.

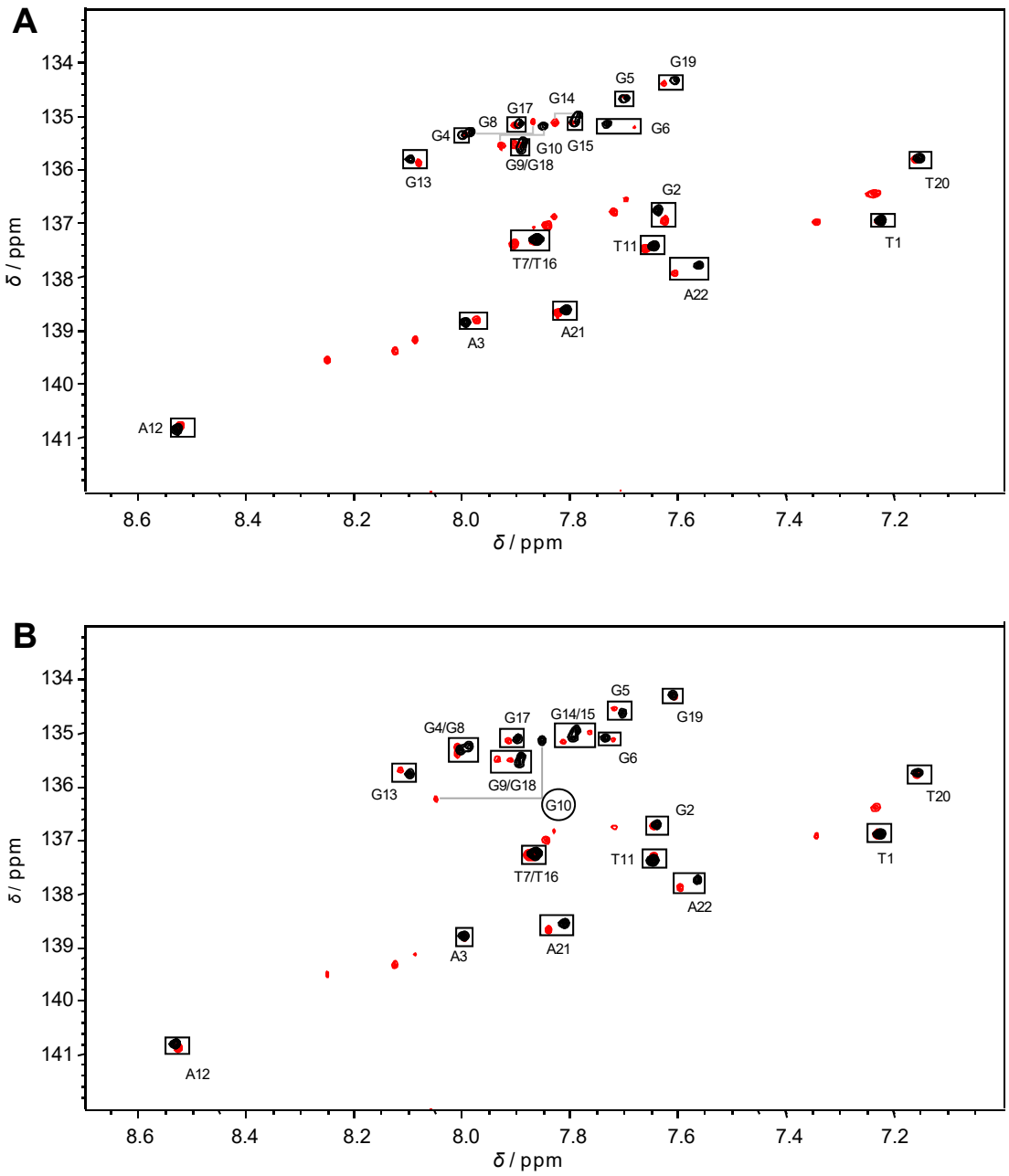

Figure S9. H6/H8–C6/C8 spectral region of ^{1}H-^{13}C HSQC spectra acquired at 40 °C. Spectrum of unmodified MYC(0) (black) is superimposed with ribose-modified (red) MYC(8) (A) and MYC(9) (B). Corresponding crosspeaks for the native and substituted quadruplex are combined within rectangular boxes or connected by horizontal and vertical lines; large chemical shift changes in both the ^{13}C and ^{1}H dimension as observed for G10 at the 3'-neighboring position of incorporated rG are highlighted in (B).

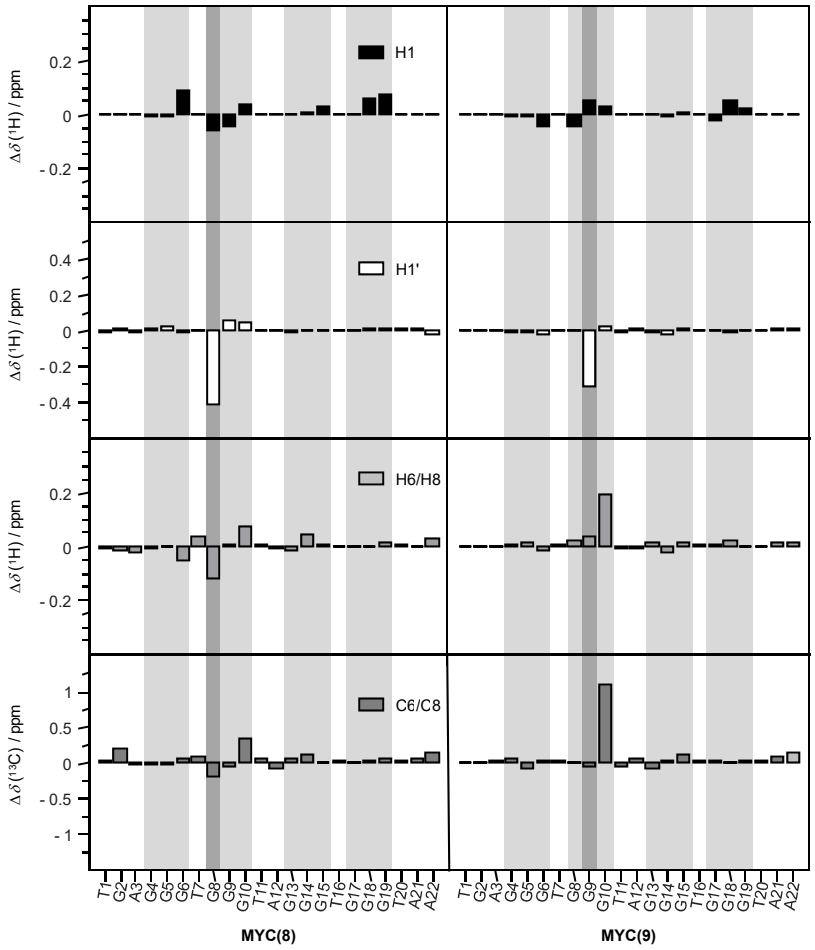

Figure S10. Chemical shift changes of H1, H1', H6/H8, and C6/C8 in rG-substituted MYC referenced against MYC(0); vertical traces in dark and light gray denote rG substitution sites and G-tracts of the quadruplex core, respectively.

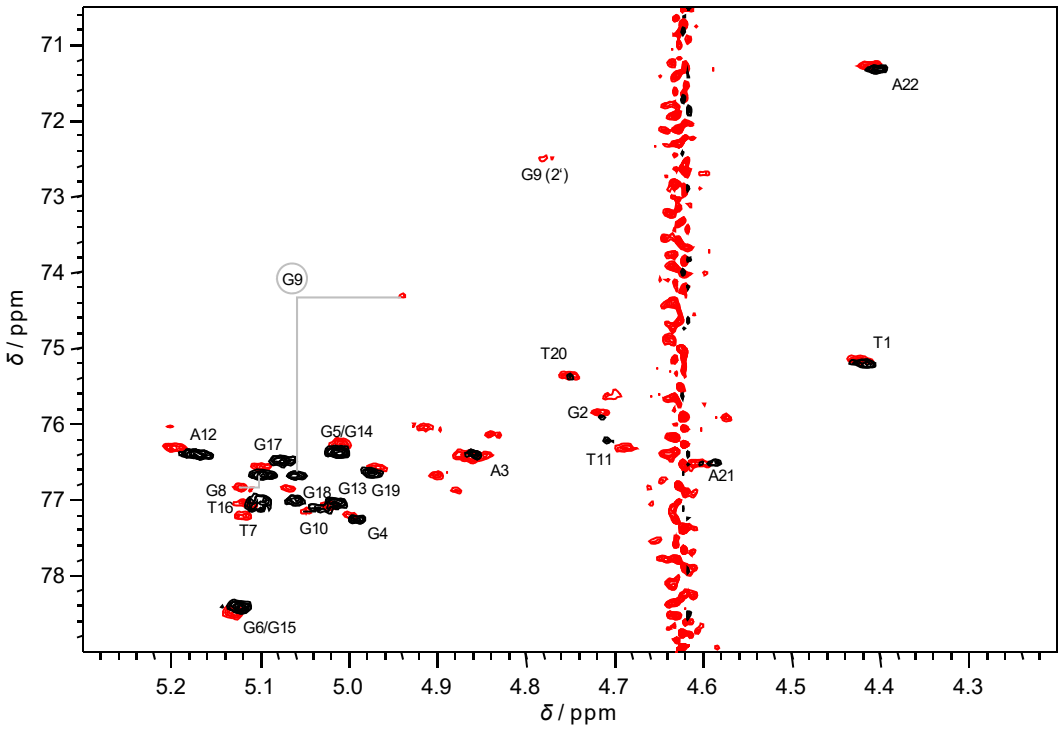

Figure S11. Superimposed H3'–C3' spectral regions of ^{1}H-^{13}C HSQC spectra acquired at 40 °C for unmodified MYC(0) (black) and ribose-modified MYC(9) (red). The large chemical shift change in both the ^{13}C and ^{1}H dimension which identifies the modified guanine base at position 9 in MYC(9) is highlighted.

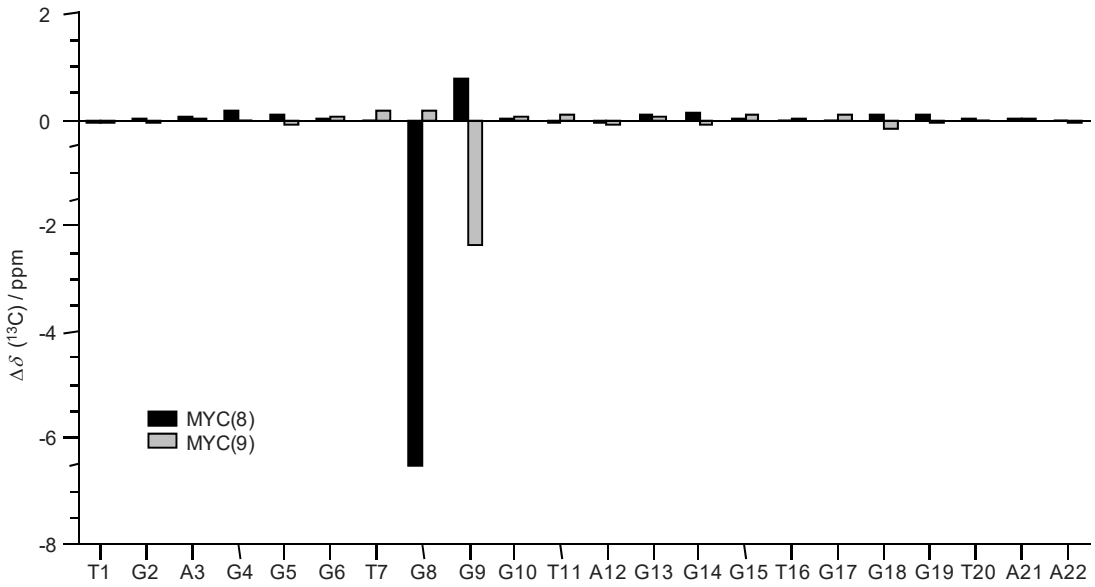

Figure S12. Chemical shift changes of C3' in rG-substituted MYC(8) and MYC(9) referenced against MYC(0).

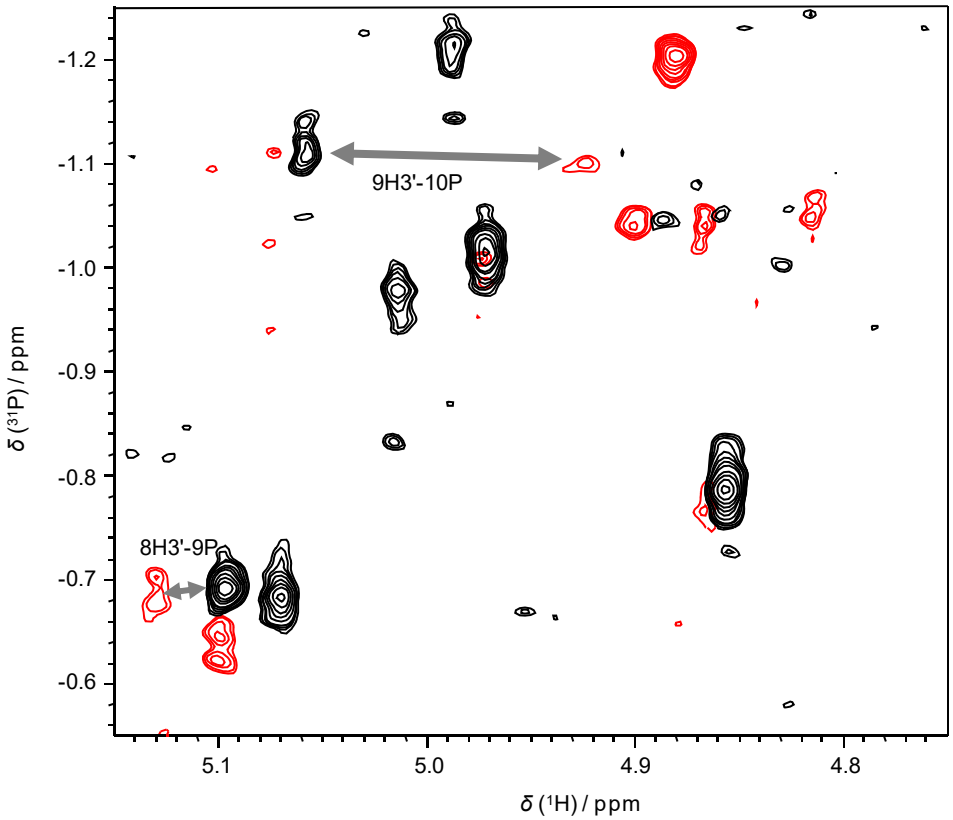

Figure S13. Superimposed H3'–P spectral regions of ^{1}H-^{31}P HETCOR spectra acquired at 40 °C for unmodified MYC(0) (black) and ribose-modified MYC(9) (red). The subtle chemical shift changes for ^{31}P adjacent to the modified G residue at position 9 are indicated by the nearly horizontal arrows.

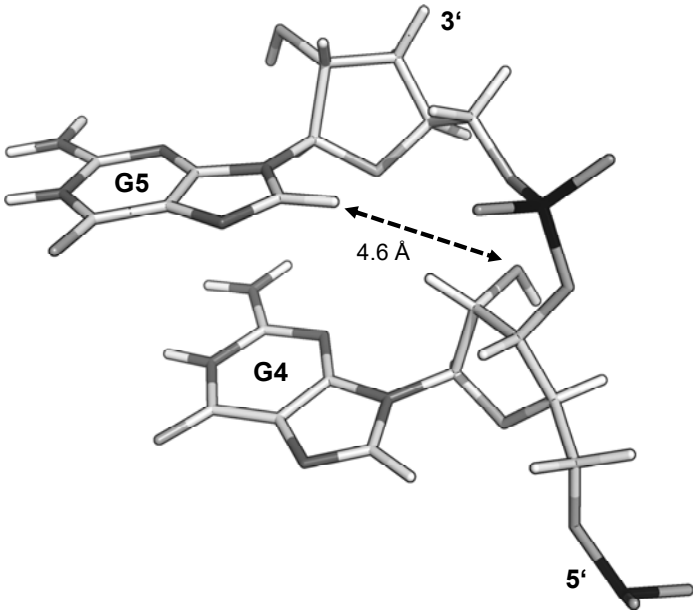

Figure S14. Geometry with internucleotide O2’-H8 distance in the G4-G5 dinucleotide fragment of the rHT RNA quadruplex solution structure with G4 in a C3’-*endo* (N) conformation (pdb code: 2KBP).

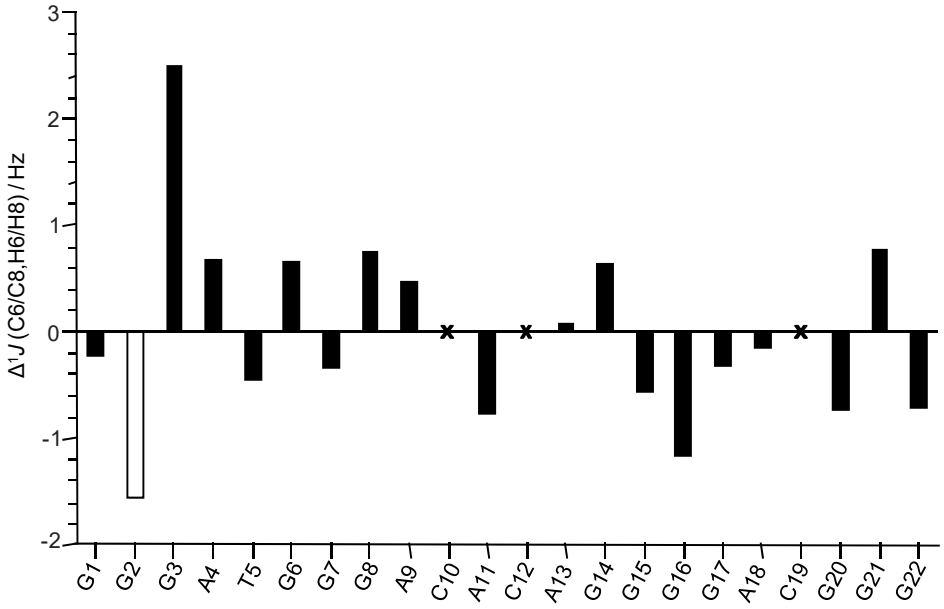

Figure S15. Changes of the C6/C8-H6/H8 ^{1}J scalar coupling in ODN(2) referenced against ODN(0); the white bar denotes the rG substitution site; experimental uncertainty ±0.7 Hz. Couplings for the cytosine bases were not included due to their insufficient accuracy.

Quantum chemical calculations. The G2-G3 dinucleotide fragment from the NMR solution structure of the ODN quadruplex (pdb code: 2LOD) was employed as a model structure for the calculations. Due to the relatively large conformational space available to the dinucleotide, the following substructures were fixed prior to geometry optimizations:

a) both guanine bases being part of two stacked G-tetrads in the quadruplex core to maintain their relative orientation

b) the deoxyribose sugar of G3 that was experimentally shown to retain its S-conformation when replacing neighboring G2 for rG2; in contrast, the deoxyribose/ribose sugar of the 5'-residue and the phosphate backbone was free to relax.

Initially, a constrained geometry optimization (HF/6-31G*) was performed on the G-G and a corresponding rG-G model structure obtained by a 2'H→2'OH substitution in the 5'-nucleotide. Examining putative hydrogen bonds we subsequently performed ^{1}H and ^{13}C chemical shift calculations at the B3LYP/6-31G** level of theory with additional polarization functions on the hydrogens.

The geometry optimized rG-G dinucleotide exhibits a 2'-OH oriented towards the phosphate backbone forming OH···O interactions with O(=P). In additional calculations on rG-G, interresidual H8···O2' distances R and C-H8···O2' angles ϑ as well as H2'-C2'-O2'-H torsion angles Θ of the ribonucleotide were constrained to evaluate their influence on the chemical shifts. As expected for a putative CH···O hydrogen bond, calculated H8 and C8 chemical shifts are found to be sensitive to R and ϑ values but also to the 2'-OH orientation as defined by Θ.

Chemical shift differences of G3 H8 and G3 C8 in the rG-G compared to the G-G dinucleotide fragment.

optimized geometry	optimized geometry with constrained R=2.40 Å	optimized geometry with constrained Θ=20°	experimental
R=2.61 Å, ϑ=132°, Θ=94°, C2'-endo	ϑ=132°, Θ=92°, C2'-endo	R=2.61 Å, ϑ=132°, C2'-endo	C2'-endo
$\Delta\delta$(H8) = +0.12 ppm	$\Delta\delta$(H8) = +0.3 ppm	$\Delta\delta$(H8) = +0.25 ppm	$\Delta\delta$(H8) = +0.1 ppm
$\Delta\delta$(C8) = +0.91 ppm	$\Delta\delta$(C8)= +1.4 ppm	$\Delta\delta$(C8)= +1.2 ppm	$\Delta\delta$(C8)= +1.1 ppm

Table S1. Sugar conformation of ribonucleotide n and geometric parameters of $(2'\text{-OH})_n\cdots(C8\text{-}H8)_{n+1}$ structural units within the G-tracts of RNA quadruplexes in solution and in the crystal.[a],[b] Only one of the symmetry-related strands in NMR-derived tetra- and bimolecular quadruplexes is presented.

structure 1 (PDB: 1MY9)[c]

	pucker	*r* (Å)	*Θ* (°)		pucker	*r* (Å)	*Θ* (°)
G1	C2'-endo	1.9	131.4	U8	C3'-endo	---	---
G2	C2'-endo	---	---	U9	O4'-endo	---	---
A3	C2'-exo	---	---	**G10**	C2'-endo	1.7	165.2
G4	C1'-exo	5.1	91.9	**G11**	C1'-exo	---	---
G5	C4'-exo	---	---	A12	C2'-exo	---	---
U6	C1'-exo	---	---	**G13**	C2'-endo	3.3	100.1
U7	C1'-exo	---	---	**G14**	C3'-exo	---	---

structure 2 (PDB: 2RQJ)[d]

	pucker	*r* (Å)	*Θ* (°)		pucker	*r* (Å)	*Θ* (°)
G1	C2'-endo	2.0	139.5	**G7**	C2'-endo	2.3	170
G2	C2'-endo	---	---	**G8**	C2'-endo	---	---
A3	C2'-exo	---	---	A9	C2'-exo	---	---
G4	C2'-exo	4.0	137.5	**G10**	C2'-exo	3.9	121.4
G5	C2'-endo	---	---	**G11**	C4'-exo	---	---
A6	C2'-endo	---	---	A12	O4'-endo	---	---

structure 3 (PDB: 2KBP)[e]

	pucker	*r* (Å)	*Θ* (°)		pucker	*r* (Å)	*Θ* (°)
U1	C3'-exo	---	---	U7	C3'-exo	---	---
A2	C2'-endo	---	---	A8	C3'-exo	---	---
G3	C2'-endo	2.2	122.6	**G9**	C2'-endo	2.9	120.8
G4	C3'-endo	4.6	126.1	**G10**	C3'-endo	3.8	119.8
G5	C2'-endo	---	---	**G11**	C3'-endo	---	---
U6	C2'-endo	---	---	U12	C3'-exo	---	---

structure 4 (PDB: 1RAU)[f]

	pucker	*r* (Å)	*Θ* (°)		pucker	*r* (Å)	*Θ* (°)
U1	C3'-endo	---	---	**G4**	C3'-endo	3.9	115.4
G2	C3'-exo	1.7	160.9	**G5**	C3'-endo	---	---
G3	C3'-endo	3.7	125.2	U6	C2'-endo	---	---

Table continued

structure 5 (PDB: 3IBK)[g]

strand a

	pucker	*r* (Å)	*Θ* (°)		pucker	*r* (Å)	*Θ* (°)
^{Br}U1	C3'-endo	---	---	U7	C3'-endo	---	---
A2	C3'-endo	---	---	A8	C2'-endo	---	---
G3	C2'-endo	2.4	134.3	**G9**	C2'-endo	2.3	135.2
G4	C3'-endo	4.1	105.1	**G10**	C3'-endo	4.1	104.7
G5	C2'-endo	---	---	**G11**	C2'-endo	---	---
U6	C1'-exo	---	---	U12	C1'-endo	---	---

strand b

	pucker	*r* (Å)	*Θ* (°)		pucker	*r* (Å)	*Θ* (°)
^{Br}U1	C3'-endo	---	---	U7	C3'-endo	---	---
A2	C3'-endo	---	---	A8	C1'-endo	---	---
G3	C3'-endo	3.8	121.2	**G9**	C3'-endo	3.8	129.1
G4	C3'-endo	3.9	107.4	**G10**	C3'-endo	3.9	116.2
G5	C2'-endo	---	---	**G11**	C3'-endo	---	---
U6	C1'-exo	---	---	U12	C2'-endo	---	---

structure 6 (PDB: 4XK0)[h]

strand a

	pucker	*r* (Å)	*Θ* (°)		pucker	*r* (Å)	*Θ* (°)
U1	C2'-endo	---	---	**G4**	C3'-endo	4.1	114.6
G2	C2'-endo	3.2	127.7	**G5**	C3'-endo	---	---
G3	C3'-endo	3.8	137.0	U6	C2'-endo	---	---

strand b

	pucker	*r* (Å)	*Θ* (°)		pucker	*r* (Å)	*Θ* (°)
U1	C3'-endo	---	---	**G4**	C3'-endo	4.0	130.7
G2	C3'-endo	3.0	125.9	**G5**	C3'-endo	---	---
G3	C3'-endo	3.9	122.9	U6	C2'-endo	---	---

structure 7 (PDB: 1J8G)[i]

strand a

	pucker	*r* (Å)	*Θ* (°)		pucker	*r* (Å)	*Θ* (°)
U1	C3'-endo	---	---	**G4**	C3'-endo	4.2	110.1
G2	C3'-endo	4.5	110.5	**G5**	C3'-endo	---	---
G3	C2'-endo	2.3	128.5	U6	C2'-endo	---	---

Table continued

strand b

	pucker	*r* (Å)	*Θ* (°)		pucker	*r* (Å)	*Θ* (°)
U1	C3'-endo	---	---	**G4**	C3'-endo	4.0	113.1
G2	C3'-endo	4.5	109.0	**G5**	C3'-endo	---	---
G3	C2'-endo	2.3	126.1	U6	C2'-endo	---	---

strand c

	pucker	*r* (Å)	*Θ* (°)		pucker	*r* (Å)	*Θ* (°)
U1	C3'-endo	---	---	**G4**	C3'-endo	4.1	109.7
G2	C3'-endo	4.4	110.6	**G5**	C3'-endo	---	---
G3	C2'-endo	2.2	131.0	U6	C2'-endo	---	---

strand d

	pucker	*r* (Å)	*Θ* (°)		pucker	*r* (Å)	*Θ* (°)
U1	C3'-endo	---	---	**G4**	C3'-endo	4.1	107.8
G2	C3'-endo	4.4	110.5	**G5**	C3'-endo	---	---
G3	C2'-endo	2.2	130.2	U6	C4'-endo	---	---

[a] Geometric parameters are defined by $H8_{n+1}\cdots O2'_n$ distance *r* and $(C8\text{-}H8)_{n+1}\cdots O2'_n$ angle *Θ*.

[b] Guanine nucleotides of G-tetrads are written in bold; nucleotide steps with geometric parameters in line with criteria set for C-H···O interactions, i.e. $r < 3$ Å and $110^o < \Theta < 180^o$, are shaded grey.

[c] H. Liu, A. Matsugami, M. Katahira, S. Uesugi, *J. Mol. Biol.* **2002**, *322*, 955–970.

[d] T. Mashima, A. Matsugami, F. Nishikawa, S. Nishikawa, M. Katahira, *Nucleic Acids Res.* **2009**, *37*, 6249–6258.

[e] H. Martadinata, A. T. Phan, *J. Am. Chem. Soc.* **2009**, *131*, 2570–2578.

[f] C. Cheong, P. B. Moore, *Biochemistry* **1992**, *31*, 8406–8414.

[g] G. W. Collie, S. M. Haider, S. Neidle, G. N. Parkinson, *Nucleic Acids Res.* **2010**, *38*, 5569–5580.

[h] M. C. Chen, P. Murat, K. Abecassis, A. R. Ferré-D'Amaré, S. Balasubramanian, *Nucleic Acids Res.* **2015**, *43*, 2223–2231.

[i] J. Deng, Y. Xiong, M. Sundaralingam, *Proc. Natl. Acad. Sci. U.S.A.* **2001**, *98*, 13665–13670.

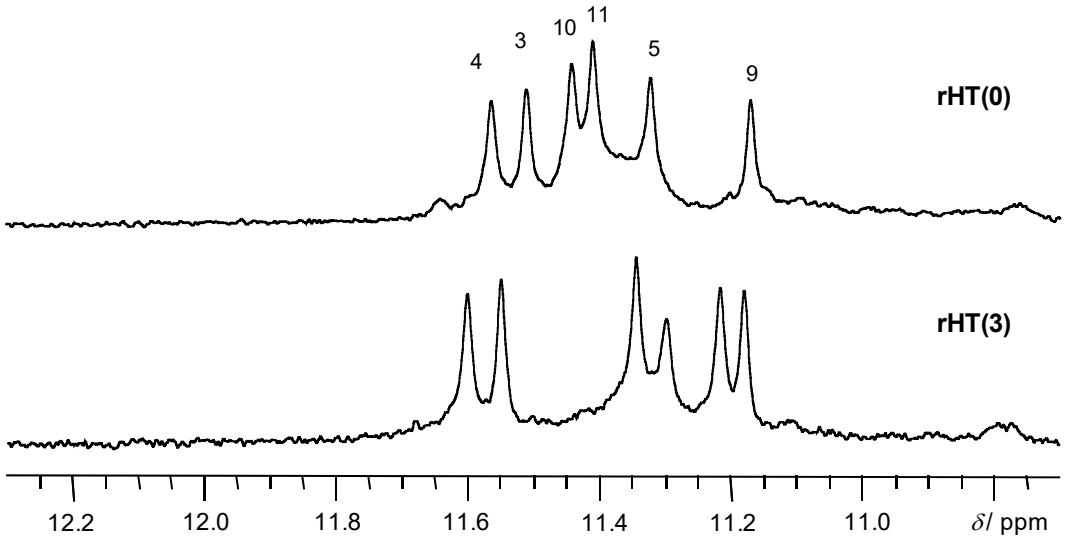

Figure S16. Imino proton spectral region of the native and dG-substituted rHT quadruplex in 10 mM potassium phosphate buffer, pH 7, at 25 °C.; peak assignments for the G-tract guanines are indicated for the native form.

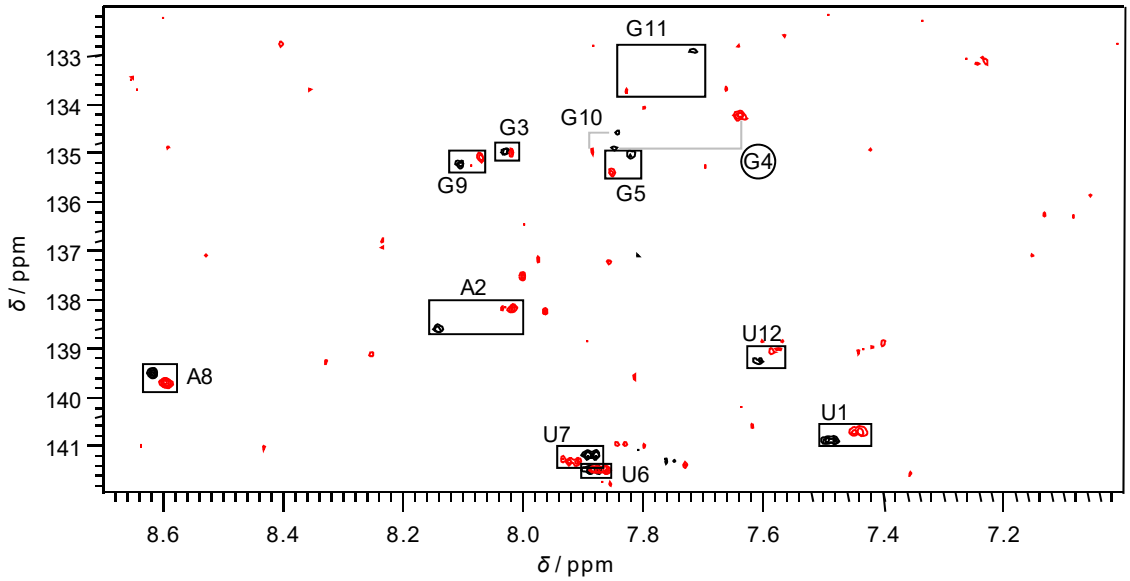

Figure S17. Portion of ^{1}H-^{13}C HSQC spectra of rHT acquired at 25 °C and showing the H6/H8–C6/C8 spectral region. Spectrum of unmodified rHT(0) (black) is superimposed with dG-modified rHT(3) (red). Corresponding crosspeaks for the native and substituted quadruplex are combined within rectangular boxes or connected by horizontal and vertical lines; large chemical shift changes in both the ^{13}C and ^{1}H dimension as observed for G4 at the 3'-neighboring position of incorporated dG are highlighted.

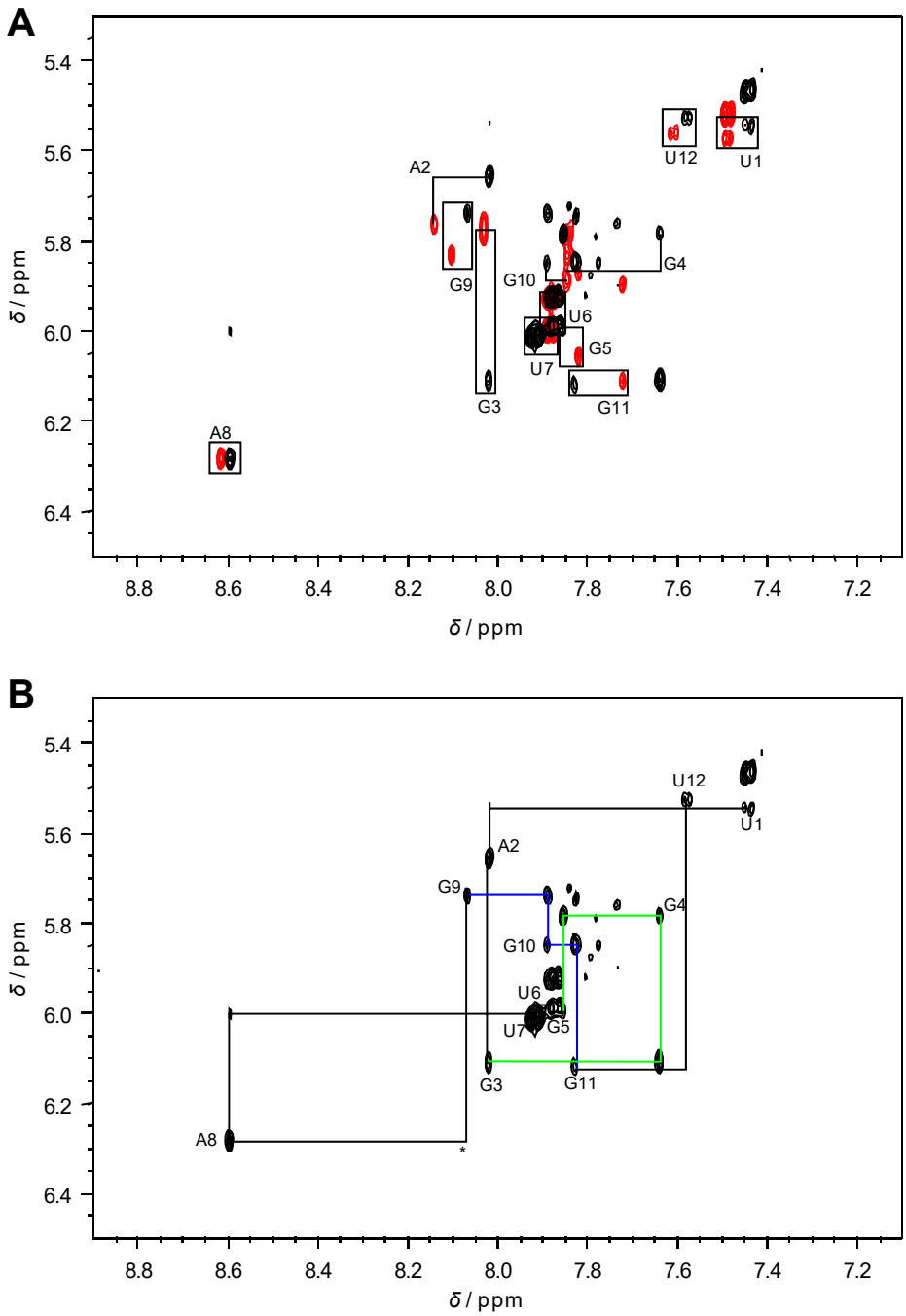

Figure S18. (A) Superposition of the H6/H8–H1' 2D NOE spectral region of rHT(0) (red) and rHT(3) (black). (B) Sequential H6/H8–H1' NOE walks for rHT(3) traced by solid lines. The NOEs along the G-tracts are shown in green and blue; non-observable NOE contacts are marked by asterisks. T = 25 °C, τ_m = 300 ms.

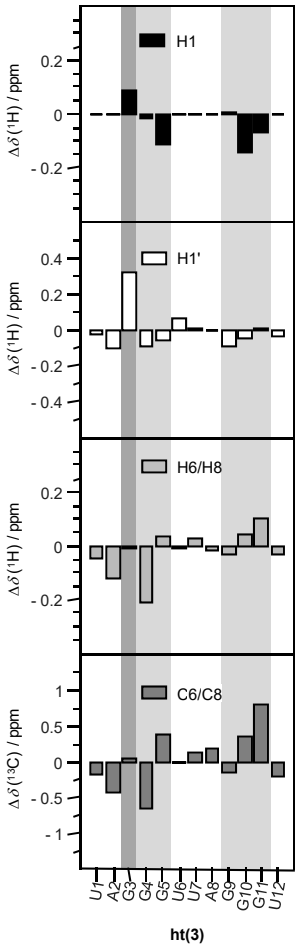

Figure S19. Chemical shift changes of H1, H1', H6/H8, and C6/C8 in dG-substituted rHT referenced against rHT(0); vertical traces in dark and light gray denote dG substitution sites and G-tracts of the quadruplex core, respectively.

Article II

G-Quadruplexes

International Edition: DOI: 10.1002/anie.201411887
German Edition: DOI: 10.1002/ange.201411887

Flipping a G-Tetrad in a Unimolecular Quadruplex Without Affecting Its Global Fold

*Jonathan Dickerhoff and Klaus Weisz**

Abstract: *A unimolecular G-quadruplex with a hybrid-type topology and propeller, diagonal, and lateral loops was examined for its ability to undergo structural changes upon specific modifications. Substituting 2′-deoxy-2′-fluoro analogues with a propensity to adopt an anti glycosidic conformation for two or three guanine deoxyribonucleosides in syn positions of the 5′-terminal G-tetrad significantly alters the CD spectral signature of the quadruplex. An NMR analysis reveals a polarity switch of the whole tetrad with glycosidic conformational changes detected for all four guanine nucleosides in the modified sequence. As no additional rearrangement of the overall fold occurs, a novel type of G-quadruplex is formed with guanosines in the four columnar G-tracts lined up in either an all-syn or an all-anti glycosidic conformation.*

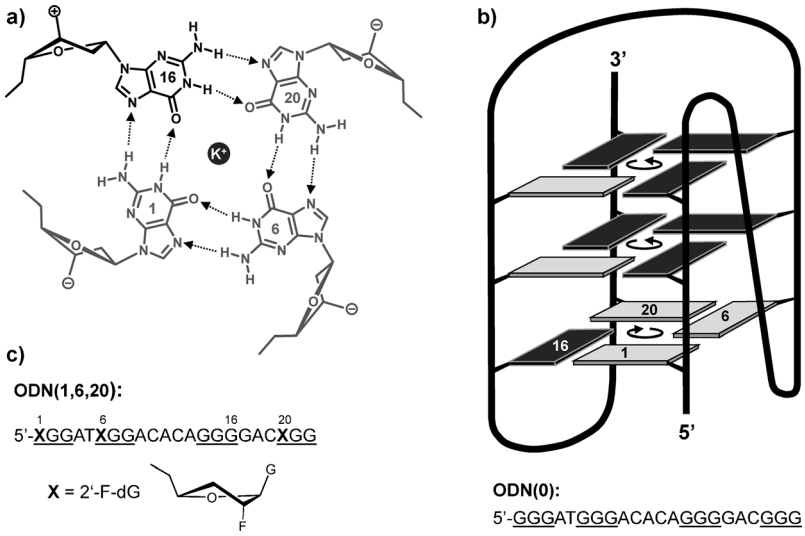

Figure 1. a) 5′-Terminal G-tetrad with hydrogen bonds running in a clockwise fashion and b) folding topology of ODN(0) with *syn* and *anti* guanines shown in light and dark gray, respectively. G-tracts in b) the native ODN(0) and c) the modified ODN(1,6,20) with incorporated 2′-fluoro-dG analogues are underlined.

Guanine-rich DNA and RNA sequences can fold into four-stranded G-quadruplexes stabilized by a core of stacked guanine tetrads. The four guanine bases in the square-planar arrangement of each tetrad are connected through a cyclic array of Hoogsteen hydrogen bonds and additionally stabilized by a centrally located cation (Figure 1 a). Quadruplexes have gained enormous attention during the last two decades as a result of their recently established existence and potential regulatory role in vivo[1] that renders them attractive targets for various therapeutic approaches.[2] This interest was further sparked by the discovery that many natural and artificial RNA and DNA aptamers, including DNAzymes and biosensors, rely on the quadruplex platform for their specific biological activity.[3]

In general, G-quadruplexes can fold into a variety of topologies characterized by the number of individual strands, the orientation of G-tracts, and the type of connecting loops.[4] As guanosine glycosidic torsion angles within the quadruplex stem are closely connected with the relative orientation of the four G segments, specific guanosine replacements by G analogues that favor either a *syn* or *anti* glycosidic conformation have been shown to constitute a powerful tool to examine the conformational space available for a particular quadruplex-forming sequence.[5] There are ongoing efforts aimed at exploring and ultimately controlling accessible quadruplex topologies prerequisite for taking full advantage of the potential offered by these quite malleable structures for therapeutic, diagnostic, or biotechnological applications.

The three-dimensional NMR structure of the artificially designed intramolecular quadruplex ODN(0) was recently reported.[6] Remarkably, it forms a (3 + 1) hybrid topology with all three main types of connecting loops, that is, with a propeller, a lateral, and a diagonal loop (Figure 1 b). We wanted to follow conformational changes upon substituting an *anti*-favoring 2′-fluoro-2′-deoxyribo analogue 2′-F-dG for G residues within its 5′-terminal tetrad. As shown in Figure 2, the CD spectrum of the native ODN(0) exhibits positive bands at $\lambda = 290$ and 263 nm as well as a smaller negative band at about 240 nm typical of the hybrid structure. A 2′-F-dG substitution at *anti* position 16 in the modified ODN(16) lowers all CD band amplitudes but has no noticeable influence on the overall CD signature. However, progressive substitutions at *syn* positions 1, 6, and 20 gradually decrease the CD maximum at $\lambda = 290$ nm while increasing the band amplitude at 263 nm. Thus, the CD spectra of ODN(1,6), ODN(1,20), and in particular of ODN(1,6,20) seem to imply a complete switch into a parallel-type quadruplex with the absence of Cotton effects at around $\lambda = 290$ nm but with

[*] J. Dickerhoff, Prof. Dr. K. Weisz
Institut für Biochemie
Ernst-Moritz-Arndt-Universität Greifswald
Felix-Hausdorff-Strasse 4, 17487 Greifswald (Germany)
E-mail: weisz@uni-greifswald.de

Supporting information for this article is available on the WWW under http://dx.doi.org/10.1002/anie.201411887.

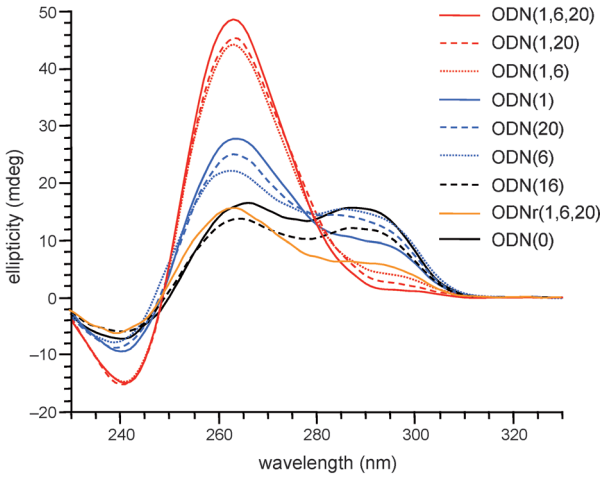

Figure 2. CD spectra of native ODN(0), rG-modified ODNr(1,6,20), and 2′-F-dG modified ODN sequences at 20 °C in 20 mM potassium phosphate, 100 mM KCl, pH 7. Numbers in parentheses denote sites of substitution.

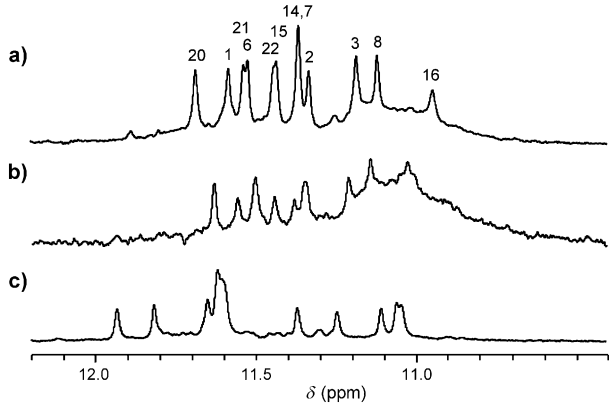

Figure 3. ^{1}H NMR spectra showing the imino proton spectral region for a) ODN(1,6,20), b) ODN(1,20), and c) ODN(0) at 25 °C in 10 mM potassium phosphate (pH 7). Peak assignments for the G-tract guanines are indicated for ODN(1,6,20).

a strong positive band at 263 nm and a negative band at 240 nm. In contrast, ribonucleotides with their similar propensity to adopt an *anti* conformation appear to be less effective in changing ODN conformational features based on the CD effects of the triply rG-modified ODNr(1,6,20) (Figure 2).

Resonance signals for imino groups detected between $\delta =$ 10.8 and 12.0 ppm in the ^{1}H NMR spectrum of unmodified ODN(0) indicate the formation of a well-defined quadruplex as reported previously.[6] For the modified sequences ODN-(1,20) and ODN(1,6,20), resonance signals attributable to imino groups have shifted but the presence of a stable major quadruplex topology with very minor additional species is clearly evident for ODN(1,6,20) (Figure 3). Likewise, only small structural heterogeneities are noticeable for the latter on gels obtained with native PAGE, revealing a major band together with two very weak bands of lower mobility (see Figure S1 in the Supporting Information). Although two-dimensional NOE experiments of ODN(1,20) and ODN(1,6,20) demonstrate that both quadruplexes share the same major topology (Figure S3), the following discussion will be restricted to ODN(1,6,20) with its better resolved NMR spectra.

NMR spectroscopic assignments were obtained from standard experiments (for details see the Supporting Information). Structural analysis was also facilitated by very similar spectral patterns in the modified and native sequence. In fact, many nonlabile resonance signals, including signals for protons within the propeller and diagonal loops, have not significantly shifted upon incorporation of the 2′-F-dG analogues. Notable exceptions include resonances for the modified G-tetrad but also signals for some protons in its immediate vicinity. Fortunately, most of the shifted sugar resonances in the 2′-fluoro analogues are easily identified by characteristic ^{1}H–^{19}F coupling constants. Overall, the global fold of the quadruplex seems unaffected by the G→2′-F-dG replacements. However, considerable changes in intranucleotide H8–H1′ NOE intensities for all G residues in the 5′-terminal tetrad indicate changes in their glycosidic torsion angle.[7] Clear evidence for guanosine glycosidic conformational transitions within the first G-tetrad comes from H6/H8 but in particular from C6/C8 chemical shift differences detected between native and modified quadruplexes. Chemical shifts for C8 carbons have been shown to be reliable indicators of glycosidic torsion angles in guanine nucleosides.[8] Thus, irrespective of the particular sugar pucker, downfield shifts of $\delta = 2$-6 ppm are predicted for C8 in guanosines adopting the *syn* conformation. As shown in Figure 4, resonance signals for C8 within G1, G6, and G20

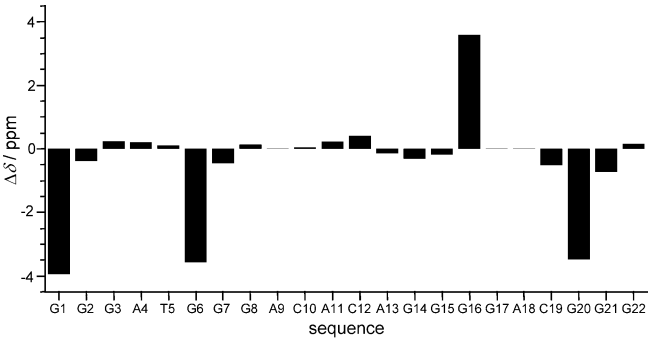

Figure 4. ^{13}C NMR chemical shift differences for C8/C6 atoms in ODN(1,6,20) and unmodified ODN(0) at 25 °C. Note, base protons of G17 and A18 residues within the lateral loop have not been assigned.

are considerably upfield shifted in ODN(1,6,20) by nearly $\delta =$ 4 ppm. At the same time, the signal for carbon C8 in the G16 residue shows a corresponding downfield shift whereas C6/C8 carbon chemical shifts of the other residues have hardly changed. These results clearly demonstrate a polarity reversal of the 5′-terminal G-tetrad, that is, modified G1, G6, and G20 adopt an *anti* conformation whereas the G16 residue changes from *anti* to *syn* to preserve the cyclic-hydrogen-bond array.

Apparently, the modified ODN(1,6,20) retains the global fold of the native ODN(0) but exhibits a concerted flip of glycosidic torsion angles for all four G residues within the

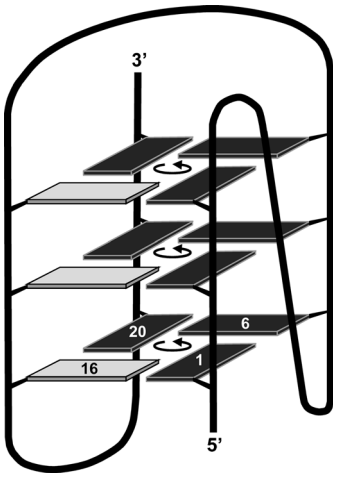

Figure 5. Schematic representation of the topology and glycosidic conformation of ODN(1,6,20) with *syn*- and *anti*-configured guanosines shown in light and dark gray, respectively.

5′-terminal tetrad, thus reversing its intrinsic polarity (see Figure 5). Remarkably, a corresponding switch in tetrad polarity in the absence of any topological rearrangement has not been reported before in the case of intramolecularly folded quadruplexes. Previous results on *anti*/*syn*-favoring guanosine replacements indicate that a quadruplex conformation is conserved and potentially stabilized if the preferred glycosidic conformation of the guanosine surrogate matches the original conformation at the substitution site. In contrast, enforcing changes in the glycosidic torsion angle at an "unmatched" position will either result in a severe disruption of the quadruplex stem or in its complete refolding into a different topology.[9] Interestingly, tetramolecular all-*trans* quadruplexes $[TG_{3\text{-}4}T]_4$ lacking intervening loop sequences are often prone to changes in tetrad polarity through the introduction of *syn*-favoring 8-Br-dG or 8-Me-dG analogues.[10]

By changing the polarity of the ODN 5′-terminal tetrad, the antiparallel G-tract and each of the three parallel G-tracts exhibit a non-alternating all-*syn* and all-*anti* array of glycosidic torsion angles, respectively. This particular glycosidic-bond conformational pattern is unique, being unreported in any known quadruplex structure, expanding the repertoire of stable quadruplex structural types as defined previously.[11,12] The native quadruplex exhibits three 5′-*syn–anti–anti* segments together with one 5′-*syn–syn–anti* segment. In the modified sequence the four *syn–anti* steps are changed to three *anti–anti* and one *syn–syn* step. UV melting experiments on ODN(0), ODN(1,20), and ODN(1,6,20) showed a lower melting temperature of approximately 10 °C for the two modified sequences with a rearranged G-tetrad. In line with these differential thermal stabilities, molecular dynamics simulations and free energy analyses suggested that *syn–anti* and *syn–syn* are the most stable and most disfavored glycosidic conformational steps in antiparallel quadruplex structures, respectively.[13] It is therefore remarkable that an unusual all-*syn* G-tract forms in the thermodynamically most stable modified quadruplex, highlighting the contribution of connecting loops in determining the preferred conformation. Apparently, the particular loop regions in ODN(0) resist topological changes even upon enforcing *syn*↔*anti* transitions.

CD spectral signatures are widely used as convenient indicators of quadruplex topologies. Thus, depending on their spectral features between $\lambda = 230$ and 320 nm, quadruplexes are empirically classified into parallel, antiparallel, or hybrid structures. It has been pointed out that the characteristics of quadruplex CD spectra do not directly relate to strand orientation but rather to the inherent polarity of consecutive guanine tetrads as defined by Hoogsteen hydrogen bonds running either in a clockwise or in a counterclockwise fashion when viewed from donor to acceptor.[14] This tetrad polarity is fixed by the strand orientation and by the guanosine glycosidic torsion angles. Although the native and modified quadruplex share the same strand orientation and loop conformation, significant differences in their CD spectra can be detected and directly attributed to their different tetrad polarities. Accordingly, the maximum band at $\lambda =$ 290 nm detected for the unmodified quadruplex and missing in the modified structure must necessarily originate from a *syn–anti* step giving rise to two stacked tetrads of different polarity. In contrast, the positive band at $\lambda = 263$ nm must reflect *anti–anti* as well as *syn–syn* steps. Overall, these results corroborate earlier evidence that it is primarily the tetrad stacking that determines the sign of Cotton effects. Thus, the empirical interpretation of quadruplex CD spectra in terms of strand orientation may easily be misleading, especially upon modification but probably also upon ligand binding.

The conformational rearrangements reported herein for a unimolecular G-quadruplex are without precedent and again demonstrate the versatility of these structures. Additionally, the polarity switch of a single G-tetrad by double or triple substitutions to form a new conformational type paves the way for a better understanding of the relationship between stacked tetrads of distinct polarity and quadruplex thermodynamics as well as spectral characteristics. Ultimately, the ability to comprehend and to control the particular folding of G-quadruplexes may allow the design of tailor-made aptamers for various applications in vitro and in vivo.

Keywords: circular dichroism · conformational analysis · glycosides · G-quadruplexes · NMR spectroscopy

How to cite: *Angew. Chem. Int. Ed.* **2015**, *54*, 5588–5591
Angew. Chem. **2015**, *127*, 5680–5683

[1] E. Y. N. Lam, D. Beraldi, D. Tannahill, S. Balasubramanian, *Nat. Commun.* **2013**, *4*, 1796.
[2] S. M. Kerwin, *Curr. Pharm. Des.* **2000**, *6*, 441–471.
[3] J. L. Neo, K. Kamaladasan, M. Uttamchandani, *Curr. Pharm. Des.* **2012**, *18*, 2048–2057.
[4] a) S. Burge, G. N. Parkinson, P. Hazel, A. K. Todd, S. Neidle, *Nucleic Acids Res.* **2006**, *34*, 5402–5415; b) M. Webba da Silva, *Chem. Eur. J.* **2007**, *13*, 9738–9745.
[5] a) Y. Xu, Y. Noguchi, H. Sugiyama, *Bioorg. Med. Chem.* **2006**, *14*, 5584–5591; b) J. T. Nielsen, K. Arar, M. Petersen, *Angew. Chem. Int. Ed.* **2009**, *48*, 3099–3103; *Angew. Chem.* **2009**, *121*,

3145 – 3149; c) A. Virgilio, V. Esposito, G. Citarella, A. Pepe, L. Mayol, A. Galeone, *Nucleic Acids Res.* **2012**, *40*, 461 – 475; d) Z. Li, C. J. Lech, A. T. Phan, *Nucleic Acids Res.* **2014**, *42*, 4068 – 4079.

[6] M. Marušič, P. Šket, L. Bauer, V. Viglasky, J. Plavec, *Nucleic Acids Res.* **2012**, *40*, 6946 – 6956.

[7] K. Wüthrich, *NMR of Proteins and Nucleic Acids*, John Wiley and Sons, New York, **1986**, pp. 203 – 223.

[8] a) K. L. Greene, Y. Wang, D. Live, *J. Biomol. NMR* **1995**, *5*, 333 – 338; b) J. M. Fonville, M. Swart, Z. Vokáčová, V. Sychrovský, J. E. Šponer, J. Šponer, C. W. Hilbers, F. M. Bickelhaupt, S. S. Wijmenga, *Chem. Eur. J.* **2012**, *18*, 12372 – 12387.

[9] a) C.-F. Tang, R. H. Shafer, *J. Am. Chem. Soc.* **2006**, *128*, 5966 – 5973; b) A. T. Phan, V. Kuryavyi, K. N. Luu, D. J. Patel, *Nucleic Acids Res.* **2007**, *35*, 6517 – 6525; c) D. Pradhan, L. H. Hansen, B. Vester, M. Petersen, *Chem. Eur. J.* **2011**, *17*, 2405 – 2413; d) C. J. Lech, Z. Li, B. Heddi, A. T. Phan, *Chem. Commun.* **2012**, *48*, 11425 – 11427.

[10] a) A. Virgilio, V. Esposito, A. Randazzo, L. Mayol, A. Galeone, *Nucleic Acids Res.* **2005**, *33*, 6188 – 6195; b) P. L. T. Tran, A. Virgilio, V. Esposito, G. Citarella, J.-L. Mergny, A. Galeone, *Biochimie* **2011**, *93*, 399 – 408.

[11] a) M. Webba da Silva, M. Trajkovski, Y. Sannohe, N. Ma'ani Hessari, H. Sugiyama, J. Plavec, *Angew. Chem. Int. Ed.* **2009**, *48*, 9167 – 9170; *Angew. Chem.* **2009**, *121*, 9331 – 9334; b) A. I. Karsisiotis, N. Ma'ani Hessari, E. Novellino, G. P. Spada, A. Randazzo, M. Webba da Silva, *Angew. Chem. Int. Ed.* **2011**, *50*, 10645 – 10648; *Angew. Chem.* **2011**, *123*, 10833 – 10836.

[12] There has been one report on a hybrid structure with one all-*syn* and three all-*anti* G-tracts suggested to form upon binding a porphyrin analogue to the *c-myc* quadruplex. However, the proposed topology is solely based on dimethyl sulfate (DMS) footprinting experiments and no further evidence for the particular glycosidic conformational pattern is presented. See: J. Seenisamy, S. Bashyam, V. Gokhale, H. Vankayalapati, D. Sun, A. Siddiqui-Jain, N. Streiner, K. Shin-ya, E. White, W. D. Wilson, L. H. Hurley, *J. Am. Chem. Soc.* **2005**, *127*, 2944 – 2959.

[13] X. Cang, J. Šponer, T. E. Cheatham III, *Nucleic Acids Res.* **2011**, *39*, 4499 – 4512.

[14] S. Masiero, R. Trotta, S. Pieraccini, S. De Tito, R. Perone, A. Randazzo, G. P. Spada, *Org. Biomol. Chem.* **2010**, *8*, 2683 – 2692.

Received: December 10, 2014
Revised: February 22, 2015
Published online: March 16, 2015

Angewandte Chemie
Eine Zeitschrift der Gesellschaft Deutscher Chemiker

Supporting Information

Flipping a G-Tetrad in a Unimolecular Quadruplex Without Affecting Its Global Fold

*Jonathan Dickerhoff and Klaus Weisz**

anie_201411887_sm_miscellaneous_information.pdf

Table of Contents

Materials and methods

Materials. Unmodified and HPLC-purified 2'-fluoro-modified DNA oligonucleotides were purchased from *TIB MOLBIOL* (Berlin, Germany) and *Purimex* (Grebenstein, Germany), respectively. Before use, oligonucleotides were ethanol precipitated and the concentrations were determined spectrophotometrically by measuring the absorbance at 260 nm. Samples were obtained by dissolving the corresponding oligonucleotides in a low salt buffer with 10 mM potassium phosphate, pH 7.0, for NMR experiments or in a high salt buffer with 20 mM potassium phosphate, 100 mM KCl, pH 7.0, for UV and CD experiments. Prior to measurements, the samples were annealed by heating to 90 ^{o}C followed by slow cooling to room temperature. Final concentrations of oligonucleotides were 5 μM for the UV and CD experiments and between 0.54 and 0.80 mM for the NMR measurements.

UV melting experiments. UV experiments were performed on a *Cary 100* spectrophotometer equipped with a Peltier temperature control unit (*Varian* Deutschland, Darmstadt). The melting curves were recorded by measuring the absorption of the solution at 295 nm with 2 data points/^{o}C in 10 mm quartz cuvettes. Heating and cooling rates of 0.2 °C/min were employed. Melting temperatures were determined by the intersection of the melting curve and the median of the fitted baselines.

Circular dichroism. CD spectra were acquired with a Jasco J-810 spectropolarimeter at 20 ^{o}C (*Jasco*, Tokyo, Japan). The spectra were recorded with a bandwidth of 1 nm, a scanning speed of 50 nm/min and 10 accumulations. All spectra were blank corrected.

Non-denaturing gel electrophoresis. To check for the presence of additional conformers or aggregates, non-denaturating gel electrophoresis was performed. After annealing in NMR buffer by heating to 90 °C for 5 min and subsequent slow cooling to room temperature, the samples (16.6 μM in strand) were loaded on a 20 % polyacrylamide gel (acrylamide/bis-acrylamide 19:1) containing TBE and 10 mM KCl. After running the gel with 4 W and 110 V at room temperature, bands were stained with ethidium bromide for visualization.

NMR experiments. All NMR spectra were acquired on a Bruker Avance 600 MHz spectrometer equipped with an inverse ^{1}H/^{13}C/^{15}N/^{31}P quadruple resonance cryoprobehead and z-field gradients. Data were processed using Topspin 3.1 and analyzed with CcpNmr Analysis.[1] Proton chemical shifts were referenced relative to TSP by setting the H_2O signal in 90% H_2O/10% D_2O

to δ_H = 4.78 ppm at 25 °C. For the one- and two-dimensional homonuclear measurements in 90% H_2O/10% D_2O a WATERGATE with w5 element was employed for solvent suppression. NOESY experiments in 90% H_2O/10% D_2O were performed at 25 ^oC with a mixing time of 300 ms and a spectral width of 9 kHz. 4K × 900 data points with 48 transients per t_1 increment and a recycle delay of 2 s were collected in t_2 and t_1. Prior to Fourier transformation data were zero-filled to give a 4K × 2K matrix and both dimensions were apodized by squared sine bell window functions.

DQF-COSY experiments were recorded in D_2O with 4K × 900 data points and 24 transients per t_1 increment. Prior to Fourier transformation data were zero-filled to give a 4K × 2K data matrix. Phase-sensitive ^1H-^{13}C HSQC experiments optimized for a ^1J(C,H) of 160 Hz were acquired with a 3-9-19 solvent suppression scheme in 90% H_2O/10% D_2O employing a spectral width of 7.5 kHz in the indirect ^{13}C dimension, 128 scans at each of 540 t_1 increments and a relaxation delay of 1.5 s between scans. ^{13}C chemical shifts were referenced relative to TMS by using the indirect referencing method.

[1] W. F. Vranken, W. Boucher, T. J. Stevens, R. H. Fogh, A. Pajon, M. Llinas, E. L. Ulrich, J. L. Markley, J. Ionides, E. D. Laue, *Proteins: Structure, Function, and Bioinformatics* **2005**, *59*, 687–696.

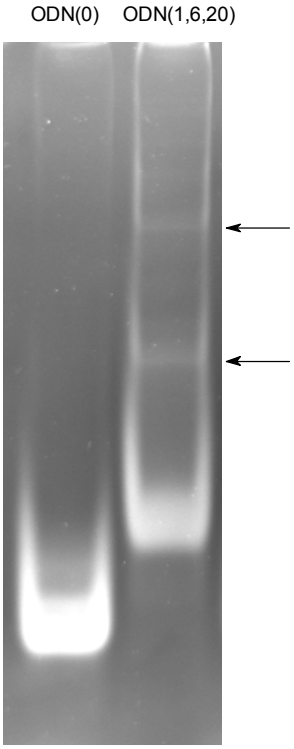

Figure S1. Non-denaturing gel electrophoresis of native ODN(0) and modified ODN(1,6,20). Considerable differences as seen in the migration behavior for the major species formed by the two sequences are frequently observed for closely related quadruplexes with minor modifications able to significantly change electrophoretic mobilities (see e.g. ref [2]). The two weak retarded bands of ODN(1,6,20) indicated by arrows may constitute additional larger aggregates. Only a single band was observed for both sequences under denaturing conditions (data not shown).

[2] P. L. T. Tran, A. Virgilio, V. Esposito, G. Citarella, J.-L. Mergny, A. Galeone, *Biochimie* **2011**, *93*, 399–408.

NMR spectral analysis of ODN(1,6,20)

H8–H2’ NOE crosspeaks of the 2’-F-dG analogs constitute convenient starting points for the proton assignments of ODN(1,6,20) (see Table S1). H2’ protons in 2’-F-dG display a characteristic ^{1}H-^{19}F scalar coupling of about 50 Hz while being significantly downfield shifted due to the fluorine substituent. Interestingly, the intranucleotide H8–H2’ connectivity of G1 is rather weak and only visible at a lower threshold level. Cytosine and thymidine residues in the loops are easily identified by their H5–H6 and H6–Me crosspeaks in a DQF-COSY spectrum, respectively (Figure S2).

A superposition of NOESY spectra for ODN(1,20) and ODN(1,6,20) reveals their structural similarity and enables the identification of the additional 2’-F-substituted G6 in ODN(1,6,20) (Figure S3). Sequential contacts observed between G20 H8 and H1', H2' and H2" sugar protons of C19 discriminate between G20 and G1. In addition to the three G-runs G1-G2-G3, G6-G7-G8 and G20-G21-G22 it is possible to identify the single loop nucleotides T5 and C19 as well as the complete diagonal loop nucleotides A9-A13 through sequential H6/H8 to H1'/H2'/H2" sugar proton connectivities (Figure S4). Whereas NOE contacts unambiguously show that all guanosines of the already assigned three G-tracts each with a 2’-F-dG modification at their 5’-end are in an *anti* conformation, three additional guanosines with a *syn* glycosidic torsion angle are identified by their strong intranucleotide H8–H1' NOE as well as their downfield shifted C8 resonance (Figure S5). Although H8–H1’ NOE contacts for the latter G residues are weak and hardly observable in line with 5’*syn*-3’*syn* steps, an NOE contact between G15 H1' and G14 H8 can be detected on closer inspection and corroborate the *syn*-*syn* arrangement of the connected guanosines. Apparently, the quadruplex assumes a (3+1) topology with three G-tracts in an all-*anti* conformation and with the fourth antiparallel G-run being in an all-*syn* conformation.

In the absence of G imino assignments, the cyclic arrangement of hydrogen-bonded G nucleotides within each G-tetrad remains ambiguous and the structure allows for a topology with one lateral and one diagonal loop as in the unmodified quadruplex but also for a topology with the diagonal loop substituted for a second lateral loop. In order to resolve this ambiguity and to reveal changes induced by the modification, the native ODN(0) sequence was independently measured and assigned in line with the recently reported ODN(0) structure (see Table S2).[3] The spectral similarity between ODN(0) and ODN(1,6,20) is striking for the 3'-tetrad as well as for the propeller and diagonal loop, demonstrating the conserved overall fold (Figures S6 and S7).

Consistent with a switch of the glycosidic torsion angle, guanosines of the 5'-tetrad show the largest changes followed by the adjacent central tetrad and the only identifiable residue of the lateral loop, i.e. C19. Knowing the cyclic arrangement of G-tracts, G imino protons can be assigned based on the rather weak but observable imino–H8 NOE contacts between pairs of Hoogsteen hydrogen-bonded guanine bases within each tetrad (Figure S4c). These assignments are further corroborated by continuous guanine imino–imino sequential walks observed along each G-tract (Figure S8).

Additional confirmation for the structure of ODN(1,6,20) comes from new NOE contacts observed between T5 H1' and G6 H8 as well as between C19 H1' and G20 H8 in the modified quadruplex. These are only compatible with G6 and G20 adopting an anti conformation and conserved topological features (Figure S9).

[3] M. Marušič, P. Šket, L. Bauer, V. Viglasky, J. Plavec, *Nucleic Acids Res*. **2012**, *40*, 6946-6956.

Table S1. ^{1}H and ^{13}C chemical shifts δ (in ppm) of protons and C8/C6 in ODN(1,6,20)[a]

	imino	H8/H6	H2/H5/Me	H1‘	H2‘/H2“[b]	H3‘	C8/C6
G1	11.57	7.99	---	6.15	5.60	4.87	134.94
G2	11.32	7.71	---	6.24	2.58/2.71	4.96	135.04
G3	11.18	7.61	---	6.19	2.58/2.64	4.99	134.81
A4	---	8.57	8.33	8.59	2.89/2.94	4.91	140.13
T5	n.d.	7.84	2.02	6.55	2.58/2.64	5.02	137.54
G6	11.52	8.01	---	6.03	5.40	4.86	135.42
G7	11.35	7.77	---	6.00	2.59/2.69	5.03	135.17
G8	11.11	7.52	---	5.92	2.13/2.41	4.95	134.14
A9	---	8.05	7.76	6.04	2.52/2.68	4.95	138.93
C10	---	7.57	5.91	5.86	1.79/2.17	4.58	140.78
A11	---	7.83	7.67	5.75	2.10/2.37	4.48	138.91
C12	---	7.02	5.18	5.51	1.73/2.00	4.38	140.98
A13	---	7.88	7.76	5.78	2.29/2.62	4.74	138.61
G14	11.37	7.22	---	6.04	3.10/3.66	n.d.	138.64
G15	11.43	7.33	---	5.81	2.81/2.93	n.d.	137.96
G16	10.94	7.52	---	5.83	2.32/2.65	n.d.	138.60
G17	n.d.	n.d.	---	n.d.	n.d.	n.d.	n.d.
A18	---	n.d.	n.d.	n.d.	n.d.	n.d.	n.d.
C19	---	7.31	5.74	5.60	2.14/2.37	4.59.	140.19
G20	11.68	8.24	---	5.85	5.81	4.97	135.98
G21	11.54	7.69	---	6.01	2.57/2.68	5.05	135.09
G22	11.43	7.87	---	6.34	2.44/2.59	4.68	134.98

[a] At 25 ^{o}C in 90% H_2O/10% D_2O, 10 mM potassium phosphate buffer, pH 7.0; n.d. = not determined.

[b] No stereospecific assignments.

Table S2. ^{1}H and ^{13}C chemical shifts δ (in ppm) of protons and C8/C6 in ODN(0)[a]

	imino	H8/H6	H2/H5/Me	H1‘	H2‘/H2”[b]	H3‘	C8/C6
G1	11.65	7.57	---	6.22	2.73/3.29	5.05	138.89
G2	11.63	7.96	---	6.01	2.56/2.75	5.07	135.44
G3	11.06	7.62	---	6.23	2.67/2.74	5.07	134.58
A4	---	8.58	8.31	6.61	2.90/2.94	4.87	139.91
T5	n.d.	7.87	2.03	6.62	2.64	5.07	137.43
G6	11.61	7.25	---	6.00	2.97/3.09	4.90	139.00
G7	11.60	7.84	---	5.78	2.63	5.09	135.62
G8	11.11	7.53	---	5.95	2.12/2.44	4.96	134.01
A9	---	8.05	7.70	6.02	2.70/2.57	4.98	138.93
C10	---	7.60	5.89	5.88	1.74/2.15	4.61	140.74
A11	---	7.88	7.61	5.74	2.05/2.36	4.43	138.68
C12	---	7.03	5.13	5.58	1.64/1.99	4.39	140.56
A13	---	7.90	7.74	5.85	2.48/2.71	4.78	138.75
G14	11.05	7.26	---	6.05	3.04/3.47	4.88	138.95
G15	11.37	7.38	---	5.79	2.54	4.99	138.13
G16	11.62	7.67	---	5.95	2.54/2.58	5.05	135.01
G17	n.d.	8.10	---	6.07	2.65/2.76	4.92	137.19
A18	---	7.80	7.59	6.06	2.13/2.37	4.75	138.37
C19	---	7.51	5.72	5.77	1.76/2.37	4.64	140.71
G20	11.82	7.42	---	6.02	2.97/3.59	n.d.	139.455
G21	11.94	7.93	---	5.82	2.53/2.71	5.07	135.82
G22	11.25	7.76	---	6.29	2.50	4.68	134.83

[a] At 25 ^{o}C in 90% H_2O/10% D_2O, 10 mM potassium phosphate buffer, pH 7.0; n.d. = not determined.

[b] No stereospecific assignments.

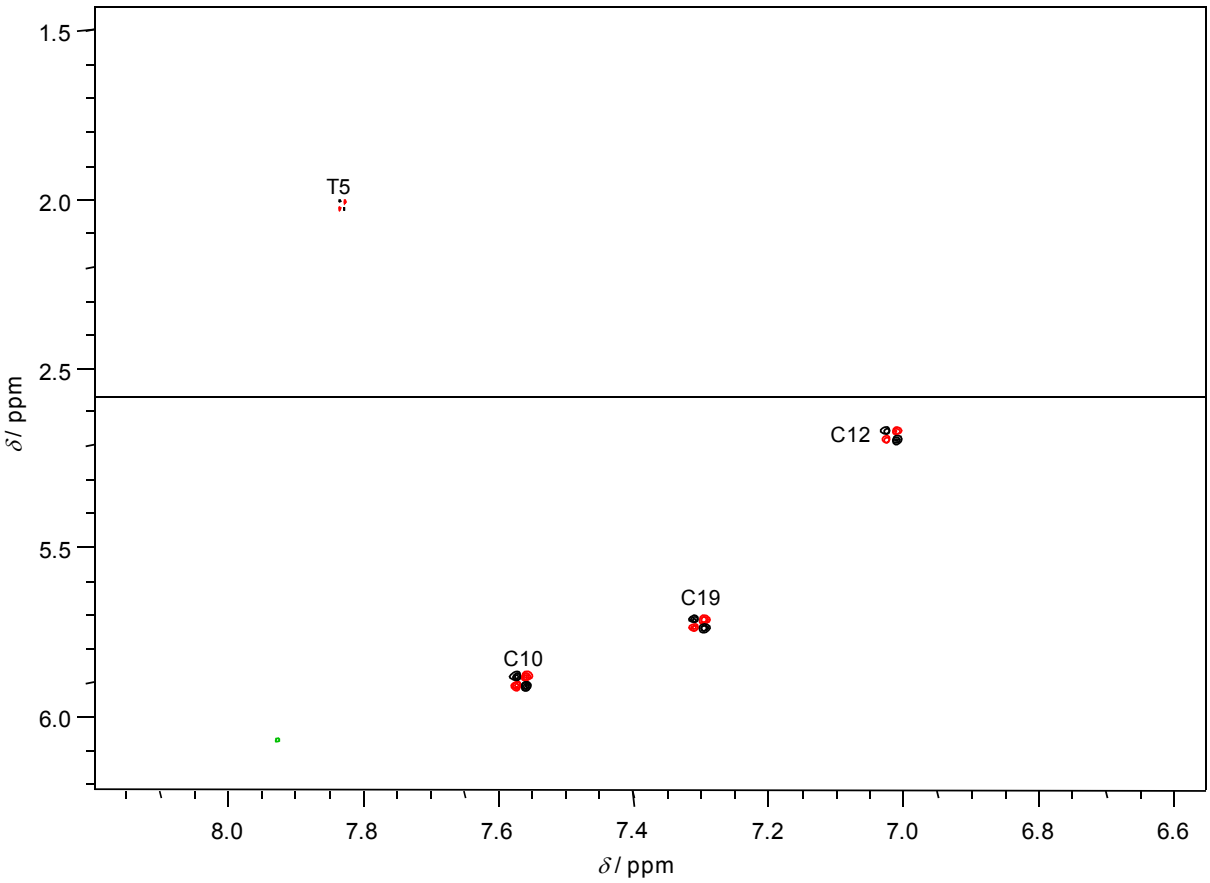

Figure S2. DQF-COSY spectrum of ODN(1,6,20) acquired in D_2O at 25 °C, showing spectral regions with thymidine H6–Me (top) and cytosine H5–H6 correlation peaks (bottom).

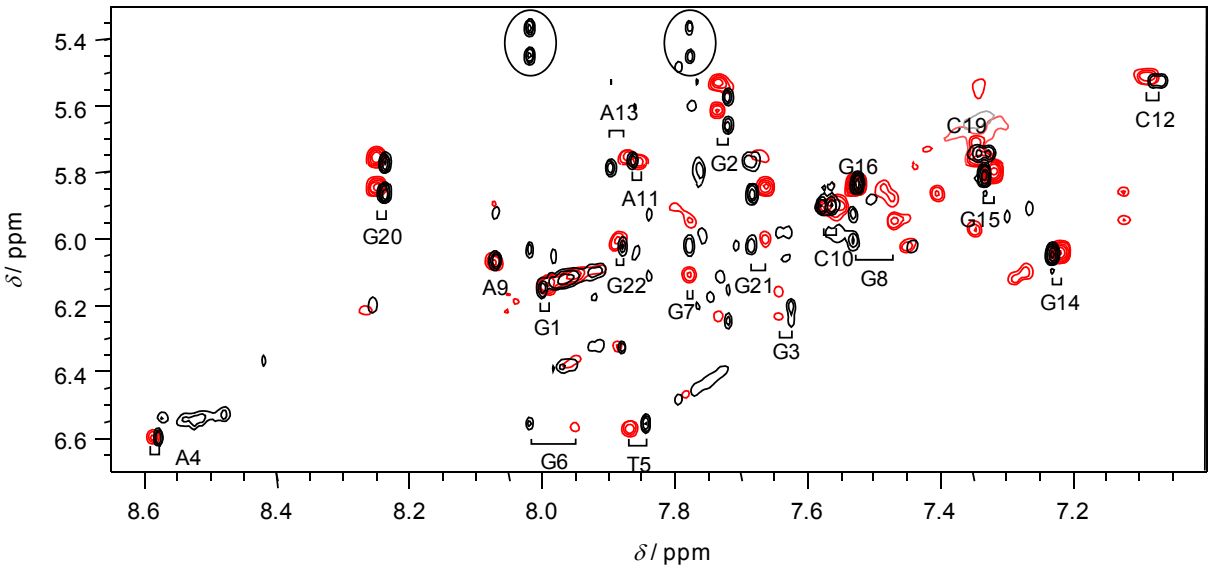

Figure S3. Superposition of the H8/H6–H1'/H5 2D NOE spectral region of ODN(1,20) (red) and ODN(1,6,20) (black); observed chemical shift changes of H8/H6 crosspeaks along ω_2 are indicated. Typical H2' doublets through ^{1}H-^{19}F scalar couplings along ω_1 are highlighted by circles for the 2'-F-dG analog at position 6 of ODN(1,6,20); T = 25 ^{o}C, τ_m = 300 ms.

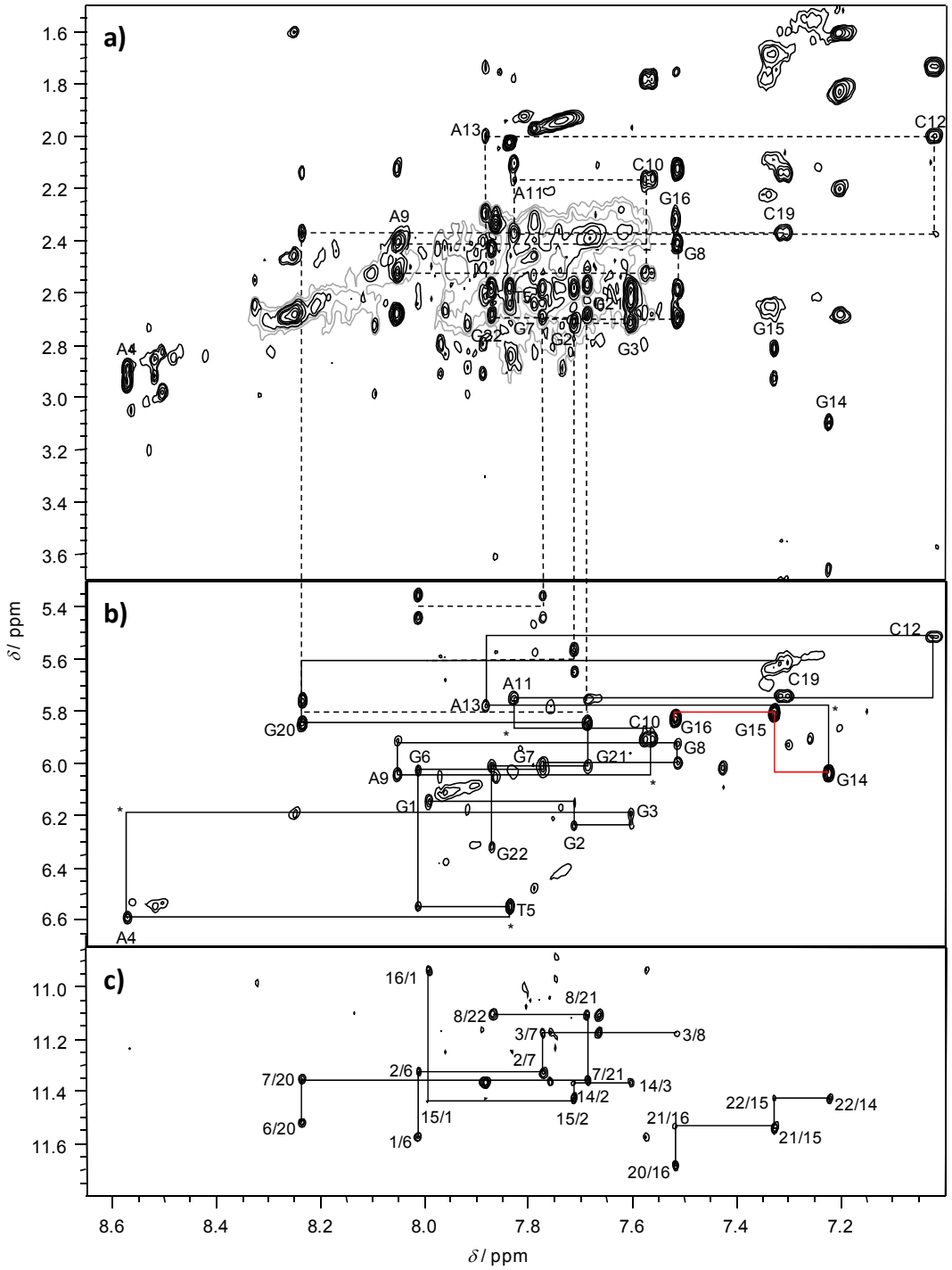

Figure S4. 2D NOE spectrum of ODN(1,6,20) acquired at 25 °C (τ_m = 300 ms). a) H8/H6–H2'/H2" region; for better clarity, only one of the two H2' sugar protons was used to trace NOE connectivities by the broken lines. b) H8/H6–H1'/H5 region with sequential H8/H6–H1' NOE walks traced by solid lines; note, that H8–H1' connectivities along G14-G15-G16 (colored red) are mostly missing in line with an all-*syn* conformation of the guanosines; additional missing NOE contacts are marked by asterisks. c) H8/H6–imino region with intratetrad and intertetrad guanine H8–imino contacts indicated by solid lines.

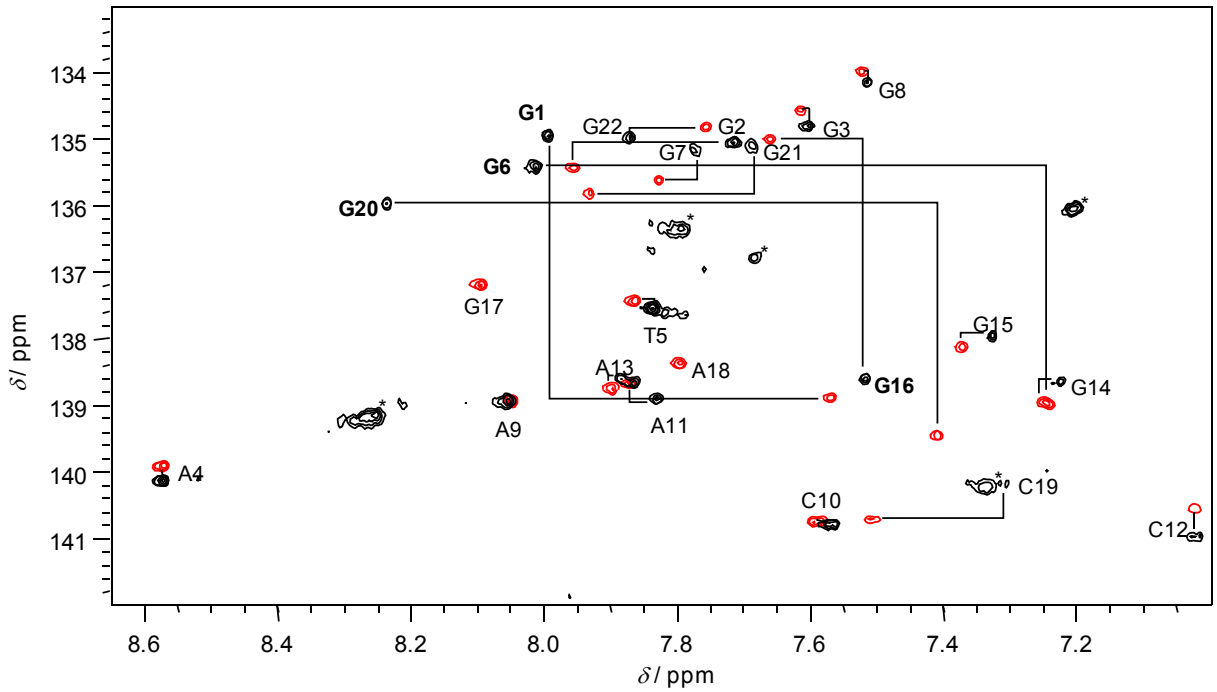

Figure S5. Superposition of ^{1}H-^{13}C HSQC spectra acquired at 25 ^{o}C for ODN(0) (red) and ODN(1,6,20) (black) showing the H8/H6–C8/C6 spectral region; relative shifts of individual crosspeaks in the two quadruplexes are indicated by the horizontal and vertical lines with emphasis on the largest chemical shift changes as observed for G1, G6, G16 and G20. Note, that corresponding correlations of G17 and A18 are not observed for ODN(1,6,20) whereas the correlations marked by asterisks must be attributed to additional minor species.

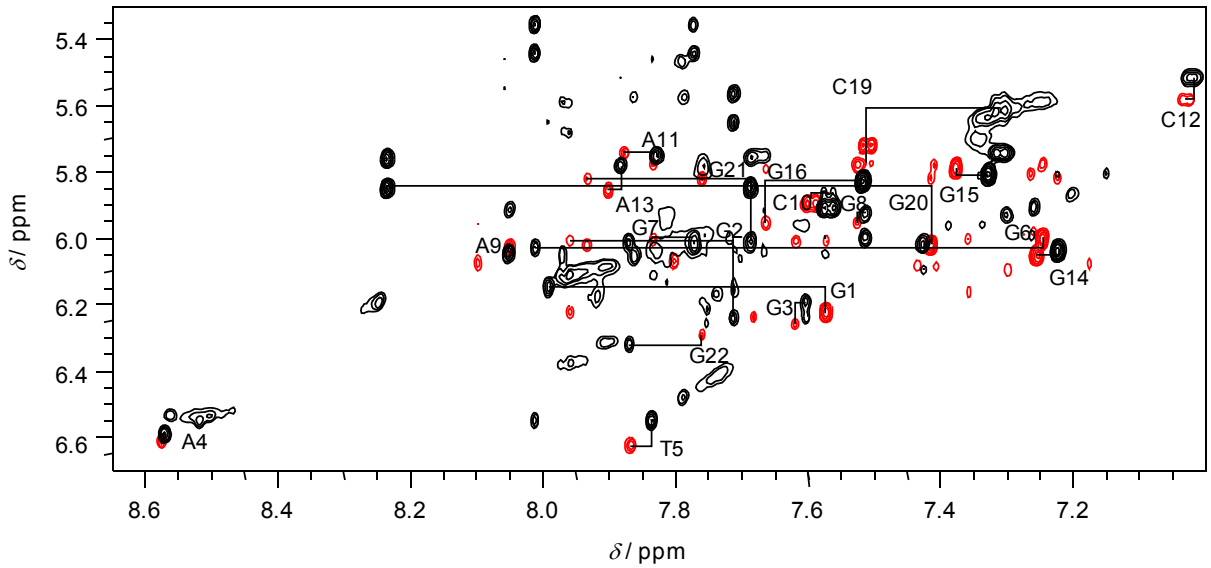

Figure S6. Superposition of the H8/H6–H1'/H5 2D NOE spectral region of ODN(0) (red) and ODN(1,6,20) (black); relative shifts of individual H8/H6–H1' crosspeaks in the two quadruplexes are indicated by the horizontal and vertical lines. Note the close similarity of chemical shifts for residues G8 to G14 comprising the 5 nt loop; T = 25 ^{o}C, τ_m = 300 ms.

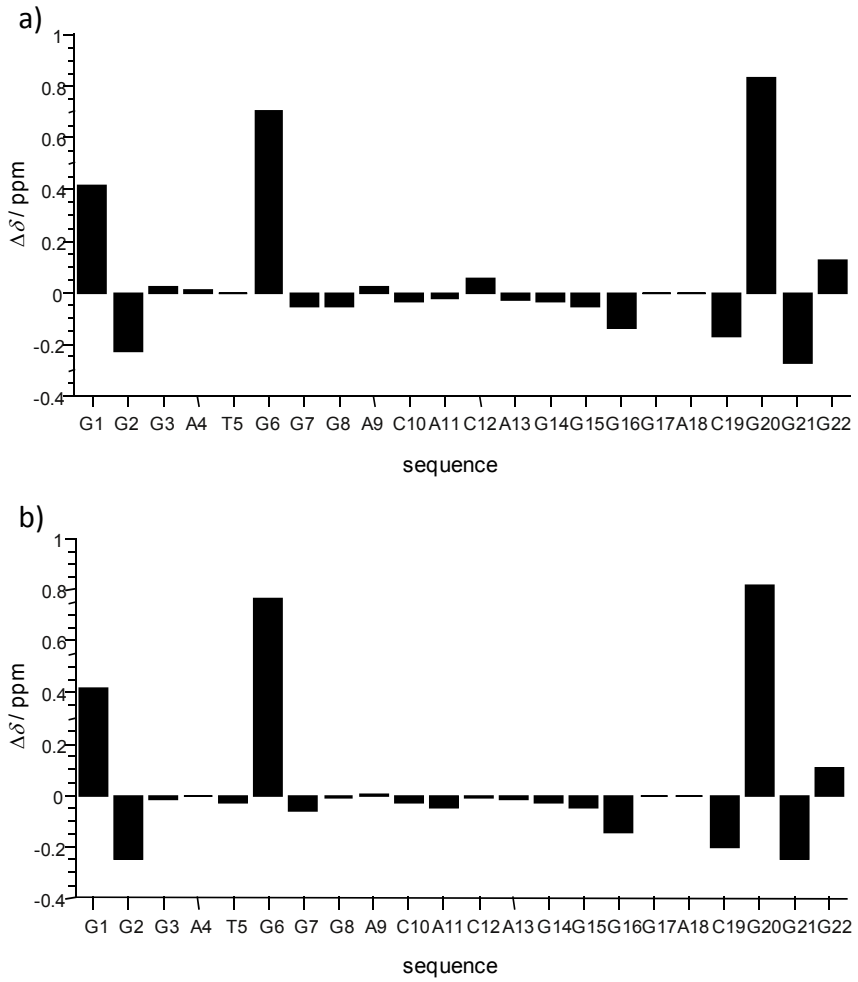

Figure S7. H8/H6 chemical shift differences in a) ODN(1,20) and b) ODN(1,6,20) when compared to unmodified ODN(0) at 25 ^{o}C; note, that the additional 2'-fluoro analog at position 6 in ODN(1,6,20) has no significant influence on the base proton chemical shift; due to their faster dynamics and associated signal broadening, base protons of G17 and A18 within the lateral loop have not been assigned.

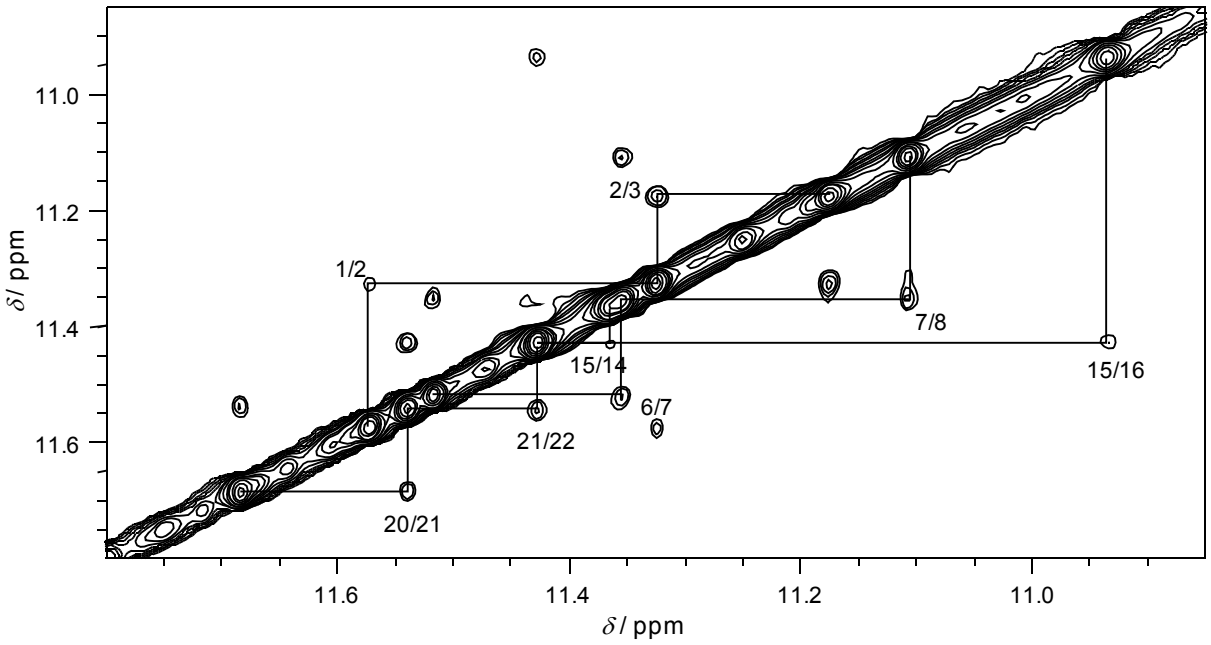

Figure S8. Portion of a 2D NOE spectrum of ODN(1,6,20) showing guanine imino–imino contacts along the four G-tracts; T = 25 ^{o}C, τ_m = 300 ms.

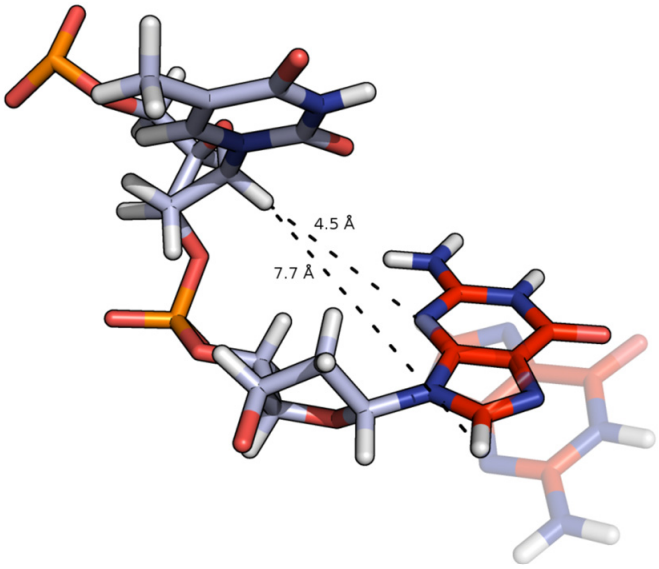

Figure S9. Interproton distance between T5 H1' and G6 H8 with G6 in an *anti* (in the background) or *syn* conformation; as a first approximation, the structure of the T5-G6 step was adopted from the published NMR structure of ODN(0) (PDB ID: 2LOD).

Article III [1]

[1] Reprinted with permission from 'Tracing Effects of Fluorine Substitutions on G-Quadruplex Conformational Changes', Dickerhoff, J., Haase, L., Langel, W., and Weisz, K., *ACS Chemical Biology*, ASAP, DOI: 10.1021/acschembio.6b01096. Copyright 2017 American Chemical Society.

Tracing Effects of Fluorine Substitutions on G-Quadruplex Conformational Transitions

Jonathan Dickerhoff, Linn Haase, Walter Langel, and Klaus Weisz*

Institute of Biochemistry, Ernst-Moritz-Arndt University Greifswald, Felix-Hausdorff-Str. 4, D-17487 Greifswald, Germany

Corresponding Author

*E-mail: weisz@uni-greifswald.de. Fax: (+49) 3834 86-4427. Phone: (+49) 3834 86-4426.

Author Contributions

The manuscript was written through contributions of all authors. All authors have given approval to the final version of the manuscript.

ABSTRACT: A human telomere sequence that folds into an intramolecular (3+1)-hybrid G-quadruplex was modified by the incorporation of 2'-fluoro-2'-deoxyriboguanosines (^{F}G) into *syn* positions of its outer tetrad. A circular dichroism and NMR spectral analysis reveals a nearly quantitative switch of the G-tetrad polarity with concerted *syn*↔*anti* transitions of all four G residues. These observations follow findings on a ^{F}G-substituted (3+1)-hybrid quadruplex with a different fold, suggesting a more general propensity of hybrid-type quadruplexes to undergo a tetrad polarity reversal independent of overhang sequences and type of loops. Two out of the three ^{F}G analogs in both modified quadruplexes adopt an S-type sugar pucker, challenging a sole contribution of N-type sugars in enforcing an *anti* glycosidic torsion angle associated with the tetrad flip. NMR restrained three-dimensional structures of the two substituted quadruplexes reveal a largely conserved overall fold but significant rearrangements of the overhang and loop nucleotides capping the flipped tetrad. Sugar pucker preferences of the ^{F}G analogs may be rationalized by different orientations of the fluorine atom and its resistance to be positioned within the narrow groove with its highly negative electrostatic potential and spine of water molecules.

Guanine-rich DNA or RNA sequences can fold into four-stranded structures called G-quadruplexes (G4). These secondary structures feature at least two stacked tetrads consisting of a planar arrangement of four guanine (G) bases that are connected via Hoogsteen hydrogen bonds and further stabilized by the coordination of cations, mostly potassium ions, in the central channel of the G-tetrad core. Despite their relatively uniform sequences, DNA quadruplexes exhibit high structural variability. Thus, folding into G4 structures can result in parallel, (3+1)-hybrid, or antiparallel topologies with four, three, or two parallel G-tracts, respectively. Structural polymorphism is strongly associated with glycosidic torsion angles of individual nucleotides, the G4 molecularity, the type of coordinated cations as well as the composition of loop and overhang sequences.[1] Interestingly, RNA quadruplexes are mostly found to adopt a parallel topology and thus contrast with DNA G4. A notable exception to this RNA topological preference involves an aptamer with a G4 core embedded in an unusual secondary structure.[2]

Based on overwhelming evidence for the existence of quadruplex structures *in vivo*, increasing efforts have recently been directed towards a better understanding of their role in cellular processes and their use as novel targets for anticancer therapeutics.[3,4] On the other hand, the quadruplex scaffold with

its unique properties has also been recognized as a powerful platform for various technological applications, e.g. as biosensor, aptamer, or DNAzyme.[5,6] Clearly, a detailed knowledge of driving forces correlating a primary sequence with its particular G-quadruplex fold is highly desirable for influencing folding pathways, for expanding the conformational landscape, and for optimizing quadruplex specific properties. One approach for disentangling contributions to folding makes use of local structural perturbations and their impact on the parent structure through the incorporation of modified residues.[7] In many cases, positions within the G4 core have been targeted through their replacement by nucleotide analogs with either matching or non-matching glycosidic torsion angles. Thus, large bromine and methyl substituents at guanine C8 favor *syn* glycosidic conformations due to steric interactions. Likewise, modified ribose sugars may enforce a *north* (N) sugar pucker thought to be strongly correlated with an *anti* glycosidic conformation.[8] The latter preference often induces a parallel topology in antiparallel or (3+1)-hybrid quadruplexes after substitutions at appropriate sites.[9,10] Alternatively, a polarity reversal for the G-tetrad following the 5'-end (5'-tetrad) in a parallel tetramolecular quadruplex was observed after substitutions with 8-bromo- or 8-methylguanosine analogs.[11,12] Recently, such a complete tetrad flip without any refolding into a parallel topology was also found for the 5'-tetrad of an artificial monomolecular (3+1)-hybrid quadruplex modified with 2'-fluoro-2'-deoxyriboguanosine (^{F}G).[13] A corresponding tetrad polarity reversal was again realized in subsequent studies through 8-bromoguanosine modifications in a parallel *MYC* quadruplex or through the incorporation of an 8-oxoguanine-xanthine pair in a human telomeric sequence (HT).[14,15]

The present studies aim to generalize the concept of an ^{F}G-induced tetrad reversal by extending substitution experiments to a (3+1)-hybrid structure with a different fold. Structural and thermodynamic studies demonstrate the presence of site-specific sugar conformations and their variable impact on G4 stability and conformational transitions. Finally, NMR restrained high-resolution structures of modified quadruplexes are presented and reveal noticeable adjustments of nucleotides in overhang and loop sequences that cap the flipped outer G-tetrad.

RESULTS AND DISCUSSION

Reverting the Tetrad Polarity of a Human Telomeric Quadruplex. Previously, G residues were substituted with ^{F}G analogs in the outer tetrad of the artificial ODN quadruplex, inducing a tetrad polarity switch.[13] The ODN structure comprises a propeller, diagonal, and lateral loop but lacks overhang sequences at both its 5'- and 3'-end (Figure 1a).[16] The question arises if such a tetrad flip is promoted by its long five-nucleotide (5-nt) loop favoring the diagonal arrangement and/or by missing

overhangs and thus limited to G4s with specific structural features. To resolve this issue and to possibly expand on past findings, we studied a human telomeric (HT) sequence likewise adopting a (3+1)-hybrid structure but with 5'- and 3'- overhang sequences.[17] Also, the diagonal loop found in ODN is replaced in HT by a second lateral loop associated with a different G-tract arrangement (Figure 1b). Notably, the HT quadruplex with its TTA loops is known to easily adopt different folds depending on the overhang composition, the cation present or molecular crowding conditions.[18,19]

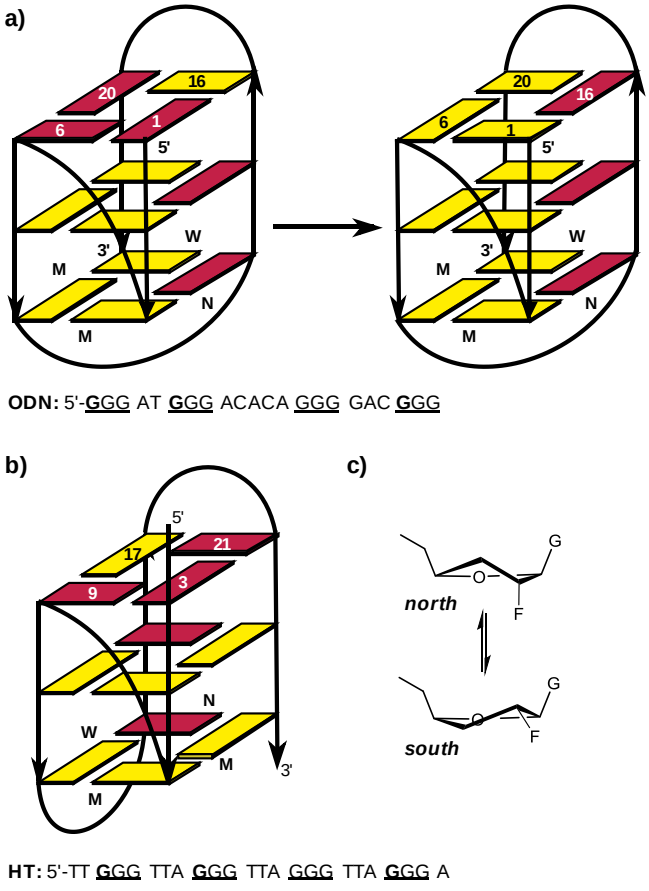

HT: 5'-TT GGG TTA GGG TTA GGG TTA GGG A

Figure 1. Schematic representation and sequence of the (a) ODN and (b) HT quadruplex with *syn* (red) and *anti* (yellow) G residues and narrow (N), medium (M), and wide grooves (W). For ODN, a transition involving a 5'-tetrad flip is indicated. (c) N-S equilibrium for the 2'-fluoro-2'-deoxyriboguanosine (^{F}G) analog.

In analogy to previous studies on ODN, the three *syn* positions 3, 9, and 21 of the 5'-tetrad were substituted with ^{F}G to yield the sequence ^{F}HT. Circular dichroism (CD) spectra were acquired for an initial structural characterization. CD spectral signatures strongly depend on the polarity of stacked tetrads and can generally be correlated with three G4 structural types.[20,21] For type I, the glycosidic

torsion angles do not change along the G-tracts resulting in a Hoogsteen hydrogen bond network of the same polarity within every tetrad. Such a homopolar stacking is indicated by negative and positive CD bands at about 240 and 270 nm, respectively. Alternation of glycosidic conformations in type III structures is responsible for the heteropolar stacking of tetrads with different polarity associated with negative and positive bands at about 270 and 295 nm. The simultaneous occurrence of both homo- and heteropolar stacking interactions (type II) as exemplified by (3+1)-hybrid structures leads to a superposition of type I and III spectra and two positive CD bands at about 270 and 295 nm.

Apparently, whereas the latter pattern is observed for native HT the CD spectrum changes noticeably towards a type I structure for the ^{F}G-modified ^{F}HT (Figure 2a). Such a transition has its precedence in ^{F}G-modified ^{F}ODN and indicates pure homopolar stacking as a result of a 5'-tetrad polarity switch or of refolding into a parallel structure.

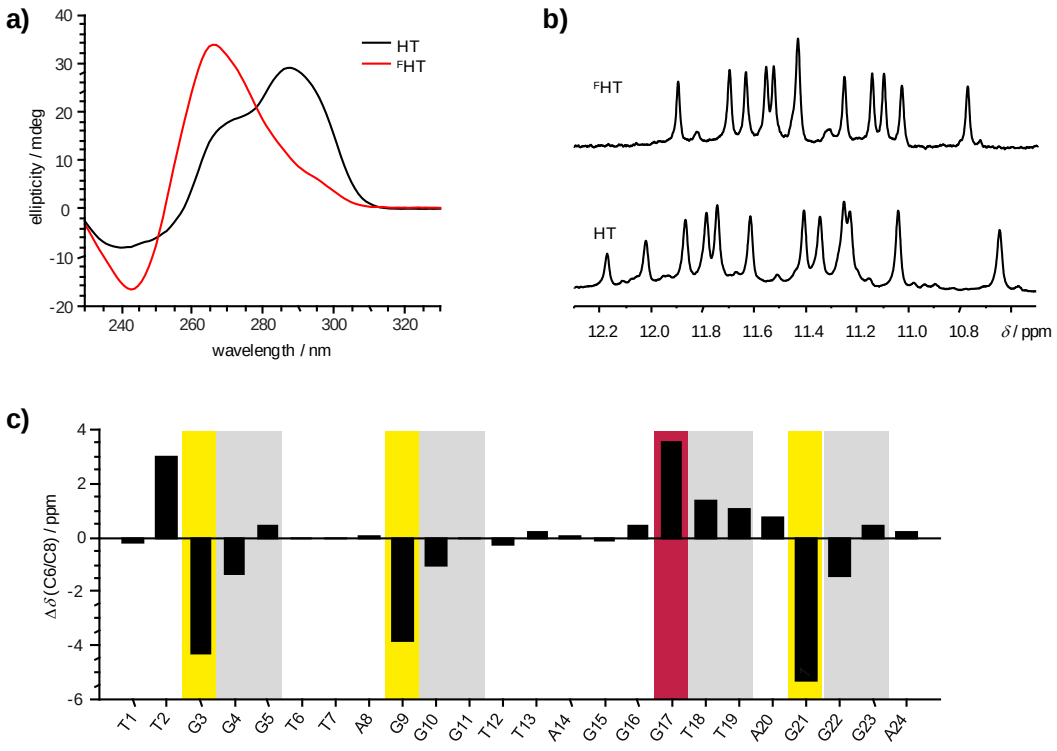

Figure 2. (a) CD spectra and (b) NMR spectra showing the imino proton spectral region of HT and the modified ^{F}HT quadruplex. (c) C6/C8 ^{13}C chemical shift differences between ^{F}HT and HT.

More structural information comes from NMR measurements. In full agreement with the presence of a single well-defined quadruplex with three tetrads, ^{1}H NMR spectra of both HT and ^{F}HT sequences

exhibit twelve sharp signals in the imino region between 10.6 and 12.2 ppm partially shifted for the ^{F}G-modified G4 (Figure 2b). The assignment of most proton and C6/C8 carbon resonances is based on NOESY, DQF-COSY, HSQC, and HMBC experiments as shown in the Supporting Information (Figures S1 and S2).

Fortunately, ^{F}G residues can easily be identified by a characteristic E.COSY-type pattern of their H1'-H2' NOE crosspeaks as well as their deshielded H2' protons, making them convenient starting points for further assignments (Figure S1). A careful inspection of NOE patterns for ^{F}HT shows that most contacts are conserved when compared to the native sequence. However, a polarity reversal of the 5'-tetrad is indicated by new H8-H1 NOE contacts and altered intensities of H8-H1' crosspeaks in line with base rotations around the glycosidic bond. Following the approach used previously for ^{F}ODN, this structural rearrangement can firmly be established through the strong dependence of C6/C8 chemical shifts on glycosidic torsion angles with *syn* and *anti* conformations differing in $\delta(^{13}C)$ by ~4 ppm.[22,23] As shown in Figure 2c, corresponding effects on chemical shift differences between ^{F}HT and HT are exclusively observed for G residues of the 5'-tetrad and T2 located in the 5'-overhang. Whereas guanine C8 resonances of G3, G9, and G21 in ^{F}HT experience a significant upfield shift typical of a *syn*→*anti* transition, C8/C6 of G17 and T2 exhibit downfield shifts indicating an *anti*→*syn* conversion. In contrast, nucleotides within the central tetrad and the 5'-lateral loop are only moderately affected due to their proximity to the flipped tetrad and there is a negligible impact on the remaining residues.

Taken together, the introduction of three ^{F}G analogs in the (3+1)-hybrid HT structure promotes a concerted flip of all four G residues within the 5'-outer tetrad as has already been observed for the correspondingly modified ^{F}ODN quadruplex.[13] Consequently, this structural rearrangement induced by specific ^{F}G perturbations seems to be a more general feature of hybrid-type G4 structures irrespective of loop composition or overhang sequences.

Sugar Pucker and Positional Differences. With the tetrad flip being a common feature of (3+1)-hybrid structures with appropriate ^{F}G modifications, the impact of sugar conformation and substitution site on the tetrad polarity reversal was assessed in more detail. The 2'-fluoro-2'-deoxyribose sugar is known to strongly favor *north* (N) over *south* (S) conformations both in solution and in duplexes (see also Figure 1c).[24–26] Moreover, it is generally accepted that this preference constitutes the major driving force for adopting an *anti* glycosidic torsion angle. To probe sugar conformations of the ^{F}G analogs within the present quadruplexes, vicinal scalar couplings between H1' and H2' protons were evaluated. These couplings are highly dependent on sugar pucker and yield typical values of $^{3}J_{H1'\text{-}H2'} > 6$ Hz for S conformers but much smaller couplings < 3 Hz for N-type sugars.[25,27]

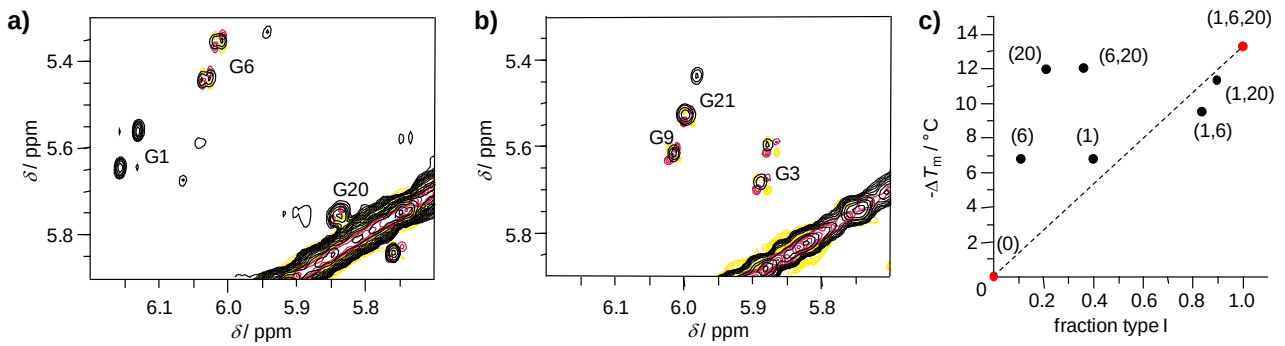

Figure 3. Superposition of NOESY (black) and DQF-COSY (colored) spectra showing H1'-H2' crosspeaks of ^{F}G residues in (a) ^{F}ODN and (b) ^{F}HT. Note, that ^{F}G nucleotides display an E.COSY-type pattern due to additional ^{19}F passive couplings. (c) Correlation between thermal destabilization and extent of structural conversion to type I quadruplexes for different ^{F}G substituted ODN analogs; numbers in parentheses denote the substitution sites.

Figures 3a and 3b show an overlay of NOESY and DQF-COSY spectra with crosspeaks between H1' and H2' protons of all ^{F}G analogs in modified ^{F}ODN and ^{F}HT quadruplexes. Although close to the diagonal (^{F}G20 in ^{F}ODN) or partially overlapped (^{F}G9 and ^{F}G21 in ^{F}HT) intranucleotide H1'-H2' NOE contacts are easily identified for all incorporated ^{F}G analogs in the 2D NOE spectra. In contrast, corresponding DQF-COSY spectra reveal H1'-H2' COSY crosspeaks for all ^{F}G residues except for ^{F}G1 in ^{F}ODN and ^{F}G21 in ^{F}HT. Apparently, the latter must adopt an N-type pucker resulting in the cancellation of crosspeaks with their characteristic antiphase pattern due to small $^{3}J_{H1'-H2'}$.couplings. This is further corroborated by their weaker H8-H2' NOE contacts.

Notably, the observation of strong DQF-COSY crosspeaks for two out of three ^{F}G analogs in each quadruplex points to $^{3}J_{H1'-H2'}$ couplings > 6 Hz and demonstrates their *south* conformation. These unexpected results being the first experimental evidence of ^{F}G adopting an S conformation raise important questions as to the correlation between sugar pucker and glycosidic torsion angle. Which contribution to the tetrad reversal if any can be expected for the differently puckered ^{F}G-modifications? In an effort to address these issues, CD spectra and thermal stabilities were compared for a family of ODN analogs. These comprise all seven possible combinations of *syn* dG to ^{F}G substitutions within the ODN 5'-tetrad and were either taken from previous studies[13] or newly prepared.

An isoelliptic point at about 280 nm observed for the entire ODN family of quadruplexes points to only a minor difference between G and ^{F}G with respect to their optical properties (Figure S3).

Consequently, a simplified analysis based on a two-state model for the structural conversion and ODN/^{F}ODN used as reference for pure type II/type I topologies was applied to derive molar fractions of the species. In Figure 3c the ^{F}G-induced decrease in melting temperatures -ΔT_m is plotted against the fraction of formed type I quadruplex. A single substitution leads to a thermal destabilization of about 7 °C at position 1 and 6 and of about 12 °C at position 20. Although additional ^{F}G modifications result in a further decrease of T_m, their effects are clearly non-additive with ^{F}G20 exerting a maximum destabilizing effect on all the quadruplexes. In contrast, ^{F}G1 seems to be most influential with regard to the conformational transition. Thus, singly substituted ODN(1) comprises about 40 % of type I G4 and is therefore as effective as ODN(6,20) bearing two ^{F}G modifications. Because ^{F}G1 was shown to be the only analog with N-type sugar, a *north* conformation is indeed suggested to play a significant role for tetrad reversal. However, for a more quantitative rearrangement with > 80 % population of homopolar stacked quadruplex at least one additional S-puckered 2'-fluoro-dG analog is required. Incorporation of an additional third analog with S conformation has only minor additional effects on the equilibrium. Overall, the N conformation seems to be a major albeit not the only contributor when driving the glycosidic torsion angle from *syn* towards *anti*.

Previously, similar shifts towards CD spectra of type I were observed for HT following single *syn* dG to ^{F}G substitutions.[28] Although positional dependencies on structure and stability have not been evaluated in more detail, similar trends with a major impact of *north* puckered ^{F}G replacements at position 21 of the HT quadruplex may be anticipated.

Structure Determination. In the following, the three-dimensional structure of ^{F}ODN and ^{F}HT was determined with molecular dynamics calculations in explicit water and NMR-derived distance and torsion angle restraints (see Table 1). Final RMSD values are similar to the values previously reported for the unmodified G4 structures.[16,17] An overlay of representative refined structures for parent and ^{F}G-substituted G4s reveal that the overall fold but also the G-core with its reversed 5'-tetrad is largely conserved for both of the modified quadruplexes (Figure 4). The largest deviations are found for the propeller loops as well as the lateral loop adjacent to the 5'-tetrad in ODN and the 5'-overhang in HT. Due to its high inherent flexibility and aggravated by recent adjustment of the applied force field with its significant impact on backbone torsions, the ODN diagonal loop with its rather broad range of conformations was excluded from a more detailed discussion.

Table 1. NMR restraints and structural statistics

	^{F}ODN	^{F}HT
distance restraints		
intramolecular	193	246
intermolecular		
sequential	99	107
long-range	34	60
other restraints		
hydrogen bonds	48	58
torsion angles	39	46
G-quartet planarity	36	36
structural statistics		
pairwise heavy atom RMSD (Å)		
G-tetrad core	0.79 ± 0.10	0.87 ± 0.12
all residues	2.66 ± 0.68	1.44 ± 0.39
violations		
mean NOE restraint violations	0.002 ± 0.001	0.004 ± 0.000
max. NOE restraint violations	0.103	0.131
max. torsion angle restraint violations	5.797	0.480
deviations from idealized geometry		
bonds (Å)	0.011 ± 0.000	0.011 ± 0.000
angles (°)	2.334 ± 0.039	2.403 ± 0.026

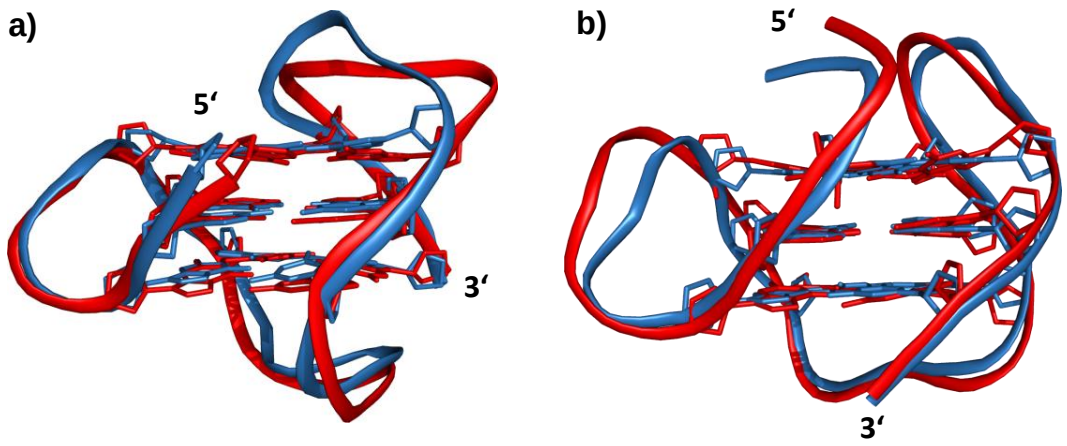

Figure 4. Superimposed representative structures of (a) ODN (blue, pdb: 2LOD) and ^{F}ODN (red) and (b) HT (blue, pdb: 2GKU) and ^{F}HT (red).

Structure of the 5'-tetrad. As expected, the modified tetrad itself is significantly altered due to the *syn*-*anti* flip of glycosidic torsions. The direction of the Hoogsteen hydrogen bond network is reversed and the stacking upon the central tetrad has changed considerably. While stacking interactions between the 5-membered rings of purines predominate in *syn*/*anti* steps, both *anti*/*anti* and *syn*/*syn* steps in the fluorinated quadruplexes result in a partial overlap between the 5- and 6-membered rings of stacked guanine bases (Figure 5).[29] As a result, they are reminiscent of parallel quadruplexes containing only tetrads of the same polarity. Energies of these different stacking interactions in quadruplexes were calculated previously by employing various dinucleotide steps but have shown only minor differences.[29–31]

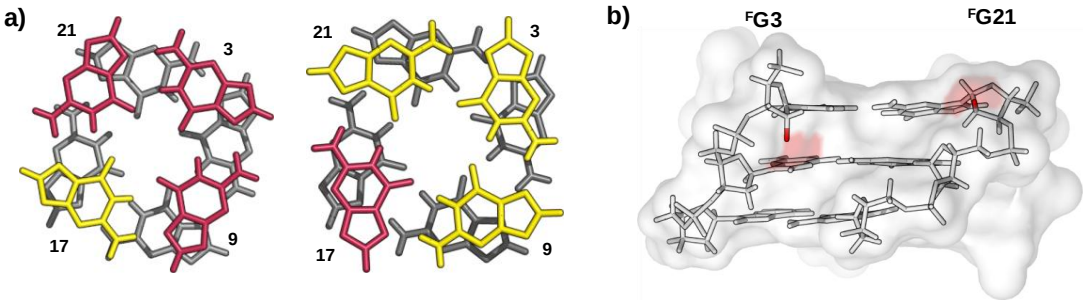

Figure 5. (a) Stacking of the 5'-tetrad on the central tetrad in HT (left) and ^{F}HT (right). (b) View into the medium-sized groove of ^{F}HT showing the orientation of fluorines (red) in ^{F}G3 and ^{F}G21.

As mentioned above, the application of different force fields and variation in methodologies hamper a more detailed comparison of backbone parameters in reported structures. However, the rigidity of the G-core ensures a limited occupancy of insignificant conformational states. Despite a base flip about the glycosidic bond accompanied by translational motions of the residues to maintain base stacking, crankshaft motions compensate for major structural aberrations along the sugar-phosphate backbone. A direct correlation is found between the glycosidic torsion angle and the dihedral angle γ (O5'-C5'-C4'-C3'), mostly adopting a gauche+ (g^+) conformation for *anti* glycosidic conformers as reported previously.[32] However, in case of *syn* nucleotides, an increase of unfavorable backbone-base interactions in particular for *N*-type puckered residues will result in a γ with increasingly populated gauche− (g^-) or trans (t) conformers. This trend is reflected by noticeable differences in γ for the native and modified sequences (see Figures S4 and S5). Thus, ^{F}G-substituted positions undergoing a *syn*→*anti* interconversion exhibit increased g^+ populations in both quadruplexes. Likewise, opposing trends are observed for the flipped (*anti*→*syn*) residue in the antiparallel G-tract. Smaller changes as

observed for ODN may be attributed to its less flexible lateral loop that spans the wide groove and may resist changes in γ. It should be noted, that actual γ populations are also sensitive towards additional environmental factors like preceding loops and overhang sequences and also show alterations as a consequence of the unrestrained backbone dihedral angles.

The sugar pucker preference for ^{F}G substitutions, thought to be linked to the quadruplex conformational transitions, seems to be of particular importance. Noticeably, both N-puckered residues ^{F}G1 (^{F}ODN) and ^{F}G21 (^{F}HT) are located adjacent to the antiparallel G-tract and border narrow and medium grooves on either side. Most strikingly, there is a correlation between the 2'-F orientation and the sugar conformation as visualized in Figure 5c for the ^{F}HT quadruplex. Adopting an S-type pucker, the fluorine of ^{F}G3 will point towards the central tetrad within the medium groove. On the other hand, a change to an N-type pucker in ^{F}G21 will reposition the fluorine away from the narrow groove and into the medium groove with 2'-F pointing away from the G-core. Apparently, as a consequence of the individual sugar puckers all fluorine atoms are located within the medium grooves and it is only the N conformation of ^{F}G21 that prevents its localization within the narrow groove. Generally, an N-type sugar pucker seems to be disfavored in the quadruplex but other interactions must override its more destabilizing effect. The narrow groove is characterized by short phosphate-phosphate distances leading to a highly negative electrostatic potential.[33] Hydration seems to be important for reducing the electrostatic repulsion as seen by a well-defined spine of water molecules in narrow grooves of antiparallel structures solved by X-ray crystallography.[34,35] This molecular arrangement can significantly be perturbed by a fluorine atom being negatively polarized but also hydrophobic.[36,37] Therefore, fluorine may not only increase the negative potential within the narrow groove but may also disrupt the compensating and stabilizing network of water molecules. Both effects will enhance the electrostatic repulsion between backbones and destabilize any G4 structure with a narrow groove. Avoiding such a situation should either favor parallel topologies or induce changes in the sugar pucker to redirect fluorine away from the narrow groove as observed in the present case. It should be noted, that these arguments likewise apply to ^{F}ODN with the same *syn*/*anti* pattern of ^{F}G analogs at corresponding substitution sites (*vide supra*, see also Figure 1).

Structure of Capping Motifs. In addition to the reversed 5'-tetrad, significant conformational changes are observed for the capping loops and overhangs in ^{F}ODN and ^{F}HT. The strained 3 nt lateral loop in native ODN spans the wide groove with a highly flexible A18 and with C19 and G17 stacked upon the G-core (Figure 6a). The tetrad reversal induces rearrangements in ^{F}ODN with a positional exchange of the two purine bases but only smaller reorientations of the cytosine base. This is a

consequence of backbone adjustments required to maintain favorable stacking interactions following the concerted flip of all G residues in the 5'-tetrad.

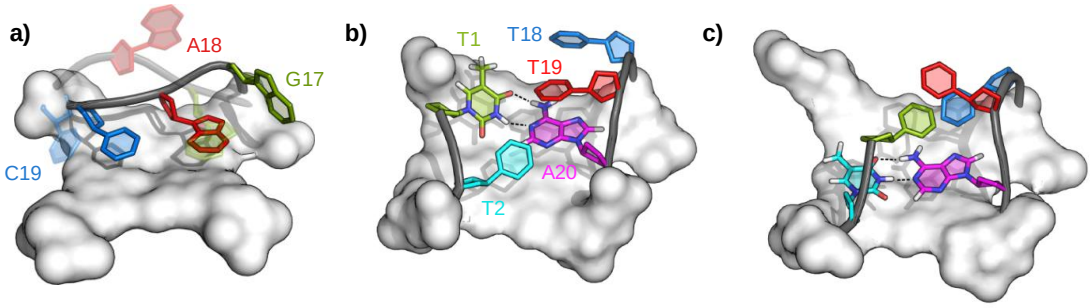

Figure 6. Capping motifs of the 5'-tetrad. (a) ODN (transparent) and ^{F}ODN (solid), (b) native HT, and (c) ^{F}HT.

On the other hand, a T1-A20 base pair formed between the 5'-overhang and the lateral loop stacks on the 5'-tetrad in HT (Figure 6b). In contrast to ODN, the 3 nt loop spans the narrow groove exhibiting a higher flexibility and a better ability to compensate for backbone conformational changes. Nevertheless, noticeable differences are found for ^{F}HT. Thus, as already indicated in Figure 2c, the T2 nucleotide changes from *anti* to *syn* and displaces T1 in the base pair with A20 (Figure 6c). Although the backbone seems to allow conservation of the native pairing, a closer look at the base pair positioning above the tetrad indicates a common stacking pattern (Figure 7). Thus, thymine is always located above the 6-membered ring of a G with its imino proton situated directly above the guanine carbonyl. Likewise, the 6-membered ring of A20 always stacks on a G carbonyl. Apparently, enabled by sufficient flexibility such a stacking pattern is preserved through a change of the T2 glycosidic torsion angle and its recruitment in a T2-A20 base pair.

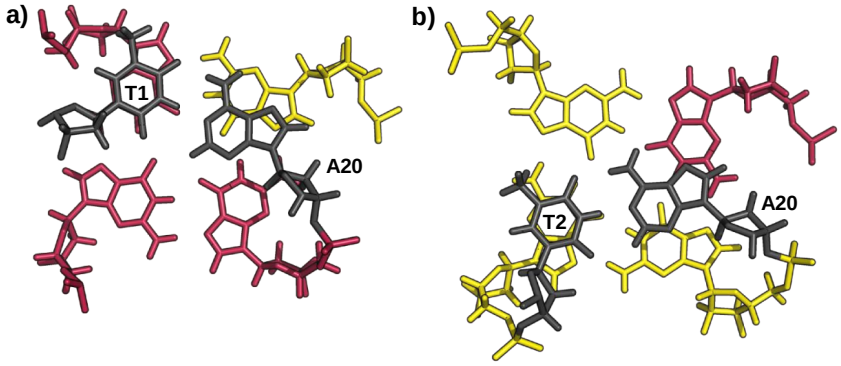

Figure 7. Stacking of overhang and loop residues on the 5'-tetrad in (a) HT and (b) ^{F}HT. Loop and overhang residues not involved in the base pairing are omitted for clarity.

CONCLUSIONS

The incorporation of nucleoside analogs with modified base or sugar into G-quadruplexes has increasingly been employed in the recent past. Being of particular importance for the quadruplex topology, pronounced preferences for a particular conformation around the glycosidic bond render G analogs powerful tools in the stabilization and refolding of G4 structures. Whereas substitutions at a matching position will often increase stability of the native fold, replacements at non-matching sites may be used for enforcing a different topology or conformation.

In the past, the 2'-fluoro-2'-deoxyguanosine residue when substituted for dG within the quadruplex core has been reported to favor *anti* conformations thought to be tightly connected with its N-type sugar. Accordingly, an *anti* preference for a single ^{F}G residue is found to play a critical role in driving the G-tetrad flip within the two different (3+1)-hybrid structures. However, a *south* sugar pucker shown to be favored for most ^{F}G analogs seems to support such a conformational transition in a similar way. Based on the analysis of NMR restrained high-resolution structures it is suggested that only an unfavorable fluorine interaction within the highly electronegative narrow groove may account for a *north*-puckered ^{F}G nucleoside. These unexpected findings testify to our still limited understanding of the delicate forces that balance within a quadruplex scaffold. It may even be speculated that in addition to other effects[38] similar unfavorable interactions of ribose 2'-OH substituents may contribute to the propensity of RNA to form parallel quadruplexes lacking a narrow groove.

Clearly, the different impact of substitution sites on stability or conformational transitions is of particular relevance to any application that makes use of G4 modifications. The present studies aim to give a structural basis for the site-specific ^{F}G perturbations and thus add to a more fundamental understanding of effects to be expected from a specific incorporation of G analogs. This not only supports a more rational design of quadruplexes for various applications but also yields a better understanding of interactions present in these highly polymorphic structures.

METHODS

Sample Preparation. Unmodified and 2'-fluoro-modified DNA oligonucleotides were purchased from *TIB MOLBIOL* (Berlin, Germany) and *Purimex* (Grebenstein, Germany), respectively. Following ethanol precipitation, the absorbance at 260 nm was used for their quantification. NMR samples with typical concentrations between 0.33 and 0.80 mM were obtained by dissolving the corresponding oligonucleotides in 10 mM potassium phosphate buffer, pH 7. For optical measurements, oligonucleotides were dissolved in 20 mM potassium phophate buffer, 100 mM KCl, pH 7, to give a

final concentration of 5 μM. Prior to measurements, the samples were annealed by heating to 90 °C followed by slow cooling to room temperature.

Cicular Dichroism. CD spectra were recorded at 20 °C with a *Jasco J-810* spectropolarimeter (*Jasco*, Tokyo, Japan) and subsequently blank corrected. Ten accumulations were acquired with a scanning speed of 50 nm/min and a bandwidth of 1 nm. To cover both bands the fraction of type I was calculated from 260-270 nm and 285-295 nm with $(\theta-\theta_{ODN})/(\theta_{FODN}-\theta_{ODN})$ and averaged.

UV Melting. Melting curves were recorded in triplicate on a *Cary 100* spectrophotometer equipped with a Peltier temperature control unit (*Varian*, Darmstadt, Germany) by following the absorbance at 295 nm between 10 and 90 °C. Quartz cuvettes of 10 mm path length were used and data points were measured in 0.5 °C intervals with heating rates of 0.2 °C/min. The intersection of the melting curve with the median of the fitted baselines was used to determine the melting point T_m.

NMR. All NMR spectra were acquired on a Bruker Avance 600 MHz spectrometer equipped with an inverse $^{1}H/^{13}C/^{15}N/^{31}P$ quadruple resonance cryoprobehead and z-field gradients. They were processed with Topspin 2.1 software and analyzed with CcpNmr Analysis.[39] Full experimental details are given in the Supporting Information.

Structure Refinement. The RED software was used to calculate the partial atomic charges on the HF/6-31G(d) level for the modified nucleotide ^{F}G.[40] Starting models from 100 extended structures were generated with a distance geometry simulated annealing protocol in Xplor-NIH 2.39.[41] Subsequently, restrained simulated annealing was performed with the Amber15 software in implicit water using the parmbsc0 force field including the χ_{OL4}, $\varepsilon\zeta_{OL1}$, and β_{OL1} corrections.[32,42–44] Ten lowest-energy structures were selected, equilibrated for 1 ns with explicit solvent, and shortly minimized in vacuum. Details of the calculation process can be found in the Supporting Information. Structural parameters were determined with the 3DNA software package.[45]

Data Deposition. Atomic coordinates of the ^{F}ODN and ^{F}HT G-quadruplexes have been deposited in the Protein Data Bank (accession codes 5MCR and 5MBR).

ASSOCIATED CONTENT

Supporting Information

The Supporting Information is available free of charge on the ACS Publications website at DOI...

Details on NMR experiments and structure calculations, 2D NMR spectra of ^{F}HT (Figures S1 and S2), CD spectra of native and ^{F}G substituted ODN quadruplexes (Figure S3), distribution of γ conformers for modified and unmodified ODN and HT (Figures S4 and S5).

REFERENCES

(1) Phan, A. T., Kuryavyi, V., Luu, K. N., and Patel, D. J. (2006) Chapter 3 in *Quadruplex Nucleic Acids* (Balasubramanian, S., and Neidle, S., Eds), RSC Publishing, Cambridge.

(2) Huang, H., Suslov, N. B., Li, N.-S., Shelke, S. A., Evans, M. E., Koldobskaya, Y., Rice, P. A., and Piccirilli, J. A. (2014) A G-quadruplex-containing RNA activates fluorescence in a GFP-like fluorophore. *Nat. Chem. Biol. 10*, 686–691.

(3) Murat, P., and Balasubramanian, S. (2014) Existence and consequences of G-quadruplex structures in DNA. *Curr. Opin. Genet. Dev. 25*, 22–29.

(4) Neidle, S. (2016) Quadruplex nucleic acids as novel therapeutic targets. *J. Med. Chem. 59*, 5987–6011.

(5) Sen, D., and Poon, L. C. H. (2011) RNA and DNA complexes with hemin [Fe(III) heme] are efficient peroxidases and peroxygenases: how do they do it and what does it mean? *Crit. Rev. Biochem. Mol. Biol. 46*, 478–492.

(6) Neo, J. L., Kamaladasan, K., and Uttamchandani, M. (2012) G-quadruplex based probes for visual detection and sensing. *Curr. Pharm. Des. 18*, 2048–2057.

(7) Sagi, J. (2014) G-quadruplexes incorporating modified constituents: a review. *J. Biomol. Struct. Dyn. 32*, 477–511.

(8) Saenger, W. (1984) *Principles of Nucleic Acid Structure* (Cantor, C. R., Ed.), Springer-Verlag, New York.

(9) Tang, C.-F., and Shafer, R. H. (2006) Engineering the quadruplex fold: nucleoside conformation determines both folding topology and molecularity in guanine quadruplexes. *J. Am. Chem. Soc. 128*, 5966–5973.

(10) Martín-Pintado, N., Yahyaee-Anzahaee, M., Deleavey, G. F., Portella, G., Orozco, M., Damha, M. J., and González, C. (2013) Dramatic effect of furanose C2′ substitution on structure and stability: directing the folding of the human telomeric quadruplex with a single fluorine atom. *J. Am. Chem. Soc. 135*, 5344–5347.

(11) Esposito, V., Randazzo, A., Piccialli, G., Petraccone, L., Giancola, C., and Mayol, L. (2004) Effects of an 8-bromodeoxyguanosine incorporation on the parallel quadruplex structure $[d(TGGGT)]_4$. *Org. Biomol. Chem. 2*, 313–318.

(12) Virgilio, A., Esposito, V., Randazzo, A., Mayol, L., and Galeone, A. (2005) 8-Methyl-2'-deoxyguanosine incorporation into parallel DNA quadruplex structures. *Nucleic Acids Res. 33*, 6188–

6195.

(13) Dickerhoff, J., and Weisz, K. (2015) Flipping a G-tetrad in a unimolecular quadruplex without affecting its global fold. *Angew. Chem. Int. Ed. 54,* 5588–5591.

(14) Karg, B., Haase, L., Funke, A., Dickerhoff, J., and Weisz, K. (2016) Observation of a dynamic G-tetrad flip in intramolecular G-quadruplexes, *Biochemistry* Epub Nov 15, 2016. DOI: 10.1021/acs.biochem.6b00925

(15) Cheong, V. V., Lech, C. J., Heddi, B., and Phan, A. T. (2016) Inverting the G-tetrad polarity of a G-quadruplex by using xanthine and 8-oxoguanine. *Angew. Chem. Int. Ed. 55,* 160–163.

(16) Marušič, M., Šket, P., Bauer, L., Viglasky, V., and Plavec, J. (2012) Solution-state structure of an intramolecular G-quadruplex with propeller, diagonal and edgewise loops. *Nucleic Acids Res. 40,* 6946–6956.

(17) Luu, K. N., Phan, A. T., Kuryavyi, V., Lacroix, L., and Patel, D. J. (2006) Structure of the human telomere in K^+ solution: an intramolecular (3+1) G-quadruplex scaffold. *J. Am. Chem. Soc. 128,* 9963–9970.

(18) Wang, Y., and Patel, D. J. (1993) Solution structure of the human telomeric repeat d[$AG_3(T_2AG_3)_3$] G-tetraplex. *Structure 1,* 263–282.

(19) Parkinson, G. N., Lee, M. P. H., and Neidle, S. (2002) Crystal structure of parallel quadruplexes from human telomeric DNA, *Nature 417*, 876-880.

(20) Karsisiotis, A. I., Hessari, N. M., Novellino, E., Spada, G. P., Randazzo, A., and Webba da Silva, M. (2011) Topological characterization of nucleic acid G-quadruplexes by UV absorption and circular dichroism. *Angew. Chem. Int. Ed. 50,* 10645–10648.

(21) Masiero, S., Trotta, R., Pieraccini, S., De Tito, S., Perone, R., Randazzo, A., and Spada, G. P. (2010) A non-empirical chromophoric interpretation of CD spectra of DNA G-quadruplex structures. *Org. Biomol. Chem. 8,* 2683–2692.

(22) Greene, K. L., Wang, Y., and Live, D. (1995) Influence of the glycosidic torsion angle on ^{13}C and ^{15}N shifts in guanosine nucleotides: investigations of G-tetrad models with alternating *syn* and *anti* bases. *J. Biomol. NMR 5,* 333–338.

(23) Fonville, J. M., Swart, M., Vokáčová, Z., Sychrovský, V., Šponer, J. E., Šponer, J., Hilbers, C. W., Bickelhaupt, F. M., and Wijmenga, S. S. (2012) Chemical shifts in nucleic acids studied by density functional theory calculations and comparison with experiment. *Chem. - Eur. J. 18,* 12372–12387.

(24) Blandin, M., Son, T.-D., Catlin, J. C., and Guschlbauer, W. (1974) Nucleoside conformations: 16. Nuclear magnetic resonance and circular dichroism studies on pyrimidine-2′-fluoro-2′-

deoxyribonucleosides. *Biochim. Biophys. Acta 361*, 249–256.

(25) Thibaudeau, C., Plavec, J., and Chattopadhyaya, J. (1998) A new generalized Karplus-type equation relating vicinal proton-fluorine coupling constants to H-C-C-F torsion angles. *J. Org. Chem. 63*, 4967–4984.

(26) Pallan, P. S., Greene, E. M., Jicman, P. A., Pandey, R. K., Manoharan, M., Rozners, E., and Egli, M. (2011) Unexpected origins of the enhanced pairing affinity of 2'-fluoro-modified RNA. *Nucleic Acids Res. 39*, 3482–3495.

(27) de Leeuw, F. A. A. M., and Altona, C. (1982) Conformational analysis of β-D-ribo-, β-D-deoxyribo-, β-D-arabino-, β-D-xylo-, and β-D-lyxo-nucleosides from proton–proton coupling constants. *J. Chem. Soc. Perkin Trans. 2*, 375–384.

(28) Li, Z., Lech, C. J., and Phan, A. T. (2014) Sugar-modified G-quadruplexes: effects of LNA-, 2'F-RNA- and 2'F-ANA-guanosine chemistries on G-quadruplex structure and stability. *Nucleic Acids Res. 42*, 4068–4079.

(29) Lech, C. J., Heddi, B., and Phan, A. T. (2013) Guanine base stacking in G-quadruplex nucleic acids. *Nucleic Acids Res. 41*, 2034–2046.

(30) Šponer, J., Mládek, A., Špačková, N., Cang, X., Cheatham, T. E., III, and Grimme, S. (2013) Relative stability of different DNA guanine quadruplex stem topologies derived using large-scale quantum-chemical computations. *J. Am. Chem. Soc. 135*, 9785–9796.

(31) Islam, B., Stadlbauer, P., Neidle, S., Haider, S., and Šponer, J. (2016) Can we execute reliable MM-PBSA free energy computations of relative stabilities of different guanine quadruplex folds? *J. Phys. Chem. B 120*, 2899–2912.

(32) Zgarbová, M., Šponer, J., Otyepka, M., Cheatham, T. E., III, Galindo-Murillo, R., and Jurečka, P. (2015) Refinement of the sugar–phosphate backbone torsion beta for AMBER force fields improves the description of Z- and B-DNA. *J. Chem. Theory Comput. 11*, 5723–5736.

(33) Marathias, V. M., Wang, K. Y., Kumar, S., Pham, T. Q., Swaminathan, S., and Bolton, P. H. (1996) Determination of the number and location of the manganese binding sites of DNA quadruplexes in solution by EPR and NMR in the presence and absence of thrombin. *J. Mol. Biol. 260*, 378–394.

(34) Haider, S., Parkinson, G. N., and Neidle, S. (2002) Crystal structure of the potassium form of an Oxytricha nova G-quadruplex. *J. Mol. Biol. 320*, 189–200.

(35) Hazel, P., Parkinson, G. N., and Neidle, S. (2006) Topology variation and loop structural homology in crystal and simulated structures of a bimolecular DNA quadruplex. *J. Am. Chem. Soc. 128*, 5480–5487.

(36) Biffinger, J. C., Kim, H. W., and DiMagno, S. G. (2004) The polar hydrophobicity of fluorinated compounds. *ChemBioChem 5*, 622–627.

(37) O'Hagan, D. (2008) Understanding organofluorine chemistry. An introduction to the C–F bond. *Chem. Soc. Rev. 37*, 308–319.

(38) Dickerhoff, J., Appel, B., Müller, S., and Weisz, K. (2016) Sugar-edge interactions in a DNA-RNA G-quadruplex: evidence of sequential C-H···O hydrogen bonds contributing to RNA quadruplex folding, *Angew. Chem. Int. Ed*., **55**, 15162-15165.

(39) Vranken, W. F., Boucher, W., Stevens, T. J., Fogh, R. H., Pajon, A., Llinas, M., Ulrich, E. L., Markley, J. L., Ionides, J., and Laue, E. D. (2005) The CCPN data model for NMR spectroscopy: development of a software pipeline. *Proteins: Struct., Funct., Bioinf. 59*, 687–696.

(40) Vanquelef, E., Simon, S., Marquant, G., Garcia, E., Klimerak, G., Delepine, J. C., Cieplak, P., and Dupradeau, F.-Y. (2011) R.E.D. server: a web service for deriving RESP and ESP charges and building force field libraries for new molecules and molecular fragments. *Nucleic Acids Res. 39*, W511–W517.

(41) Schwieters, C. D., Kuszewski, J. J., Tjandra, N., and Clore, G. M. (2003) The Xplor-NIH NMR molecular structure determination package. *J. Magn. Reson. 160*, 65–73.

(42) Cornell, W. D., Cieplak, P., Bayly, C. I., Gould, I. R., Merz, K. M., Ferguson, D. M., Spellmeyer, D. C., Fox, T., Caldwell, J. W., and Kollman, P. A. (1995) A second generation force field for the simulation of proteins, nucleic acids, and organic molecules. *J. Am. Chem. Soc. 117*, 5179–5197.

(43) Krepl, M., Zgarbová, M., Stadlbauer, P., Otyepka, M., Banáš, P., Koča, J., Cheatham, T. E., III, Jurečka, P., and Šponer, J. (2012) Reference simulations of noncanonical nucleic acids with different χ variants of the AMBER force field: quadruplex DNA, quadruplex RNA, and Z-DNA. *J. Chem. Theory Comput. 8*, 2506–2520.

(44) Zgarbová, M., Luque, F. J., Šponer, J., Cheatham, T. E., III, Otyepka, M., and Jurečka, P. (2013) Toward improved description of DNA backbone: revisiting epsilon and zeta torsion force field parameters. *J. Chem. Theory Comput. 9*, 2339–2354.

(45) Lu, X.-J., and Olson, W. K. (2003) 3DNA: a software package for the analysis, rebuilding and visualization of three-dimensional nucleic acid structures. *Nucleic Acids Res. 31*, 5108–5121.

Supporting Information

Tracing Effects of Fluorine Substitutions on G-Quadruplex Conformational Transitions

Jonathan Dickerhoff, Linn Haase, Walter Langel, and Klaus Weisz*

Institute of Biochemistry, Ernst-Moritz-Arndt University Greifswald, Felix-Hausdorff-Str. 4, D-17487 Greifswald, Germany

*Corresponding author: weisz@uni-greifswald.de

METHODS

NMR experiments. All spectra were acquired at 25 °C with proton chemical shifts referenced relative to TSP by setting the H_2O signal to 4.78 ppm. For one-dimensional and NOESY experiments a WATERGATE with w5 element was employed for solvent suppression. 2D NOE spectra were recorded with mixing times of 80, 150, 250, and 300 ms either in 90% H_2O/10% D_2O or 100 % D_2O. DQF-COSY spectra were acquired in D_2O with a 3-9-19 solvent suppression scheme that was also used for the phase-sensitive ^{1}H-^{13}C HSQC experiments in 90% H_2O/10% D_2O. The latter were optimized for a ^{1}J(C,H) of 160 Hz and ^{13}C chemical shifts were referenced relative to DSS by using the indirect referencing method. A JRHMBC spectrum with a jump and return water suppression scheme was recorded for the ^{F}HT quadruplex in order to correlate H1 and H8 protons within the same guanine base through their long-range *J* coupling to C5.[1]

NMR structure calculations. Crosspeaks in the NOESY spectra were classified as strong (2.9 ± 1.1 Å), medium (4.0 ± 1.5 Å), weak (5.5 ± 1.5 Å), and very weak (6.0 ± 1.5 Å). In case of exchangeable protons the categories were set to medium (4.0 ± 1.2 Å), weak (5.0 ± 1.2 Å), and very weak (6.0 ± 1.2 Å). Distances of 5.0 ± 2.0 Å were assigned to strongly overlapped signals. Glycosidic torsion angles were restrained to 170-310° and 200-280° for *anti* conformers outside and within the G-core, respectively. Due to a very weak H8-H2' contact a dihedral of 90-240° was assigned to ^{F}G1 in ^{F}ODN. Glycosidic torsions for s*yn* conformers were set to 25-95°. The signal intensity of H1'-H2' and H1'-H2" crosspeaks in DQF-COSY spectra was used for an estimation of sugar pucker with the pseudorotation phase angle restricted to 144-180° for *south*-type and 0-36° for *north*-type sugars. Due to spectral overlap this parameter could not be determined for residues 2 and 6 in ^{F}HT as well as for residues 12, 17, 18, and 19 in ^{F}ODN.

The protocol for simulated annealing of the 100 starting structures included a 5 ps equilibration period at 100 K followed by heating to 1000 K during 10 ps. After 30 ps the system was cooled to 100 K during 45 ps and finally to 0 K during the last 10 ps. Force constants for NMR-derived distance and hydrogen bond restraints also including the A-T base pair in ^{F}HT were set to 50 kcal·mol^{-1}·Å^{-2}, for glycosidic torsion angle and sugar pucker restraints to 200 kcal·mol^{-1}·rad^{-2}, and for planarity restraints of G-tetrads to 30 kcal·mol^{-1}·Å^{-2}.

For a refinement in water the ten lowest-energy quadruplex structures were neutralized with K^+ and two cations manually moved between tetrads. The system was solved with water molecules (TIP3P) in a truncated octahedral box of 10 Å.[2] During initial equilibration the DNA

was fixed with 25 kcal·mol^{-1}·Å^{-2}. After 500 steps each of steepest descent and conjugated gradient minimization, the system was heated from 100 to 300 K during 10 ps under constant volume followed by a decrease in force constants to 5, 4, 3, 2, 1, and 0.5 kcal·mol^{-1}·Å^{-2} and further equilibration. The final simulation of 1 ns duration was performed with restraints only for NMR-derived distances and Hoogsteen hydrogen bonds as well as for the sugar pucker of ^{F}G residues. The trajectories were subsequently averaged over the last 100 ps and shortly minimized in vacuum for 2000 steps.

References

(1) Phan, A. T. (2000) Long-range imino proton-13C J-couplings and the through-bond correlation of imino and non-exchangeable protons in unlabeled DNA. *J. Biomol. NMR 16*, 175–178.

(2) Jorgensen, W. L., Chandrasekhar, J., Madura, J. D., Impey, R. W., and Klein, M. L. (1983) Comparison of simple potential functions for simulating liquid water. *J. Chem. Phys. 79*, 926-935.

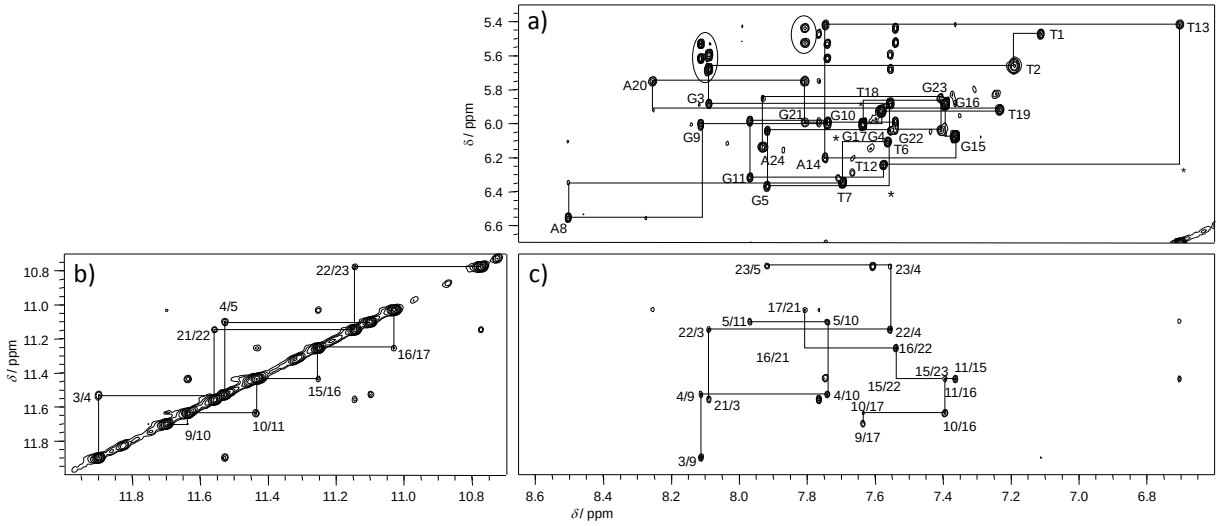

Figure S1. 2D NOE spectral regions of ^{F}HT acquired at 25 °C with τ_m = 300 ms. (a) H8/H6(ω_2)–H1'(ω_1) region tracing continuous NOE connectivities; missing NOE contacts are marked by asterisks and prominent H8-H2' crosspeaks of ^{F}G used as starting points are circled. (b) Imino–imino contacts along the four G-tracts. (c) H8/H6(ω_2)–imino(ω_1) region with intratetrad and intertetrad guanine H8–imino contacts indicated by solid lines.

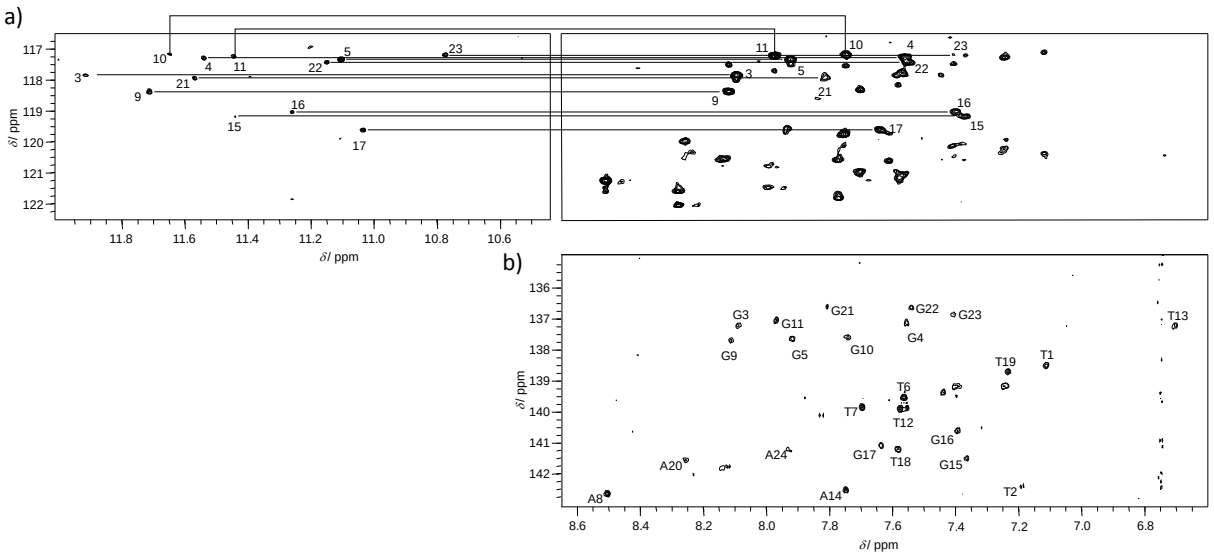

Figure S2. (a) ^{1}H-^{13}C JRHMBC spectral regions of ^{F}HT at 25 °C showing guanine H1-C5 (left) and H8-C5 (right) correlations. H1 imino and H8 protons within the same guanine base are correlated via their through-bond coupling with C5 as indicated by the solid lines. (b) ^{1}H-^{13}C HSQC spectral region of ^{F}HT at 25 °C showing correlations between H6/H8 and C6/C8.

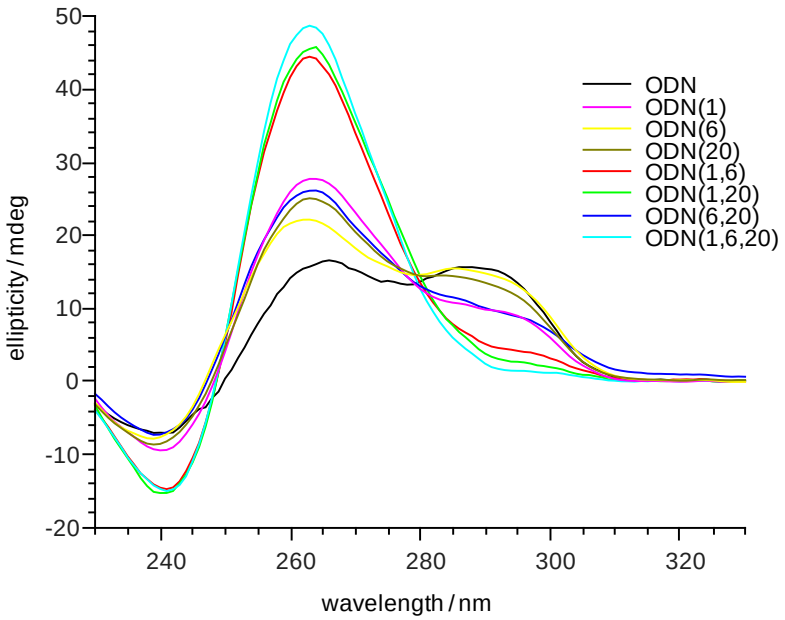

Figure S3. Superimposed CD spectra of native ODN and ^{F}G modified ODN quadruplexes (5 μM) at 20 °C. Numbers in parentheses denote the substitution sites.

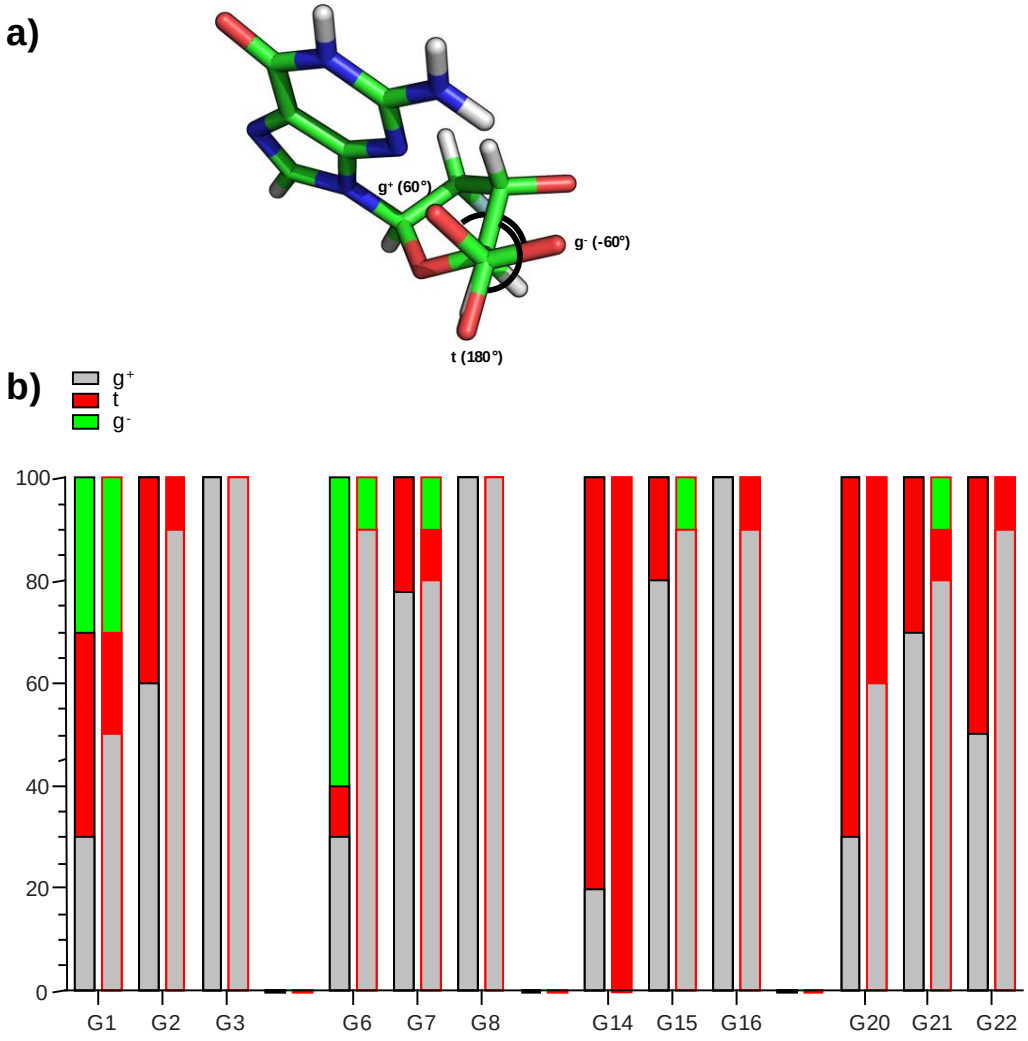

Figure S4. (a) Model of a *syn* guanosine with the sugar O5'-orientation in a gauche+ (g^+), gauche- (g^-), and trans (t) conformation for torsion angle γ (O5'-C5'-C4'-C3'). (b) Distribution of γ conformers in ODN (left black-framed bars) and ^{F}ODN (right red-framed bars). Relative populations of g^+ (0-120°), t (120-240°), and g^- (240-360°) for each residue within the G-tetrad core are based on the analysis of all deposited 10 low-energy conformations for each quadruplex NMR structure (pdb: 2LOD and 5MCR).

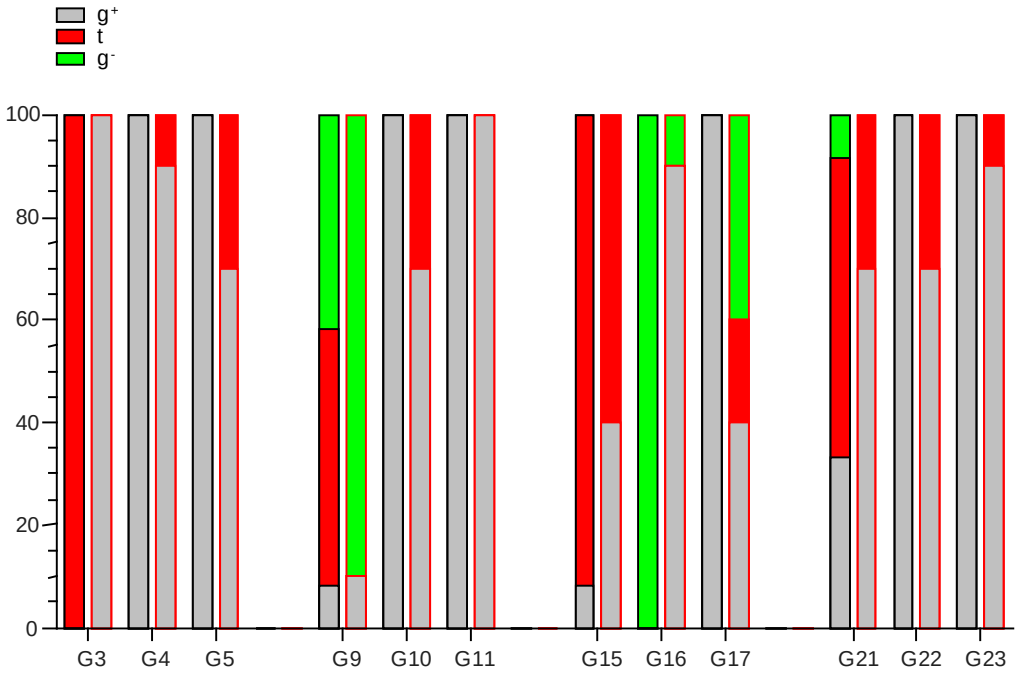

Figure S5. Distribution of γ conformers in HT (left black-framed bars) and ^{F}HT (right red-framed bars). Relative populations of g^+ (0-120°), t (120-240°), and g^- (240-360°) for each residue within the G-tetrad core are based on the analysis of all deposited 12 and 10 low-energy conformations for the two quadruplex NMR structures (pdb: 2GKU and 5MBR).

Affirmation

The affirmation has been removed in the published version.

Curriculum vitae

The curriculum vitae has been removed in the published version.

Published Articles

1. Dickerhoff, J., Riechert-Krause, F., Seifert, J., and Weisz, K. Exploring multiple binding sites of an indoloquinoline in triple-helical DNA: A paradigm for DNA triplex-selective intercalators. *Biochimie* 2014, 107, 327–337.

2. Santos-Aberturas, J., Engel, J., Dickerhoff, J., Dörr, M., Rudroff, F., Weisz, K., and Bornscheuer, U. T. Exploration of the Substrate Promiscuity of Biosynthetic Tailoring Enzymes as a New Source of Structural Diversity for Polyene Macrolide Antifungals. *ChemCatChem* 2015, 7, 490–500.

3. Dickerhoff, J., and Weisz, K. Flipping a G-Tetrad in a Unimolecular Quadruplex Without Affecting Its Global Fold. *Angew. Chem. Int. Ed.* 2015, 54, 5588–5591; *Angew. Chem.* 2015, 127, 5680 – 5683.

4. Kohls, H., Anderson, M., Dickerhoff, J., Weisz, K., Córdova, A., Berglund, P., Brundiek, H., Bornscheuer, U. T., and Höhne, M. Selective Access to All Four Diastereomers of a 1,3-Amino Alcohol by Combination of a Keto Reductase- and an Amine Transaminase-Catalysed Reaction. *Adv. Synth. Catal.* 2015, 357, 1808–1814.

5. Thomsen, M., Tuukkanen, A., Dickerhoff, J., Palm, G. J., Kratzat, H., Svergun, D. I., Weisz, K., Bornscheuer, U. T., and Hinrichs, W. Structure and catalytic mechanism of the evolutionarily unique bacterial chalcone isomerase. *Acta Cryst. D* 2015, 71, 907–917.

6. Skalden, L., Peters, C., Dickerhoff, J., Nobili, A., Joosten, H.-J., Weisz, K., Höhne, M., and Bornscheuer, U. T. Two Subtle Amino Acid Changes in a Transaminase Substantially Enhance or Invert Enantiopreference in Cascade Syntheses. *ChemBioChem* 2015, 16, 1041–1045.

7. Funke, A., Dickerhoff, J., and Weisz, K. Towards the Development of Structure-Selective G-Quadruplex-Binding Indolo[3,2- b]quinolines. *Chem. Eur. J.* 2016, 22, 3170–3181.

8. Dickerhoff, J., Appel, B., Müller, S., and Weisz, K. Sugar-Edge Interactions in a DNA-RNA G-Quadruplex: Evidence of Sequential C-H$\cdots$ Hydrogen Bonds Contributing to RNA Quadruplex Folding. *Angew. Chem. Int. Ed.* 2016, 55, 15162-15165; *Angew. Chem.* 2016, 128, 15386 – 15390.

9. Karg, B., Haase, L., Funke, A., Dickerhoff, J., and Weisz, K. Observation of a Dynamic G-Tetrad Flip in Intramolecular G-Quadruplexes. *Biochemistry* 2016, 55, 6949–6955.

10. Dickerhoff, J., Haase, L., Langel, W., and Weisz, K. Tracing Effects of Fluorine Substitutions on G-Quadruplex Conformational Transitions. *submitted*.

Poster

1. 07/2012: EUROMAR in Dublin, Ireland, 'NMR Spectroscopic Characterization of Coexisting DNA-Drug Complexes in Slow Exchange'

2. 09/2013: VI. Nukleinsäurechemietreffen in Greifswald, Germany, 'Multiple Binding Sites of a Triplex-Binding Indoloquinoline Drug: A NMR Study'

3. 05/2015: 5th International Meeting in Quadruplex Nucleic Acids in Bordeaux, France, 'Editing Tetrad Polarities in Unimolecular G-Quadruplexes'

4. 07/2016: EUROMAR in Aarhus, Denmark, 'Systematic Incorporation of C2'-Modified Analogs into a DNA G-Quadruplex'

5. 07/2016: XXII International Roundtable on Nucleosides, Nucleotides and Nucleic Acids in Paris, France, 'Structural Insights into the Tetrad Reversal of DNA Quadruplexes'

Acknowledgements

An erster Stelle danke ich Klaus Weisz für die Begleitung in den letzten Jahren: für das Vertrauen, die vielen Ideen, die Freiheiten in Forschung und Arbeitszeiten und die zahlreichen Diskussionen. Ohne all dies hätte ich weder meine Freude an der Wissenschaft entdeckt noch meine wachsende Familie so gut mit der Promotion vereinbaren können.

Ich möchte auch unseren benachbarten Arbeitskreisen für die erfolgreichen Kooperationen danken. Prof. Dr. Müller und Bettina Appel halfen mir beim Einstieg in die Welt der RNA-Quadruplexe und Simone Turski und Julia Drenckhan synthetisierten die erforderlichen Oligonukleotide. Die nötigen Rechnungen zur Strukturaufklärung konnte ich nur dank der von Prof. Dr. Langel bereitgestellten Rechenkapazitäten durchführen und ohne Norman Geist wären mir viele wichtige Einblicke in die Informatik entgangen.

Andrea, Petra und Trixi danke ich für die familiäre Atmosphäre im Arbeitskreis, die täglichen Kaffeerunden und die spannenden Tagungsreisen. Außerdem danke ich Jenny, ohne die ich die NMR-Spektroskopie nie für mich entdeckt hätte.

Meinen ehemaligen Kommilitonen Antje, Lilly und Sandra danke ich für die schönen Greifswalder Jahre innerhalb und außerhalb des Instituts. Ich freue mich, dass der Kontakt auch nach der Zerstreuung in die Welt erhalten geblieben ist.

Schließlich möchte ich meinen Eltern für ihre Unterstützung und ihr Verständnis in den Jahren meines Studiums und der Promotion danken. Aber vor allem freue ich mich, die Abenteuer Familie und Wissenschaft zusammen mit meiner Frau und meinen Kindern erleben zu dürfen. Ich danke euch für Geduld und Verständnis, wenn die Nächte mal kürzer und die Tage länger sind oder ein unwilkommenes Ergebnis die Stimmung drückt. Ihr seid mir ein steter Anreiz, nicht mein ganzes Leben mit Arbeit zu verbringen.